NASA Contractor Report 3213

Noise of a Model Helicopter Rotor Due to Ingestion of Turbulence

Robert W. Paterson and Roy K. Amiet

CONTRACT NAS1-15094
NOVEMBER 1979

NASA

NASA Contractor Report 3213

Noise of a Model Helicopter Rotor Due to Ingestion of Turbulence

Robert W. Paterson and Roy K. Amiet
United Technologies Research Center
East Hartford, Connecticut

Prepared for
Langley Research Center
under Contract NAS1-15094

National Aeronautics
and Space Administration

**Scientific and Technical
Information Branch**

1979

TABLE OF CONTENTS

TABLE OF CONTENTS (Cont'd)

SUMMARY

A theoretical and experimental investigation of the noise of a model helicopter rotor due to ingestion of turbulence was conducted. Experiments were performed with a 0.76 m dia, articulated model rotor at the United Technologies Research Center (UTRC) Acoustic Research Tunnel for a range of inflow turbulence and rotor operating conditions. Inflow turbulence levels varied from approximately 2 to 19 percent and tip Mach number was varied from 0.3 to 0.52. Test conditions included ingestion of atmospheric turbulence in outdoor hover as well as ingestion of grid generated isotropic turbulence in the wind tunnel airstream. In wind tunnel testing, both forward flight and vertical ascent (climb) were simulated. Far-field noise spectra and directivity were measured in addition to incident turbulence intensities, length scales and spectra.

Measured inflow turbulence statistics and rotor operating parameters were employed in a theoretical procedure to predict turbulence ingestion noise. This theory, which had been published in the open literature but not assessed prior to this study, represented a rotating blade extension to an earlier theory that had been shown to predict, accurately, isolated airfoil incident turbulence noise spectra and directivity without recourse to empirical or adjustable constants. While noise prediction accuracy was found to be generally less favorable in the present rotor case then the previous isolated airfoil case, the narrowband random nature of turbulence ingestion noise at low frequency and broadband nature at high frequency was predicted. In addition, broadband noise levels measured in wind tunnel experimentation were well predicted. Theoretical predictions of pitch and blade number effects were partially confirmed. An anisotropic inflow turbulence model was shown to be necessary to predict atmospheric turbulence ingestion noise measured during outdoor hover testing. Inclusion of anisotropic inflow turbulence effects and treatment of the forward flight case represented extensions to the theoretical noise prediction method performed as part of this study.

Ingestion of atmospheric turbulence and steady blade loading were found to be the principal model rotor noise mechanisms in outdoor tests simulating hover. Except for the first few harmonics of blade passage frequency (BPF), the turbulence ingestion mechanism dominated, causing narrowband random noise to extend to approximately 25 harmonics of BPF. This was attributed to interaction of axially elongated eddies with the rotor. A fundamental conclusion of this study, therefore, is that ingestion of atmospheric turbulence is the dominant helicopter rotor hover noise mechanism at the moderate to high frequencies which determine perceived noise level.

In addition to turbulence ingestion experimentation, ingestion of a tip vortex generated by a blade located upstream of the rotor was observed to cause significant harmonic noise and an impulsive waveform. Such ingestion appears to be a relevant main rotor-tail rotor interaction noise mechanism; this noise would be additive to interaction noise resulting from ingestion of rotor wake turbulence.

LIST OF SYMBOLS

b	Airfoil semichord
B	Number of blades
c	Airfoil chord
c_o	Sound speed
d	Semispan of airfoil segment
E	Energy
$E[\ ]$	Expected value
F	Force
fo	Doppler shifted frequency
f_s	Source frequency
g	Airfoil response function; Eq. (B 24)
$\hat{i},\hat{j},\hat{k}$	Unit vectors along x, y, z coordinates
K	Constant
k_x, k_y, k_z	Wavenumber components of turbulence
K_x	ω/V_c
K_y	$\omega y'/(c_o \sigma')$
$K_z(n)$	Defined by Eq. (B 37)
ℓ	Defined in Fig. 24
$\mathcal{L}$	Integrated airfoil response function; Eq. (B 31)
M_a	Spanwise component of flight Mach number
M_c	Chordwise component of Mach number

M_f	Flight Mach number
M_n	Mach number component in observer direction
M_s	Mach number of source relative to fluid
M_t	Mach number of source relative to observer
M_{tip}	Tip Mach number
M_z	Axial Mach number
P	Pressure
R_{pp}	Autocorrelation function of the far-field noise
$R_{pp}^{(n)}$	Cross-correlation of the far-field sound from the zeroth blade passage with that from the n'th blade passage
$R_{qq}^{(n)}$	Cross-correlation of surface pressure on the zeroth blade passage with that on the n'th blade passage
R_{ww}^{I}	Cross-correlation function of transverse velocities for isotropic turbulence
R_{ww}^{NI}	Cross-correlation function of transverse velocities for nonisotropic turbulence
R	Radius at which blade segment rotates
r	Source to observer distance
r_e	Distance from observer to retarded source point
$S_{pp}^{(n)}$	Cross-spectrum of the far-field sound from the zeroth blade passage with that from the n'th blade passage
$S_{pp}(\gamma)$	Instantaneous far-field spectrum
S_{pp}	Far-field spectrum averaged over azimuth

LIST OF SYMBOLS (Cont'd)

t	Time
T	Time between blade passages
T_1	Time between eddy chops
T_r	Time for sound to propagate from source to observer
V_c, V_f, V_t, V_z	c_o times the corresponding Mach number
V	Velocity of airfoil relative to observer
w	Gust component normal to airfoil
$\underline{x}_p$	Present source position
$\underline{x}_s$	Retarded source position
$\underline{x}$	Coordinate system with origin at rotor hub, the z coordinate lying along the axis and the observer in the xz plane
$\underline{x}'$	Coordinate system with y' along airfoil span and x' along chord pointing from leading to trailing edge and origin at the present source position of the rotor segment
$\underline{x}''$	Coordinate system with z" along rotor axis and y" along rotor span and origin at the present source position of the rotor segment
$\underline{x}'''$	Coordinate system translated from the $\underline{x}$ system so that the origin lies at the present source position of the rotor segment
Z	Minimum distance between a chopped eddy and the succeeding blade
α	Stretching factor for nonisotropic turbulence
α'	Angle of airfoil with respect to rotor plane
β	Prandtl-Glauert factor $(1-M_c^2)^{1/2}$

γ	Aximuthal angle of rotor blade
η	$y_1 - y_2$
θ	Angle of microphone from tunnel centerline
θ_M	Measured value of θ
θ_c	Value of θ corrected for shear layer refraction
θ'	Angle of observer from rotor axis
$\textcircled{H}$	Angle defined by Eq. (B 8)
Λ_f	Longitudinal correlation length of turbulence
Λ_g	Transverse correlation length of turbulence
ν	Kinematic viscosity
ρ	Density
σ'	Effective distance defined by Eq. (B 31)
τ	Dummy time variable
ϕ	Angle of microphone as measured in a plane perpendicular to the tunnel axis
ϕ'	Angle which the non-axial component of flow, M_f, makes with the y axis; see Fig. 23
Φ	Angle between the x' axis and a line from the observer to the rotor blade segment; see Eq. (B 15d)
Φ_{ww}	Spectrum of turbulence velocity normal to the rotor blade
$\tilde{\Phi}_{ww}$	Integral of Φ_{ww} over the wavevector normal to the blade; see Eq. (B 29)
Φ_{ww}^{I}, Φ_{ww}^{NI}	Spectrum of transverse turbulence velocities for iostropic and nonisotropic turbulence, respectively

LIST OF SYMBOLS (Cont'd)

ω	Radian frequency of source
ω_o	Radian frequency heard by observer

INTRODUCTION

Helicopter Rotor Noise Sources

Generalized conclusions as to the relative importance of various helicopter noise mechanisms are difficult to draw due to complications introduced by the four variables of rotor geometry, operating condition, far-field noise frequency and noise directivity angle. While one mechanism may dominate far-field noise for a set of these values, other mechanisms will dominate the noise for other sets. This coexistence of mechanisms of various strengths and different frequency and directivity characteristics, significantly complicates both data interpretation and attempts to assess the accuracy of theories developed to treat one mechanism.

The list of possible rotor noise mechanisms is lengthy and is, in fact, a matter of contention among specialists in the area of helicopter noise research. A useful list of possible mechanisms and the state of understanding of each, as of 1977, was given by George in reference 1. Noise due to turbulent inflow is included in this list. Only in the past five years, however, has this mechanism been regarded as a potentially important helicopter noise source.

Arising from the interaction of random velocity fluctuations with a blade, the turbulence ingestion mechanism is always operative to some degree. For reasons cited above it is difficult to obtain a universally valid ranking of helicopter noise sources in order of importance and then to assign the turbulent inflow mechanism an appropriate position in the list.

The objective of the present study was to attempt to obtain a quantitative understanding of the contribution of turbulence ingestion noise to model rotor noise spectra and directivity as a function of relevant variables. These variables included the intensity, length scale and degree of anisotropy of the inflow turbulence as well as rotor operating conditions (tip speed, orientation of the rotor with respect to the inflow etc.). The study was undertaken as an extension to the isolated airfoil turbulence interaction study reported in reference 2.

In the reference 2 study, an absolute level spectrum and directivity theory was shown to predict, accurately, the noise of an isolated airfoil in a homogeneous, isotropic turbulence field. Reported here is an experimental assessment of the rotating blade extension of this theory.

Previous Investigations

A detailed review of theoretical and experimental research directed toward non-rotating blade, turbulence interaction noise was given in reference 2. In addition to being a stationary blade broadband noise source, interaction of inflow turbulence with a rotating blade was demonstrated by Sharland in 1964 (reference 3) to be a significant source of fan broadband noise.

Although Sofrin and McCann in 1966 (reference 4) pointed to ingestion of turbulence as a possible source of rotating blade harmonic noise, it was not until Hanson's 1974 study (reference 5) that experimental data supporting this hypothesis was obtained. Hanson concluded that the spectrum peaks of propellers, helicopter rotors and fans that had previously been considered harmonics due to fixed inflow distortion were likely narrowband random noise associated with ingestion of atmospheric turbulence.

As a result of a number of subsequent studies, turbulence ingestion has come to be recognized as an important source of rotating blade narrowband random noise as well as broadband noise. In the case of propellers, Pegg et. al. (reference 6) have shown that turbulence ingestion under static test conditions produces significant harmonic noise, while in flight, where turbulence effects are significantly less, steady loading and thickness noise dominate. For the case of fans, Feiler and Groeneweg in a review paper (reference 7), show similar effects of flight on turbulence ingestion noise. To date, however, there have been no corresponding full-scale experimental studies of helicopter rotor turbulence ingestion effects. A detailed review of theoretical and experimental research directed toward rotating blade turbulence ingestion noise is provided in Appendix A.

From a noise prediction standpoint, the theories of Amiet (reference 8) and Homicz and George (reference 9) represent the most rigorous treatments of propeller and hovering rotor turbulence ingestion noise. These theories proceed from a statistical description of the inflow turbulence field to predict far-field noise spectra and directivity on an absolute level basis. Empirical or adjustable constants are not employed; neither is knowledge of unsteady blade pressure statistics required.

George, in reference 1, concluded that there was a strong need for experiments on rotor-turbulence interaction where turbulent inflow properties and acoustic data were measured simultaneously. Hawkings more recently, in reference 10, noted that there were no experimental data on the nature and level of the turbulence entering a helicopter rotor.

Present Study

Objectives - The overall objectives of the present study were to provide turbulent inflow and noise data such as described above for a model helicopter rotor and use these results to assess the accuracy of the turbulence ingestion noise prediction method developed by Amiet (reference 8). It was desired to treat not only the hovering rotor case (or simulated vertical ascent) but also simulated forward flight.

A second objective was to assess noise prediction accuracy not only for isotropic, homogeneous inflow turbulence but also for the more complicated anisotropic inflow anticipated in outdoor hover. As part of this objective, it was desired to obtain an indication of the role of atmospheric turbulence ingestion in the generation of hover noise.

A third objective was to obtain exploratory experimental data on the effect of the ingestion of an isolated tip vortex on the noise of a model rotor. Such ingestion is a possible main rotor-tail rotor interaction noise mechanism that could produce noise in addition to that created by ingestion of main or tail rotor mean and turbulent wakes.

Approach - A 0.76m dia articulated rotor was tested in an anechoic wind tunnel with and without turbulence grids located upstream. Noise and inflow turbulence statistics were measured for a number of test conditions and predictions of theory compared to experiment. Rotor tip Mach number, pitch, number of blades and inflow turbulence intensity and length scale were varied. Comparisons were made for both simulated vertical ascent and forward flight; as part of the study the prediction method of Amiet was extended to treat the forward flight case. Noise and inflow turbulence statistics were measured simultaneously at two outdoor hover test conditions. Noise data and predictions of theory (as modified to account for anisotropic turbulent inflow) were compared. In addition, measurements of the effect of the ingestion of a tip vortex by the model rotor were obtained in the wind tunnel.

THEORETICAL FORMULATION

General Approach

The theory employed in this study to predict rotor turbulence ingestion noise represents an extension to that given by Amiet in reference 8 for the case of axial inflow to a rotor or propeller. The reference 8 noise prediction method was, in turn, based on earlier theory for the acoustic radiation produced by a blade moving in rectilinear motion through turbulence. This theory was described in detail in reference 11 and was validated in isolated airfoil experimentation conducted in the UTRC Acoustic Research Tunnel as reported in references 2 and 12. In that experimental study, homogeneous, isotropic turbulence, generated by grids in the tunnel inlet, convected into the open-jet tunnel test section and interacted with the airfoil producing broadband noise. Incident turbulence statistics were measured as well as airfoil far-field noise spectra and directivity.

Measurement and prediction were found to be generally in close agreement. Of particular importance was that there were no empirically derived or adjustable constants employed in the prediction method. This theory, therefore, provided a useful base from which to treat the more complicated rotating blade case.

Treatment of Rotation Effects

Application of the rectilinear motion case to that of a rotating blade is reasonably direct. For the case of small scale turbulence entering a rotor, an eddy is completely chopped by a rotor blade and the sound of the interaction is radiated away before the blade undergoes significant angular rotation. Noise generation in this case is similar to that of an isolated airfoil in a turbulent stream since the rotation time is long compared to the time for sound generation. The effect of rotation can be put in more quantitative terms by examining the expression given by Lowson (reference 13) for the pressure field of an accelerating dipole of strength F(t). This is

$$(4\pi\ c_o)\ P = \left[r^{-2}\ (1-M_n)^{-2}\ \underline{r} \cdot \{ \dot{\underline{F}} + \dot{M}_n \underline{F}/(1-M_n) \} \right] \qquad (1)$$

where the square brackets imply evaluation at the retarded time, r is the vector joining source to observer and M_n is the component of source Mach number in the observer direction.

For a dipole fluctuating in amplitude with angular frequency, ω, and moving along a circular path with angular frequency, Ω, the F term, which represents the far-field contribution, will outweight the $\dot{M}_n$ (or near field) term if $\omega >> \Omega$ and M_n is not near 1. This result justifies treating the sound of the rotating airfoil in the present study as if the airfoil were in instantaneous rectilinear motion. The basic theory of reference 11 can thus be applied.

To arrive at a rotating blade prediction method, several extensions of the theory of reference 11 are required. First, the average of the spectrum around the azimuth must be taken. This is not a direct average, but a weighted average to account for the different amounts of retarded time spent by the rotor in the different azimuthal positions. This weighting factor is just the Doppler factor due to the source and observer being in relative motion. If the source on the blade has a frequency, ω, and the far-field observer hears a Doppler shifted frequency ω_o, then the weighting factor for averaging over the azimuth is ω/ω_o. If the instantaneous spectrum is $S_{pp}(\gamma)$ and the averaged spectrum is S_{pp}, then

$$S_{pp} = \frac{1}{2\pi}\int_o^{2\pi} S_{pp}(\gamma)\frac{\omega}{\omega_o}\, d\gamma \qquad (2)$$

Averaging instantaneous spectra in this manner is a standard technique discussed further by Bendat and Piersol (reference 14).

Because the Mach number varies with spanwise position on the rotor, in contrast with the case rectilinear motion, an average should be taken over span. Reasonable results can usually be obtained by assuming an effective radius of about 0.8 of the tip radius, as in reference 8, but the results presented here use the more rigorous integration over span.

The spectrum, S_{pp}, represents the energy per unit radian frequency whereas the spectrum analyzer used in reduction of experimental data employs a significantly greater bandwidth. For broadband noise this can be accounted for by dividing the experimental results by the analyzer bandwidth. For narrowband random noise, such as encountered here, the width of the tone may be comparable to the measurement bandwidth, and no simple correction factor can be used. An integration of the theoretical result over the bandwidth of the measurement is therefore required. This integration was performed in the results presented in this report.

Blade-To-Blade Correlation Considerations

The final modification which must be made to the theory for rectilinear airfoil motion is to include the effects of blade-to-blade correlation. The turbulence field is assumed to be frozen as it moves through the rotor. If the eddy convection time through the rotor is greater than blade passage period, the eddies will be chopped by more than one blade giving a nonzero blade-to-blade correlation. As discussed in reference 15, this causes no appreciable change in overall acoustic energy, but concentrates sound energy around blade passage harmonics in the case of an axial inflow field. In forward flight, the effect is more complicated. The means by which blade-to-blade correlation is introduced into the prediction method is given in Appendix B.

Forward Flight

The theory developed in reference 8 was for the case of axial inflow. Since the noise spectrum is calculated on an instantaneous point-by-point basis, the theory can be extended to the case of nonaxial flow as shown in Appendix B. The Mach number impinging on the rotor then becomes a function of the aximuthal position of the rotor. Also, in calculating the blade-to-blade correlation, account must be taken of the fact that the eddies no longer move axially through the rotor. Thus, an eddy is chopped on a time scale different from blade passage period. This tends is smooth out the harmonic peaks and shift them away from multiples of blade passage frequency.

Anisotropic Turbulence

The theoretical development is valid for either isotropic or anisotropic turbulence. In reference 8 and 15, all calculations were for the case of isotropic turbulence. This assumption is convenient because of the readily available analytical expressions for the turbulence spectrum (such as those of von Kármán or Liepmann given in reference 16).

In the case of nonisotropic turbulence, the analytical form to use for the spectrum is not obvious since there is no general expression available. For tests conducted in the wind tunnel in the present study, an isotropic model was satisfactory since there was little contraction of the flow as it passed through the rotor. For outdoor hover tests, however, there was no external flow; in this case, there is significant contraction of the inflow streamlines. Even if the ambient atmospheric turbulence were isotropic, it would be significantly distorted and stretched in the axial direction in the process of convecting into the rotor. Such distortion was observed in the present experiment.

The model used here for the nonisotropic turbulence is based on the above physical reasoning. Denoting the isotropic spectrum function by Φ^{I}_{ww}, the anisotropic spectrum function Φ^{NI}_{ww} used here is

$$\Phi^{NI}_{ww}(k_x, k_y, k_z) = \alpha \Phi^{I}_{ww}(k_x, k_y, \alpha k_z) \tag{3}$$

This model gives the same rms intensity for the turbulence velocity fluctuation in both isotropic and nonisotropic cases as can be shown by integration of the above equation over k_x, k_y, k_z. It reduces to the isotropic spectrum when the parameter, α, approaches one and yields an elongation of the turbulence length scale in the axial (z) direction for $\alpha > 1$.

This stretching can be more clearly seen by examining the expression for the velocity cross-correlation; i.e., the Fourier transform of Φ with respect to k_z.

$$\begin{aligned} R^{NI}_{ww}(k_x, k_y, Z) &= \int_{\infty}^{\infty} \Phi^{NI}_{ww}(k_x, k_y, k_z)\, e^{ik_z z} dk_z \\ &= \int_{\infty}^{\infty} \Phi^{I}_{ww}(k_x, k_y, k_z')\, e^{ik_z' z/\alpha} dk_z' \\ &= R^{I}_{ww}(k_x, k_y, Z/\alpha) \end{aligned} \tag{4}$$

Thus, if the correlation length in the z direction for the isotropic case is L, for the nonisotropic case it will be αL. The correlation lengths in the x and y directions continue to be L for the nonisotropic case. Thus, there is a stretching in the z direction by the factor α.

Sound produced by convection of anisotropic turbulence of this form into a rotor is approximately the same as that resulting from ingestion of isotropic turbulence at an assumed axial velocity that is a factor of α smaller than the actual axial velocity. That is, if the convection of a nominally spherical eddy through the rotor disk is artificially slowed down by a factor α, the noise prediction method will view this as an interaction with an elongated eddy.

This approach correctly models the essential feature of the anistropic inflow in that the retarded spherical eddy is chopped the same number of times as the unretarded elongated eddy. This approach was used in the

present program. The measured transverse turbulence length scale defined the radial extent of the eddy and the measured ratio of axial-to-transverse length scale defined the retarding (elongation) parameter.

In addition to accounting for enhanced eddy chopping due to elongation, the above approach correctly treats the other two factors (turbulence intensity and transverse length scale) that affect noise generation. That is, the measured root-mean-square value of the axial turbulence component defines the magnitude of the incident velocity fluctuation sensed by the blade while the measured transverse length scale of the axial component defines the width of the eddy.

The procedure described above does not give exactly the same result that would be obtained by using equation (3) for the turbulence spectrum. First, the effect on the noise of relative motion between source and fluid is not precisely modeled since the measured inflow velocity is decreased by a factor α, giving a slight error in relative velocity. This is a small effect for the low axial Mach numbers encountered here because the relative velocity of the blade and turbulent eddy is virtually unchanged when the axial velocity is decreased.

Second, predicted noise directivity is somewhat altered by the velocity contraction. This is because the prediction method assumes that each radial blade segment is aligned with the local inflow relative velocity. When the inflow velocity is retarded, the prediction program assigns a different orientation to each blade segment. This again was not considered a major effect in the present study because rotor tip speed was high relative to the axial velocity. In this case, the blade lies nearly in the rotor plane.

Theory Limitations

The prediction method described here has been developed by progressively including additional effects in their assumed order of importance. Additional modifications would be required to eliminate three current limitations.

First, a specified blade twist distribution could be incorporated, replacing the current assumption that each blade segment is aligned with the blade relative velocity vector. The purpose of the modification would be to more accurately define the noise directivity pattern of each blade segment.

Second, the program could be modified to account for a radially non-uniform incident mean velocity field. The current assumption is one of uniform incident velocity. Either experimental data or existing rotor inflow prediction methods could serve as input. Third, the anisotropic turbulence inflow case could be treated more rigorously by using a modified spectrum function rather than the retardation approach described above.

While the prediction capability of the theory in its present form is reasonably good considering the absolute nature of the prediction, the limitations discussed above may account for some of the disagreement with experiment reported here.

DESCRIPTION OF THE EXPERIMENT

Experimental Arrangement

This study was conducted at the UTRC Acoustic Research Tunnel. Forward flight testing was performed in the tunnel airstream while outdoor hover tests were conducted at a test stand located on the roof of the tunnel anechoic chamber.

The tunnel, described in detail in reference 17, is a controlled turbulence level, open-jet, open-circuit wind tunnel designed specifically for aerodynamic noise research. Models placed within the test section generate noise which propagates through the open-jet velocity field to microphones located in the quiescent region of the sealed chamber that surrounds the open-jet test section. The shear layer causes refraction of sound wave fronts which must be accounted for in data interpretation. The chamber is lined with fiber glass wedges which have been demonstrated through acoustic calibrations to provide an anechoic test environment for broadband and tone noise above 250 Hz. In the absence of turbulence generating grids in the tunnel inlet, a low test section turbulence level of approximately 0.2 percent is obtained. This level varies somewhat with freestream velocity.

Figure 1 shows the test arrangement in the UTRC Acoustic Research Tunnel for both simulated forward flight and vertical ascent testing. The model consisted of a 0.76 m dia articulated rotor equipped with four (or two) untwisted NACA 0012 blades of 5.1 cm chord.

For both simulated vertical ascent and forward flight testing the rotor hub was located 0.6 m downstream of the 1.3 m dia tunnel inlet nozzle on the tunnel centerline. Although a farther downstream position would have been desirable to provide a greater noise directivity measurement range, noise measurements with a clean tunnel inflow (no grid installed) showed that the rotor tip ingested the turbulent open jet test section shear layer at a hub position approximately 0.9 m downstream from the nozzle. This caused significant turbulence ingestion noise and therefore constituted an unsuitable test arrangement.

To provide various intensities and length scales of turbulence for ingestion by the rotor, various bi-plane turbulence generating grids were installed in the tunnel nozzle 1.6 m upstream of the nozzle exit plane in a 1.1 m dia section. The nozzle diffused from this minimum diameter section to 1.3 m dia at the exit plane. This small diffusion was predicted and experimentally determined not to produce boundary layer separation in the nozzle.

Instrumentation

Far-field noise was measured with 0.635 cm dia condenser microphones. The frequency response of these microphones was flat for the range relevant to this study (250 to 10,000 Hz).

For wind tunnel testing, microphones were located on arcs with radii of 3 and 2.5 m depending on microphone position. Atmospheric attenuation of far-field sound was neglected due to the low frequencies (maximum of 10 KHz) and small sound propagation distances involved in the present experiment. While figures contained in the report include a schematic of the microphone measurement position for each noise spectrum presented, a brief description of the microphone measurement array is given here.

Two noise measurement planes were used. In vertical ascent testing, microphones were located in a horizontal plane, parallel to the anechoic chamber floor, passing through the axis of the rotor. The angle, θ, defines the angular position of the microphones relative to the upstream tunnel (rotor) axis. Thus, a microphone located in the plane of rotation was at 90 deg. Measurement positions ranged from 60 to 140 deg providing data from 30 deg ahead of the plane of rotation to 50 deg aft. In forward flight testing, microphones were also located in a vertical plane passing through the $\theta = 90$ position and the rotor hub. The angle, ϕ, defines the angular position of the microphones in this plane.

Spectrum analysis was conducted with a 500 line, narrow bandwidth, real-time spectrum analyzer-ensemble averager. The effective noise bandwidth of the analyzer was measured to be 20 Hz for an analysis range of 0 to 5 KHz. Bandwidths for other ranges were in direct proportion. Noise data presented here are given as sound pressure level in decibels (referred to 0.0002 μ bar) in a specified effective noise bandwidth. Correlations were performed with a 100 line, real-time correlation and probability analyzer.

Turbulence data were acquired with single and crossed hot film probes operating in conjunction with a four channel, linearized, constant temperature anemometer system. A sum and difference network was employed to measure two components of the mean and turbulence velocity for certain test conditions.

Tunnel Mach number was determined from a pitot-static probe located in the tunnel airstream. In conjunction with tunnel inlet total temperature, these measurements defined tunnel velocity.

Vortex Shedding Noise

In model scale testing such as that considered here, a decision must be made as to how to treat the phenomenon of discrete frequency vortex shedding noise. The origin of this mechanism and its treatment in the present program is discussed below.

In isolated airfoil studies reported by Paterson et al. in 1971 (reference 18), it was shown that laminar boundary layers can cause vortex shedding noise at discrete frequencies. This pure tone noise was observed to occur only when the boundary layer on one or both airfoil surface(s) remained laminar to the trailing edge. This noise mechanism was also shown to cause a strong broadband hump in the noise spectrum of a full-scale tail rotor; the broadband nature of the noise in this case was shown to be associated with the variation of blade relative velocity, and hence tone frequency, with radius. These results were published in the open literature as reference 19.

Since this study, vortex shedding noise has been the subject of a number of model rotor, propeller and airfoil studies. In virtually all full-scale applications, however, this noise mechanism does not exist since both suction and pressure surface boundary layers are turbulent at the blade trailing edge. From a practical standpoint, therefore, discrete frequency vortex shedding noise is an unimportant mechanism. If it exists, it can be readily eliminated by tripping the boundary layer as was shown in the initial investigation of this mechanism (reference 19). The phenomenon is common, however, in model testing where the typically low Reynolds numbers favor the persistance of a laminar boundary layer to the blade trailing edge of the pressure surface.

As shown in figure 2, this extraneous noise occurred during initial test work in the present study. The solid line shows a spectrum obtained with a clean airfoil in which vortex shedding noise occurred. The dashed line shows the result of tripping the blade boundary layer(s).

Prediction of the frequency range of this vortex shedding noise is possible. If f_s is the tone frequency generated by a radial segment of the blade, the Doppler shifted frequency range detected by a fixed observer at directivity angle, θ, relative to the rotor axis is:

$$f_o = \frac{f_s}{1 \mp M_{tip} \sin\theta} \tag{5}$$

Using the tone frequency prediction reported in reference 19,

$$f_s = \frac{KV^{3/2}}{(c\nu)^{1/2}} \tag{6}$$

where V is the local velocity, c is chord, ν is kinematic viscosity and K is a constant with an empirically derived value of 0.011. Based on this, the tone frequency, f_s, would be expected to vary from a minimum of 2900 Hz at the root cutout to 25,700 at the tip. From equation (5), this would result in a vortex shedding noise frequency range from 2500 to 36,000 Hz.

Since the original empirical correlation described above, Fink (reference 20) has shown this phenonenon to be caused by the interaction of Tollmein-Schlichting waves with the blade trailing edge and has developed a first-principles theory for predicting tone frequencies. When this theory was applied, the predicted tone frequency range was 2800 to 41,500 Hz. This predicted range is shown in figure 2 to be in reasonable agreement with data.

In the present study it was desired to trip the boundary layer with the minimum size surface protrusion so as to avoid an unnaturally large or distorted trailing edge turbulent boundary layer. The reason for this was that data acquired in the present study under clean inflow conditions (no grid installed in the tunnel inlet) were intended to be used for two purposes. First, clean inflow results would provide a reference case to which turbulent inflow results could be compared. While the manner of eliminating vortex shedding noise would not be important for this purpose, the second purpose would be to provide clean inflow rotor broadband noise data. Data of this nature, acquired under very low inflow turbulence inflow conditions, are not readily available in the open literature and are needed to test various trailing edge noise theories currently under development.

To cause transition with minimum boundary layer distortion, a variant of the triangular configuration tripping device reported in reference 21 was employed. The leading edge of a strip of aluminum tape (width of 0.8 cm and thickness of 0.15 mm) was cut with pinking shears and installed on the pressure surface of the blades with the leading edge of the tape at 25 percent chord. This installation, shown in figure 2, part (b), reduced rotor broadband noise from the solid line of part (a) to the dashed line. Installation of a second pressure surface trip at 63 percent chord and a suction surface trip at 38 percent chord caused no further noise reduction. Based on these results, a single pressure surface trip at 25 percent chord was employed in all program testing.

ISOTROPIC TURBULENCE INGESTION

Objective

The objective of this phase of the study was to assess the accuracy of the isotropic inflow turbulence noise prediction method described in this report over a range of rotor operating and turbulence inflow conditions.

Since a turbulence field that is precisely homogeneous and isotropic may rarely exist in practical applications, it is reasonable to question the relevance of experimentation with such turbulence. Both theoretical and practical reasons, however, support this approach. From a theoretical standpoint, isotropic turbulence is the simplest and best understood free turbulence field. For example, established expressions exist for the turbulence spectrum. In addition, measurement of only one length scale and turbulence intensity is required to define the wavenumber spectrum of the turbulence needed for noise prediction. Fundamental shortcomings of a noise prediction method will be more evident in isotropic, homogeneous turbulence than in a more complex turbulent field where more parameters are required to describe the field and the turbulence spectrum model is less certain.

From a practical standpoint, an isotropic turbulence assumption (or simple anisotropic variant of this assumption) may have to be invoked in many model and full-scale rotor tests due to the difficulty of obtaining detailed inflow turbulence statistical information. While several single-wire hot-wire probes can be used conveniently in such testing, provision for traversing a number of multi-wire probes may not be feasible. Complicated arrangements of this nature would be required to define, rigorously, turbulence length scales and intensities in more general inflow turbulence fields.

Approach

To provide a nominally isotropic and homogeneous inflow turbulence field, tests were conducted in an anechoic wind tunnel with turbulence generating grids located upstream of the model rotor. Hot-wire anemometry was employed to document inflow turbulence statistics. To provide a comprehensive assessment of theory, tests were conducted in both simulated forward flight and vertical ascent at a number of tunnel speeds and rotor tip Mach numbers. Both pitch and number of blades were varied.

Vertical ascent conditions were included in the test plan since this rotor configuration results in the simplest turbulence interaction process. It therefore represents an important test case by which to identify any shortcomings in the theoretical formulation. In vertical ascent, turbulence

is convected primarily in the axial direction and a single eddy convection velocity can be measured for input to theory. The trajectory of a turbulent eddy through the rotor can be assumed to be perpendicular to the disk.

In simulated forward flight the interaction is more complicated with the convection velocity skewed relative to the disk. This results in a variation in the radial and azimuthal position of the intersection of a particular eddy with successive blades.

Two additional noise measurements were required to permit separating turbulence ingestion noise from other sources. Noise data acquired with a turbulence grid installed and the rig operating, but with the blades removed from the rig, provided a measurement of background noise. A second set of noise data, acquired with the blades installed, rig operating and grid removed from the inlet, provided a measurement of clean inflow rotor noise. By comparing turbulence ingestion noise data to these two cases, turbulence ingestion noise could be separated from tunnel background noise and other rotor noise that existed in the absence of inflow turbulence.

Inflow Measurements

Hot wire anemometry was employed to define the rotor inflow velocity field. For simulated forward flight test conditions, a crossed-film probe was used to define the mean velocity components parallel and perpendicular to the plane of the rotor that were required in the noise prediction method. These measurements were acquired with the rotor operating. Turbulence inflow statistics, however, were obtained with the rotor rig removed from the tunnel since the particle velocity of the rotor acoustic field contaminated the hot-film signal. Blade passage frequency noise caused not only errors in rms turbulence intensities but introduced a periodic component in the autocorrelation function. Presence of such a component prevents measurement of the Eulerian time scale required to calculate turbulence integral length scale.

For vertical ascent test conditions, a single hot-film probe was used to define the axial mean velocity with the rotor operating. Turbulence measurements, as in the case of simulated flight, were acquired with the rotor rig removed from the tunnel. These measurements were obtained in a plane perpendicular to the tunnel airstream at an axial location that corresponded to the rotor plane of rotation.

Appendix C contains typical correlation and spectral data which showed good agreement with the von Karman isotropic turbulence model.

Simulated Forward Flight Noise Results

High Turbulence Level - Figure 3 compares measured and predicted noise spectra at nine directivity angles for a grid configuration designed to produce a high inflow turbulence level (designated Grid L). The simulated flight speed was 22.9 m/sec., rotor tip Mach number was 0.47, shaft angle was -2.8 deg and the turbulence intensity was 18.5 percent. Other operating and turbulence inflow conditions are defined in Table I under Test Condition FF-L-1.

Considering first the measured spectra, the general character is broadband in nature with several discernable tones and narrowband random peaks at low frequency. Spectra obtained under clean inflow conditions (no grid) are shown on several plots for reference purposes. This clean inflow noise is generally below the turbulence interaction noise except at blade passage frequency (BPF) and twice BPF where it sets the tone level. This clean inflow tone noise is due to blade loading and as would be expected, decays rapidly with harmonic number into a broadband spectrum.

Theoretically predicted spectra calculated from measured mean inflow velocity components, turbulence intensity and length scale and an isotropic inflow assumption are shown as open circles in figure 3. Except for the last spectrum shown in the figure (corresponding to a measurement in the plane of rotation) where the prediction is some 20 dB low, predicted levels tend to bracket measured spectra. Although theory significantly underpredicts noise levels in this plane, both theory and experiment show this to be the directivity position with least noise.

Figure 3 shows a consistent trend to overpredict low frequency noise and more accurately predict high frequency noise. The general trend of a change from narrowband random tones to broadband noise in the frequency range from 1000 to 2000 Hz is observed in both measured and predicted spectra. Theory, however, tends to overpredict the tone peak-to-trough height in this instance.

Although difficult to ascertain from figure 3 due to the scale, a general feature of both data and theory is that turbulence-induced narrowband random peaks are not centered precisely on multiples of blade passage frequency. This will be discussed in more detail subsequently.

Moderate Turbulence Level - Figure 4 compares measured and predicted noise spectra at three directivity angles for a grid configuration designed to produce a moderate inflow turbulence level (designated Grid M). The simulated flight speed was 22.9 m/sec., rotor tip Mach number was 0.52, shaft angle was -2.8 deg and the turbulence intensity was 6.9 percent. Other operating and turbulence inflow conditions are defined in Table I under Test Condition FF-M-1.

The results were generally similar to those of figure 3 obtained at a higher inflow turbulence level and lower tip speed. Theory tends to overpredict low frequency noise and underpredict noise at high frequency.

Effect of Tip Mach Number - The effect of a change in rotor tip Mach number for a fixed inflow turbulence condition is shown in figure 5. In part (a) of the figure, the dashed curve corresponds to a tip Mach number of 0.37 whereas the solid curve shows the spectrum obtained at the same directivity angle for a higher tip Mach number of 0.47.

The higher rotor tip Mach number results in higher noise levels as would be anticipated. Reference 15 contains a detailed discussion of the dependence of turbulence ingestion noise level on rotor tip Mach number. The ultimate cause is the unsteady lift force which is directly proportional to the relative velocity between the blade and the turbulence field at low frequency and the square root of this velocity at high frequency. For comparisons carried out at equal harmonic number, low frequency noise spectrum level is predicted to increase with relative velocity to the third or fourth power depending on whether the noise in tonal or broadband. At high frequency, broadband noise spectrum level is predicted to vary as relative velocity squared.

Part (b) of figure 5 compares measurement and prediction for the 0.37 tip Mach number case. Figure 3, discussed previously showed a comparison at the same directivity angle for the 0.47 Mach number case. In both instances, low frequency noise was overpredicted while agreement between theory and experiment at mid-to-high frequency was good. In this region of good agreement, the present theory appears to predict, reasonably well, the dependence of noise level on tip Mach number.

Effect of Blade Number - Figure 6 shows the effect of blade number on turbulence ingestion noise at two directivity angles. The dashed curves correspond to the four-bladed test condition of figure 4 (Test Condition FF-L-1) while the solid lines are measured spectra for a two-bladed rotor configuration (Test Condition FF-L-3). All other parameters were identical for the two test conditions.

The major effect observed in this comparison is a general decrease in noise on the order of 3 to 4 dB at frequencies above 1500 Hz. From simple arguments, a decrease of 3 dB would be predicted. That is, at high frequency, turbulence ingestion noise is due to the interaction of small turbulent eddies with individual blades. The small eddies convect through the disk in a time short compared to blade passage period and are not cut by more than one blade. The resultant noise is broadband as in the case of the interaction of turbulence with an isolated airfoil. The blades act as independent noise sources and the resultant noise is directly proportional to the number of blades.

At low frequency, where eddy transit time is comparable to or larger than blade passage period, the situation is more complicated. In general, however, noise at a fixed frequency should be lower for the two bladed case since fewer multiple choppings of an eddy will occur.

Theory predictions for the four-bladed case were shown in figure 3. Predictions for the two-bladed case are shown in figure 6. In agreement with the above arguments, the theoretical method predicts a decrease of 3 dB at high frequency. The observed 3 to 4 dB decrease is considered verification of this prediction considering noise measurement accuracies. A more detailed examination of blade number effects is given subsequently where a vertical ascent configuration provided more pronounced low frequency tone noise. In that case it will be shown that theory predicted a larger change in low frequency tone noise than was observed.

Effect of Non-Axial Inflow - In hover and vertical ascent, the inflow velocity at the rotor disk is predominantly axial. In this case, the large turbulent eddies responsible for quasi-tonal noise production convect through the disk axially. From a frozen-flow viewpoint, multiple choppings of a single eddy by successive blades occur at the same radial and azimuthal position of the disk. The time scale for the choppings is blade passage period and the predicted result is narrowband random noise centered on harmonics of blade passage frequency.

It is useful to consider the consequences of a non-frozen-flow situation; that is, if there were a random wandering of the radial position of the eddy with time as it passed through the disk, choppings would still occur on this time scale. Noise at BPF multiples would result although the amplitude of the resultant tone noise would wander since the relative velocity between the blade and the eddy varied with radial position.

If, however, there were a random wandering of the azimuthal position of the eddy with time as it passed through the disk, choppings would occur at random time periods although the most probable time period would remain blade passage period. This would result in a narrowband random peak of lower amplitude scattered over a wider frequency band. Wandering of an eddy in the azimuthal direction, therefore, provides a mechanism for shifting noise away from BPF multiples; as discussed subsequently relative to outdoor hover results, this mechanism is believed to account for the relatively high measured levels of noise at half harmonics of BPF as compared to the lower predictions of theory.

In forward flight, an additional means to shift the frequency of turbulence ingestion noise away from BPF multiples exists. In this case the inflow velocity vector is skewed relative to the rotor axis. The velocity component parallel to the disk causes an eddy to convect through a series

of different azimuthal positions during its residence time in the disk. In simple terms, the front of an eddy may be chopped at one azimuthal position whereas the back of the eddy will be chopped further downstream at a different azimuthal position.

As in the case of the azimuthal wandering mechanism discussed above, chops of a single eddy by successive blades occur at different time intervals. This is a stronger mechanism for frequency shifting than random wandering since there is no obvious most probable chop period. Consequently, turbulence ingestion noise can peak at frequencies other than BPF multiples. Such noise would also be expected to be far less coherent than that obtained in the axial inflow case. Low frequency noise would be expected to be far more broadband in nature and narrowband random peaks would not be expected to persist to the high frequencies where tonal noise was observed in the axial inflow situation.

Figure 7 confirms this physical reasoning. The spectrum at the top of the figure was obtained in a vertical ascent configuration. Narrowband random noise peaks were centered on BPF multiples. The spectrum in the middle of the figure was obtained with the same grid at the same rotor tip Mach number and tunnel speed but in a forward flight configuration. A shifting of tone peaks away from BPF multiples was apparent.

The spectrum at the bottom of the figure was obtained with the same grid and rotor tip Mach number but at a higher simulated flight speed. Increased frequency shifting was observed as well as a further reduction in tonal behavior. Above 2000 Hz, the noise was principally broadband in nature while this did not occur in the vertical ascent case until a frequency of about 5000 Hz was reached.

A conclusion resulting from these physical arguments and experimental results is that the degree of tone-like behavior will decrease as the ratio of the inflow velocity component in the plane of the rotor to that perpendicular to the plane, increases. In flight, therefore, high thrust and low forward speed favor the occurance of turbulence ingestion tones.

The effect reported here may account for some of the tones observed in the main rotor-tail rotor interaction noise spectra reported by Pegg and Shidler in reference 23. Although tones were observed at various combinations of main and tail rotor blade passage frequencies, tones at other frequencies appear to have been present.

Vertical Ascent (Climb) Noise Results

High Turbulence Level - Figure 8 compares measured and predicted noise spectra at four directivity angles for a grid configuration designed to

produce a high inflow turbulence level (designated Grid L). The tunnel speed was 9.1 m/sec., rotor tip Mach number was 0.47 and the turbulence intensity was 14 percent. Other conditions are defined in Table I under Test Condition VA-L-3.

The solid line shows spectra obtained with the grid installed whereas the dashed line shows spectra obtained under clean inflow conditions (no grid). The clean inflow spectra are characterized by pure tones at BPF and one or two higher harmonics which rapidly decay with increasing harmonic number. This tone noise is believed due to steady blade loading. The rapid harmonic decay is in agreement with theories for such noise.

At frequencies above this harmonic noise, the clean inflow spectra are generally broadband in nature showing little decay with increasing frequency. The cause of such broadband noise has not been definitively established in propeller and rotor noise research conducted to date. Since the blade boundary layers were tripped to turbulent in the present study, the laminar boundary layer mechanism identified by Paterson et al. (reference 19) is not responsible. It is believed that the operative noise mechanism, in this case, is the interaction of the blade turbulent boundary layer with the trailing edge (trailing edge noise).

Noise spectra obtained with the grid installed are significantly different, displaying a persistence of tones to about the 20th harmonic of BPF. Although centered on harmonics of BPF, the width of the tones indicates that these are not due to a precisely periodic phenomenon. The width increases with frequency and the peak-to-trough height decreases, eventually resulting in a broadband noise spectrum at moderate to high frequency.

At high frequency, the turbulent inflow noise levels are not always 10 dB or more above the clean inflow levels. In such circumstances, a problem in interpretation occurs. If it is assumed that the clean inflow noise is caused by a trailing edge noise mechanism which is unaltered when a turbulent inflow is imposed, the two mechanisms can be considered independent. In this case, the clean inflow results represent an effective background noise for the turbulent inflow measurement. The turbulent inflow spectra could then be adjusted downward to account for contributions from the second noise source resulting in a spectrum associated only with turbulence ingestion. Conversely, the high incident turbulence could modify boundary layer development and hence alter trailing edge noise. Due to the above considerations, spectra have not been adjusted in this report. The result is that in certain cases, some uncertainty exists in comparing theory to experiment at high frequency.

To provide turbulence information for input to the noise prediction method, root-mean-square turbulence intensity was measured and an auto-correlation analysis performed. These measurements provided the intensity and turbulence length scale required for noise prediction.

Theoretically predicted spectra are shown as open circles in Figure 8. At low frequency, where narrowband random tones exist, levels have been calculated for the spectrum peaks which occur at multiples of BPF as well as for the troughs (which occur at half harmonics). There is a consistent trend to overpredict low frequency tone levels. The merger of tones into broadband noise in the frequency range from 3500 to 4500 Hz is observed in both measured and predicted spectra. At mid-to-high frequencies, the agreement between theory and experiment is considered good. In this range, the maximum deviation of theory from measurement shown in figure 8 was 3 dB.

Moderate Turbulence Level - Figure 9 compares measured and predicted far-field noise spectra at four directivity angles for a grid configuration designed to produce a moderate inflow turbulence level (designated Grid M). The turbulence intensity was 8.8 percent, the tunnel speed was 9.1 m/sec. and the rotor tip Mach number was 0.52. This was the highest tip Mach number employed in the present study. Other conditions are defined in Table I under test condition VA-M-1.

Spectra measured with and without the grid installed are shown as solid and dashed lines, respectively. The agreement between predicted noise spectra (circles) and measured turbulent inflow spectra is similar to that discussed in the previous section relative to figure 8; that is, low frequency tone levels are overpredicted, trough levels at half-harmonics of BPF are better predicted and mid-to-high frequency broadband noise is well predicted.

The test conditions for figures 8 and 9 were identical (including turbulence length scale) with the two exceptions that the tip speed was a factor of 1.1 higher and the inflow turbulence level a factor of 1.6 lower for the test condition of figure 9. In the mid-to-high frequency region where agreement between theory and experiment was good in both cases, the theory appears to account for these changes in tip speed and turbulence level.

Effect of Blade Number - Figure 10, parts (a) and (c) compare predicted and measured noise spectra at two directivity angles for a two-bladed rotor in a vertical ascent configuration. The effect of blade number on turbulence ingestion noise was previously shown in figure 6 for a forward flight configuration, lower tip speed and higher inflow turbulence level.

As in other vertical ascent comparisons, tone noise at low frequency is overpredicted. The maximum error is 8 dB. Levels at half-harmonics are

predicted more accurately while broadband noise levels at frequencies above 2500 Hz are predicted within 2 1/2 dB.

Parts (b) and (d) of figure 10 show the effect of blade number directly. The solid line shows the predicted difference between 4 and 2 bladed configurations at frequencies corresponding to BPF and higher harmonics. The measured difference between 4 bladed spectra (Test Condition VA-M-1) and two bladed spectra (Test Condition VA-M-4) are shown as open circles. These two test conditions were identical except for the difference in number of blades.

As found in the previous forward flight comparison (figure 6), predicted and measured results both show a 3 dB decrease in noise at high frequency due to halving the number of blades. At low frequency, theory predicts a 6 dB decrease at a given frequency. The measured decrease is observed to be significantly less. Two and four bladed comparisons performed at a lower tip Mach number of 0.41 showed results similar to the above.

Based on these results it is concluded that the theory does not accurately predict the effect of blade number at low frequency where eddy chopping results in primarily tonal noise. This failure may be related to the general disagreement observed between theory and experiment at low frequency.

Effect of Pitch - A fundamental assumption of the theory considered in this report is that local section angle of attack has no effect on the generation of noise due to interaction with turbulence. This is because the airfoil unsteady response functions employed in the theory assume linearized flow. This is believed to be a good assumption below stall. At present there is no available theory which adequately accounts for the effects of finite angle of attack on the unsteady response of an airfoil in compressible flow.

A discussion of the effect of finite angle of attack on the noise of an isolated airfoil interacting with isotropic turbulence was given by Paterson and Amiet in reference 2. Based on an incompressible flow theory of Horlock (reference 22), it was shown in reference 2 that the additional gust contribution due to a change in angle of attack from zero to ten degrees would cause only a 1 dB increase in far-field noise. Noise measurements at a number of velocities and directivity angles, reported in reference 2, confirmed that the effect was on this order.

Assuming that a change in rotor pitch would not alter the properties of the turbulence field interacting with the rotor, the theory considered here would predict no effect of a pitch change on rotor turbulence ingestion noise. To attempt to assess the validity of this result, data were acquired for two different inflow turbulence conditions and several pitch settings. Figure 11 summarizes the most important results of the investigation. For

a high inflow turbulence level of 14 percent and rotor tip Mach number of 0.47, figure 11, part (a) shows that an increase in pitch from 3 to 9 deg had only a small effect on the noise spectrum. There was an increase of several dB at low frequency and no change at high frequency. Similar small effects were obtained at the other six directivity positions for which spectra are not shown.

For a lower inflow turbulence level of 8.8 percent and tip Mach number of 0.37, figure 11, parts (b) and (c) show that an increase in pitch from 3.7 to 15.7 deg also produced but a small change in spectrum level at directivity angles of 60 and 120 deg. In addition to the two directivity angles shown in this figure, spectrum comparisons made at intermediate directivity angles of 80 and 100 deg also showed a negligibly small effect of a change in pitch.

There are two factors that complicate comparisons such as this, where an attempt is made to hold all conditions nominally constant and alter only one variable (pitch) to isolate its influence. The first is that a change in pitch alters the noise directivity pattern of each blade segment by the amount of the pitch change. The integrated effect of these changes in blade segment directivity patterns is to alter the far-field directivity pattern to some degree. Since microphone positions were held fixed when pitch was changed, an observed change in level could be related to a directivity pattern shift rather than a change in turbulence ingestion noise source strength.

Since the pitch changes were relatively small and the far-field directivity pattern was observed to vary slowly with angle at positions other than near 90 deg, this possible directivity pattern shift is not considered to be of major importance. It may account for some of the changes observed.

A second complicating factor is that the isotropic, homogeneous wind tunnel turbulence field can be distorted by the presence of the operating rotor. While azimuthal symmetry is preserved, there is a contraction of the capture streamlines. This can alter the incident turbulence field and also cause a radial variation in the convection velocity of turbulent eddies through the disk. The distortion is proportional to thrust; hence a pitch change at fixed rotor tip Mach number can result in a change in the turbulence field seen by the rotor and the resultant noise. This is believed to account for increases on the order of 5 dB which were observed when the pitch was increased to 15 deg from the values of 3 and 9 deg shown in figure 11, part (a). An increase of 4 dB was also noted for the lower turbulence inflow condition of figure 11 when the pitch change shown in parts (b) and (c) was conducted at a higher thrust condition (tip Mach number of 0.47).

Conflicting data regarding pitch effects therefore exist. At the lower thrust conditions where the uniform, homogeneous, isotropic field of the wind tunnel would be expected to be less affected by the rotor, the effect of pitch on measured noise was observed to be small. Based on this and the isolated airfoil research results of reference 2, it is likely that the theory assumption that local section angle of attack does not significantly affect turbulence induced noise generation, is correct. A complete mapping of the mean and turbulent inflow field with the rotor operating would be required to determine whether changes in inflow conditions with pitch account for the discrepancies noted here.

Noise Directivity - Figure 12 compares measured and predicted directivity patterns of turbulence ingestion noise at six frequencies between 5 and 35 times BPF. Triangular symbols, which show measured turbulence ingestion noise levels, are plotted at angles that have been corrected for the small effect of wind tunnel shear layer refraction.

Measurements were restricted to a range of approximately 60 to 130 deg due to wind tunnel constraints. The solid line shows predicted levels for all angles. Also shown in figure 12 as square symbols are clean inflow noise levels (no grid installed) at a directivity angle of 91 deg.

While measurements show a pronounced decrease in noise near the plane of rotation (90 deg), theory predicts a sharper decrease at this angle in the form of a cusp. At other angles, agreement between theory and experiment is considered good, the only exception being low frequency (5xBPF) where discrepancies have previously been noted.

The theoretical prediction of a sharp decrease near the plane of rotation arises from modeling the unsteady pressure jump across the rotor blade by dipoles oriented perpendicular to the chord. This is considered to be an accurate representation of the noise generation process. The reason for the disagreement between theory and experiment near the plane of rotation is uncertain although two causes can be postulated.

The first possible cause is the new "unsteady thickness noise" mechanism proposed by Hawkings (reference 10) in 1978. This mechanism is predicted to cause in-plane rotor noise due to an interaction between blade thickness and turbulence. It is an analogue of the more conventional thickness noise associated with tip speed and results in an in-plane quadrupole field. This tonal and broadband noise mechanism has only been advanced as a possibly significant noise source. Detailed comparisons of theory predictions to inflow turbulence data such as reported here will be required to assess its importance.

Another source of in-plane noise, not included in the present theory, is blade trailing edge noise. Clean inflow noise levels shown in figure 12 as square symbols are believed caused by this mechanism. These levels are lower than measured turbulent inflow noise levels at 90 deg but higher, in some cases, then predicted turbulence ingestion noise levels. This mechanism would contribute to noise levels measured during turbulence ingestion tests and may account for the lack of a cusp in the directivity pattern at 90 deg. While square symbols show noise levels obtained under clean inflow conditions (no grid), higher levels of trailing edge noise may result when tests are conducted with turbulent inflow conditions.

In summary, possible reasons exist for the disagreement between the present turbulence ingestion noise theory and experiment near the plane of rotation. The most probable cause cannot be identified at this time. Excluding this angle, the present theory tends to predict the measured variations in sound pressure level of five to ten dB that were measured in the directivity range from 60 to 130 deg.

ATMOSPHERIC TURBULENCE INGESTION

Objectives

The overall objective of this phase of the study was to determine the importance of atmospheric turbulence ingestion in the generation of helicopter rotor noise in hover. It was also desired to obtain noise and rotor inflow data in sufficient detail that it could serve as a set of reference data for use in assessing current and future atmospheric turbulence ingestion noise prediction methods. Another objective was to assess, specifically, the accuracy of anisotropic inflow turbulence noise prediction method described in this report.

Establishing the contribution of atmospheric turbulence ingestion to hover noise is important since whirltower and hover noise data have traditionally been used by helicopter noise research specialists (more often than forward flight data) to assess the noise benefits of rotor system design changes. This is a natural result of the high cost of forward flight experimentation.

The potential problem with this approach is that if turbulence ingestion noise dominates whirltower and hover noise spectra but not noise in flight, incorrect conclusions may be drawn regarding the flight noise benefits of proposed design changes. Masking of design change effects by ingestion of atmospheric turbulence during static testing has been a serious turbofan engine fan noise problem (reference 7).

In addition, helicopter noise research specialists have employed outdoor and indoor hover test stands to study rotor noise mechanisms and to develop noise amplitude and frequency scaling laws. Without knowledge of the contribution of turbulence ingestion (whether due to atmospheric turbulence or turbulence contained within hover test chamber circulations), to hover noise, errors in understanding could result. For both the designer and research specialist working in a hover environment, therefore, a means to predict turbulence ingestion noise spectra and directivity is needed.

Approach

To establish the importance of atmospheric turbulence ingestion in the generation of hover noise, both a direct and indirect approach were adopted. The direct approach was to test the model rotor at the same pitch settings and rotor tip speeds in both an outdoor hover environment and in the wind tunnel. For the wind tunnel test, a clean inflow was provided (no grid

installed) and the rotor was operated in a low speed vertical ascent (climb) condition. By comparing noise spectra for these two cases, a direct indication of the contribution of inflow turbulence to noise was obtained.

The indirect approach was to categorize inflow turbulence statistics in outdoor hover by use of hot-film anemometry, input these data to the absolute level noise prediction method employed here and compare measured noise spectra and directivity with predictions of theory. If the agreement between theory and experiment were found to be reasonable (and confidence in the theoretical method existed based on isotropic inflow wind tunnel tests), then it could be concluded that ingested turbulence was the cause of the noise measured in hover.

Experimental Arrangement

General Description - Figure 13 shows both an overall and a close-up view of the outdoor hover test arrangement. The drive rig was mounted on the roof of the Acoustic Research Tunnel anechoic chamber. The corner location was chosen to provide a free-space acoustic environment and also to minimize mean velocity inflow distortion (and consequent spurious tone generation). The rotor axis was two rotor diameters above the roof and the plane of rotation was approximately one-half rotor diameter inboard of the corner. This distance between the roof and rotor would be expected to provide a uniform mean inflow.

A far-field microphone, positioned on a boom at 2.44 m radius (3.2 rotor diameters), was traversed to obtain noise measurements over an arc from on-axis (zero deg) to 130 deg aft. A cup anemometer provided ambient wind speed data. The signal from the anemometer was tape recorded simultaneously with the far-field microphone signal.

Two hot film probes were mounted 11.4 cm in front of the rotor plane to measure mean and turbulent inflow velocities. The upper probe was fixed at 70 percent rotor radius. The lower probe was mounted on a traverse can to permit the probe to be positioned at various distances from the fixed probe. A detailed description of hot film test arrangements and signal processing considerations is given in Appendix D.

Required Measurements - Noise measurements were required in the arc from 60 to 130 deg to permit comparison with clean inflow tunnel noise data. In addition, an on-axis measurement was desirable since steady blade loading noise is predicted to be zero at this position. Furthermore, this is a common measurement location in rotor testing and a convenient location, free of Doppler shift effects, for comparisons between theory and experiment.

Measurement of ambient wind speed was required to limit data acquisition to quiescent periods. This constraint was imposed for two reasons: First, wind gusts can blow tip vortices and rotor wakes into the disk causing significant increases in harmonic noise. When this occurred it was easily perceptible to observers on the ground. Moreover, cross-wind velocities can both skew the inflow velocity vector and cause it to be time varying. This would alter two-point turbulent velocity correlations used to determine transverse length scale as well as autocorrelations. In the present study, axial length scale was calculated from an autocorrelation function by invoking Taylor's frozen-flow hypothesis (reference 16). This hypothesis is invalid if the mean flow is either unsteady or skewed.

Documentation of rotor inflow turbulence statistics was required to provide data for input to the noise prediction method. Since an anisotropic field was anticipated, measurement of the intensities of at least two turbulence components and determination of both an axial and traverse turbulence length scale were needed.

Outdoor Hover Turbulence Measurements

Hot film probes mounted forward of the rotor disk measured both the inflow turbulence field and the particle velocity in the sound wave generated by the rotor. Appendix D contains a description of the filtering techniques applied to eliminate this problem. In addition, the appendix discusses the extremely low frequency nature of the ingested atmospheric turbulence field and the special D.C. coupling and high-pass filtering techniques used to extract turbulence functions.

In addition to the above complications, rotor inflow turbulence statistics were found to be non-stationary. Non-stationarity is interpreted here as a measurable change in one or more time averaged turbulence functions (rms intensity, spectrum or autocorrelation) in a time interval on the order of that required to complete one test run (several minutes) or compute an autocorrelation or spectrum with a real-time analyzer (less than one minute).

This property of atmospheric turbulence ingestion produces significant complications in test work since test conditions are not reproducible. Measurements made in sequence cannot rigorously be assigned to one test condition. It was therefore necessary to tape record inflow turbulence statistics and far-field noise simultaneously. This simultaneous measurement permitted the time-averaged noise spectrum to be computed for the same time interval as that used in the computation of time-averaged inflow turbulence functions. With this approach, however, it had to be demonstrated that wakes from hot film probes in the rotor inflow field did not alter the rotor noise spectrum.

This was demonstrated to be the case by comparing noise measurements with and without probes installed.

All of the outdoor hover noise and turbulent inflow data presented in this report, except as noted otherwise, were acquired during a single, low-wind, one-hour test period. Noise measurements were tape recorded sequentially at nine microphone angles for one rotor tip Mach number and then a second. At each microphone position, the fixed and moveable hot-film probe signals were recorded simultaneously. For each tape record at a different microphone position, a different separation distance of the moveable and fixed probes was used. This generated data required for turbulence transverse length scale determination.

Figure 14, part (a) shows typical inflow turbulence spectra. These results are significantly different from isotropic turbulence spectra which display a slope of zero at low frequency and a negative slope of 5/3 at high frequency.

Figure 14, part (b) shows the variation of cross-correlation coefficient between the axial velocities measured by the two hot film probes as a function of transverse probe separation distance for the two test tip Mach numbers. The point at which the functions decayed to 1/e of the zero separation distance value was taken as a measure of the transverse length scale of the turbulence, Λ_g. These cross-correlation measurements, by necessity, had to be taken sequentially and there was no assurance that inflow statistics were effectively similar for measurements at different probe separations due to the non-stationary nature of the inflow field. This may account for the considerable scatter in data at separation distances greater than 3 cm. Based on figure 14, a transverse length scale of 3.6 cm was assumed to apply to all test runs conducted during the hour test period. This length scale represented the least reliably measured quantity used in the present prediction method since it was based on cross-correlation measurements distributed over the one hour test period.

In contrast, inflow turbulence axial length scale was computed for each test run (i.e., microphone position) based on the same portion of the tape record used to simultaneously record far-field noise. The time delay corresponding to the 1/e point of the autocorrelation function was used to define the Eulerian time scale. By invoking Taylor's frozen flow hypothesis, this time scale and the mean velocity measured by the fixed probe allowed determination of the axial length scale. Typical autocorrelation functions are shown in Appendix D. This appendix also discusses the signal processing techniques that were employed.

Table II summarizes the inflow properties measured for all fifteen hover test conditions during the one-hour test period. Inflow turbulence levels were reasonably constant, varying only from 2 percent to 3 percent during this period. Table II shows, however, that the axial turbulence length scale varied by a factor of 3.5. This occurred even though the table shows that measured average and maximum wind speeds were low and the rotor inflow mean velocity was reasonably constant. Table II provides a clear indication of the magnitude of the non-stationary nature of the atmospheric inflow turbulence field alluded to above.

Anisotrophy - Of particular importance in Table II is the calculated ratio of axial to transverse length scale, Λ_f/Λ_g. Values range from 18 to 59. Since this ratio is two for isotropic turbulence, it is clear that the rotor inflow in this experiment was highly anisotropic.

Crossed-film probe measurements acquired during a different test period showed the axial length scale of the transverse turbulent velocity component to be large (within ten percent of the axial scale of the axial component). The ratio of the rms turbulence level of the transverse component to the axial component was approximately 1.2 for a rotor tip Mach number of 0.41 and 1.1 for the lower test tip Mach number of 0.37. This does not represent a strong deviation from the isotropic case where these components are equal.

From a comparison of transverse and axial turbulence intensities, therefore, the turbulence field appeared to be relatively isotropic. Transverse and axial velocity component length scales in the flow (axial) direction, however, were found to be an order of magnitude larger than the transverse scale of the axial component. The flow field was therefore strongly anisotropic with the large structure characterized by eddies of elongated axial extent.

These results are in general agreement with the original atmospheric ingestion duct measurements of Hanson (reference 5). He found a similar intensity level for the transverse component (2.5 percent) and a large ratio of axial to transverse length scale. In Hanson's experiment, however, the length scale ratio was an order of magnitude greater than that found here and the axial component intensity was about three times smaller than that for the transverse component.

Invoking Kelvin's theorem on the constancy of circulation in a circuit moving with the fluid, Prandtl (reference 24) showed that the effect of streamline contraction on turbulence is to stretch eddies in the streamwise direction, contract them in the transverse direction and attenuate the axial turbulence intensity relative to the transverse intensity. The degree of stretching and attenuation were predicted to increase with increased streamline contraction.

Since the rotor in the present case or the duct inlet (in Hanson's case) appears to the surrounding atmosphere as a sink, the resultant inflow experiences a nominally infinite contraction ratio. While quantitative prediction of the turbulence properties at the rotor or duct inlet from a statistical description of the atmospheric turbulence is difficult, the degree of axial stretching would be expected to depend on the diameter of the rotor (or duct inlet) and the mass flowrate. A higher effective contraction would occur for a small rotor with a high inflow mass flowrate (high thrust).

In Hanson's experiment, the duct inlet diameter was comparable to the rotor diameter employed here but the mass flowrate was a factor of approximately eight larger. More pronounced eddy stretching and attenuation of the transverse turbulence component would therefore be expected, in Hanson's experiment, as was observed.

Outdoor Hover Noise Results

Typical Results - Figure 15 shows typical spectra at two directivity angles obtained in simulated hover on the outdoor test stand shown in figure 13. Both the on-axis spectrum and the spectrum obtained at 60 deg from the rotor axis display the same general characteristics; that is, a persistence of narrowband random noise peaks to approximately the twenty-fifth harmonic of BPF and a broadband spectrum at higher frequency. Measured ambient background noise, shown by dashed lines in figure 15, influenced measured rotor noise levels for only low frequencies below blade passage frequency.

The on-axis spectrum is of particular interest since tone noise due to steady loading is predicted to be zero for this location. At other directivity angles, such as the 60 deg position shown here, clean inflow data acquired in the tunnel at the same rotor operating condition but with a small vertical ascent velocity of 9.1 m/sec, showed negligible tone noise at frequencies above two or three times BPF (as would be predicted by steady loading theory). These spectra are shown in Appendix E. The conclusion drawn, therefore, is that steady loading cannot account for the quasi-tonal noise observed in hover in the present experiment.

A school of thought exists in the helicopter noise research community that the origin of the quasi-tonal noise shown in figure 15 is blade interaction with the tip vortex field of the rotor. Conversely, propeller, fan and compressor research, discussed in Appendix A, indicates that ingestion of atmospheric turbulence is responsible for tonal noise observed during static operation. Such operation resembles a hovering rotor in that both involve sink-type atmospheric flows and Prandtl's eddy stretching mechanism is operative in both cases. In summary, the source of the noise is clearly

not steady loading but disagreement exists regarding the relative importance of turbulence ingestion and vortex interaction.

Comparison of Theory with Experiment - Figure 16 shows a measured outdoor background noise spectrum as well as hover noise spectra for rotor tip Mach numbers of 0.41 and 0.37 at a number of directivity angles ranging from on-axis to forty degrees aft of the plane of rotation. As discussed previously, inflow turbulence statistics were non-stationary over the one-hour time period required to acquire these data. With each spectrum, therefore, is a listing of the turbulence level and axial length scale measured during the same time interval used to compute the time-averaged noise spectrum at each directivity angle. A list of relevant variables for the fifteen hover cases of figure 16 is given in Table II.

The general character of all spectra shown in figure 16 is similar to the typical results discussed above. Quasi-tonal noise is observed to extend to high frequency. Since inflow turbulence statistics varied over the test period, determination of the noise directivity pattern for a fixed set of inflow conditions was not possible. Noise levels at, and near, the plane of rotation, however, are observed to be lower than at other angles as was the case with wind tunnel turbulence ingestion noise data discussed previously.

Predictions of theory at BPF harmonics are shown as open circles in figure 16. These predictions were based on the anisotropic flow model discussed in the section entitled "Theoretical Formulation" and used measured axial component turbulence intensity, axial length scale, transverse length scale and mean velocity as input.

Theory is generally observed to overpredict low frequency tone levels except, in some circumstances, blade passage frequency level. In these cases, steady loading noise set this level. The steady loading noise mechanism was not included in the present prediction method.

While low frequency tone levels are overpredicted, at high frequency there is a tendency to underpredict levels; this is most evident near the plane of rotation where turbulence ingestion noise reaches a minimum.

In the plane of rotation, the predictions of theory are off-scale. As previously discussed relative to wind tunnel data, theory predicts a sharp drop in levels near the plane of rotation which appears as a cusp in the directivity pattern. A detailed microphone traverse was not conducted in small increments between 80 and 100 degrees to establish whether such a cusp occurred in the present study. Since the rotor pitch was non-zero in the experiment, the dipole radiation pattern of blade segments would not result in a cusp at precisely 90 deg, if one did occur.

Resolution of this plane of rotation discrepancy, which arose in both wind tunnel and outdoor hover testing, would require both additional experimentation and improvement of the blade segment orientation assumption implicit in the theory.

Although failure to predict the lower levels measured in the plane of rotation may not be particularly important from a practical standpoint, a single instance of a general breakdown of agreement between theory and experiment can cast doubt on the validity of the assumed noise mechanism. For reasons discussed above and the possible role of Hawkings (reference 10) recently proposed turbulence mechanism (which would be additive to that addressed in the present theory) lack of agreement reported here is considered a problem area requiring additional investigation rather than proof that another mechanism is responsible for the observed results.

In addition to plane of rotation results, an additional major discrepancy between theory and experiment occurred in comparing levels at half-harmonics of blade passage frequency (BPF). While figure 16 shows predicted levels at BPF and higher harmonics, predicted half-harmonics (or trough levels) were off-scale.

Large peak-to-trough ratios on the order to 40 dB, such as predicted here, are never observed in far-field or blade pressure spectra. Either another noise mechanism fills in the troughs or the phenomenon is not precisely periodic to the degree necessary to result in such peak-to-trough ratios.

A calculation is presented in Appendix F that shows that if 1.3×10^{-2} of the energy contained in a peak, is frequency shifted (scattered) into an adjacent trough having a level 50 dB below the peak, the trough level will rise by 30 dB. This would result in 20 dB peak-to-trough levels such as observed in the present study.

The peak-to-trough ratio predicted by the present theory depends on the streamwise coherence of the turbulence. For the elongated eddies measured in hover, this theory predicts large ratios which are not observed, whereas for isotropic wind tunnel grid turbulence the theory predicts ratios and trough levels reasonably accurately. The reasons for the lack of agreement in hover are believed associated with the "frozen flow" and axial inflow assumptions of theory.

Frozen flow assumes that the turbulent eddy structure does not change in a time period comparable to its convection time through the rotor. Although approximately correct in certain circumstances, such as wind tunnel generated grid turbulence, deviations from frozen flow can shift energy from

BPF multiples into adjacent frequency bands. Wandering in the azimuthal position of a turbulent eddy as it passes through the rotor was previously discussed as a source of frequency shifting. Similarly, a slight non-axial component to the inflow can shift noise away from BPF multiples much as in the case of the simulated flight results presented previously.

Considering the small amount of peak sound energy that can change trough levels by 30 dB and the considerations presented above, the disagreement observed between theoretically predicted and measured trough levels is not considered to invalidate the conclusion that turbulence ingestion is the source of the tonal noise obtained in hover. Neither is the disagreement important from the standpoint of predicting perceived noise.

In summary, the ability to predict trough levels in wind tunnel tests, where conditions were stationary and ambient wind effects were not present, suggests the basic theoretical formulation is correct. Trough levels in outdoor hover appear to be very sensitive to details of the turbulence field which cannot be treated theoretically at the present time.

The next section considers the sensitivity of the present turbulence ingestion noise prediction procedure to variations in the assumed input parameters. This provides a basis for interpreting the degree of agreement between theory and experiment shown in figure 16.

Sensitivity of Noise Prediction to Input Parameters - Given the uncertainties inherent in the measurement of outdoor hover inflow turbulence statistics, it is useful to ascertain the sensitivity of the present noise prediction procedure to variations in assumed input parameters. If the procedure were highly sensitive (say a 10 dB noise level change resulted from a ten percent change in one input parameter), the experimental approach taken here to assess theory would have been invalid. Agreement or lack of agreement would have proved little.

Uncertainty in measured atmospheric turbulence statistics arises in several ways. First, the turbulence inflow field in hover has been shown to be non-stationary. This produces uncertainty in time averaged quantities. As previously discussed, the long test time required to measure transverse length scale could produce significant error in this non-stationary environment. Second, uncertainty is introduced when a hot film at one position in space is used to categorize the entire rotor inflow turbulence field (inhomogeniety considerations). Third, there are the usual hot-film measurement uncertainties associated with probe calibration, temperature changes and calibration drift due to accumulation of foreign particles on the film.

Although difficult to assess, uncertainties in outdoor hover turbulence quantities of 25 percent would not appear unreasonable. Conversely, 100 percent uncertainties appear unlikely. Table III shows the effect of 25 percent uncertainties on predicted noise levels for one hover test case at blade passage frequency (BPF), and two higher BPF multiples. The dependence on turbulence intensity is straightforward; the change in sound pressure level due to a change in rms turbulence velocity from u_1 to u_2 is given by $20 \log_{10} (u_2/u_1)$. Dependence on length scale is more complicated as discussed in reference 15.

The noise level changes shown in Table III are observed to be relatively small. This tends to confirm the validity of the turbulence measurement approach taken in the present study. A second observation is that a decrease in transverse length scale would result in lower noise levels at low frequency and higher levels at high frequency. Changes of this nature would generally improve the agreement between theory and experiment shown in figure 16. This is the only turbulence quantity which affects spectrum slope. Although there is no basis for assuming that a higher than actual length scale was measured here, this was the least reliably measured turbulence parameter.

In summary, the estimated error in measured quantities and the resultant effect on predicted noise levels suggests that the turbulence measurement approach taken here was reasonable.

Overall Noise Level Prediction - The ability to predict overall noise level is of practical interest. As an integral of the spectrum over frequency, however, it represents a less sensitive measure of the accuracy of a noise prediction method than spectrum comparisons.

Table IV compares predicted and measured overall noise levels for the fifteen hover test cases for which spectra were shown in figure 16. As previously noted, there was a large underprediction at 90 deg and lesser underpredictions at angles near this plane. For reasons discussed earlier, this significant underprediction at 90 deg is not considered an indication that a mechanism other than turbulence ingestion accounts for the hover noise measured here. In addition to significant disagreement in the plane of rotation, there is a 10 dB discrepancy between theory and experiment for Hover Case -10.

Despite these significant errors, theory and experiment were observed to agree within 3 dB for about 50 percent of the test cases; 75 percent of the cases were within 5 dB.

Importance of Anisotropic Inflow Model - Of interest is the importance of accounting for the measured anisotropic nature of the inflow field in the

prediction of turbulence ingestion noise in hover. This is clearly shown in figure 17.

In part (a) of the figure, the anisotropic inflow theory employed in this study was applied. Noise at BPF multiples is predicted within 5 dB.

In part (b), the inflow was assumed to be isotropic with an axial length scale equal to the measured large axial length scale (large spherical eddies). This automatically assigned the transverse length scale a value one-half as large. The isotropic mode of the prediction method was applied, resulting in the poor results shown. Errors of as much as 25 dB occurred. If only a single probe is used to define inflow statistics, the only derivable length scale is the axial scale of the axial component. Use of this scale in an isotropic calculation procedure is clearly invalid.

In part (c), the inflow was assumed to be isotropic with an axial length scale equal to twice the measured small transverse length scale (small spherical eddies). This automatically assigned the transverse length scale a value one-half as large. The isotropic mode of the prediction method was applied, again resulting the the poor results shown. Errors of as much as 20 dB occurred. Use of either a small or large spherical eddy assumption, therefore, resulted in very poor agreement of prediction with measurement.

In references 8 and 9, isotropic inflow was assumed and inflow turbulence parameters selected to match theory to a measured hover noise spectrum where inflow turbulence statistics were not available. As a demonstration of concept and a cross-check between two theories, this was useful; the results shown here, however, indicate that the isotropic model is inadequate in hover.

The conclusion drawn here is that inclusion of anisotropic inflow effects is essential to reasonable prediction of turbulence ingestion noise in hover.

TIP VORTEX INGESTION

Objective

The objective of this phase of the study was to obtain exploratory noise data on the effect of the ingestion of a tip vortex from an upstream airfoil on the noise of the model rotor. The incentive for such experimentation is that main rotor-tail rotor interactions involve tip vortex ingestion. In particular, the wake of the main rotor, ingested by the tail rotor (or vice versa) contains, in addition to turbulence, tip vortices. Furthermore, interaction of a rotor with its own tip vortex field is a known cause of impulsive noise in descent and certain forward flight conditions.

Absolute level prediction of noise due to tip vortex ingestion is not presently possible. Simplified vortex encounter experiments, such as that performed here are considered useful in formulating a joint theoretical and experimental approach leading to prediction of such noise.

Approach

The simplest vortex encounter situation was selected for study; that is, axial convection of a tip vortex through a rotor operating in vertical ascent. This interaction geometry has some relevance to the case where a tail rotor ingests a main rotor tip vortex but is unrepresentative of the case where a rotor tip vortex interacts with its own vortex field. The test geometry, because of its simplicity, however, provided a useful case for initial experimental study.

Experimental Arrangement

Figure 18 shows the wind tunnel arrangement employed in the present exploratory study. A 10.8 cm chord, NACA 0012 airfoil was mounted upstream of the model rotor on a traverse can capable of motion in the vertical direction. Turbulence grids were removed from the tunnel inlet to provide a clean inflow. The tip vortex from the airfoil convected downstream with the tunnel flow and inward toward the rotor axis due to the streamline contraction induced by the rotor. The vortex intersected the rotor blades at radial positions that could be varied by traversing the airfoil vertically.

The tunnel speed was 9.1 m/sec and pitch was 15 deg for all tests. Tip vortex strength was varied from zero (upstream airfoil at zero degree angle of attack) to three other values corresponding to airfoil angles of attack of 5, 10 and 20 degrees. For the 5 and 10 degree cases the upstream airfoil was unstalled, based on flow visualization with tufts, while for the 20 degree case the airfoil was stalled.

Tip Vortex Ingestion Noise Results

Effect of Radial Intersection Position - Figure 19 shows rotor noise spectra at a directivity angle of 120 deg relative to the rotor axis for a rotor tip Mach number of 0.47 and various vertical separation distances between the airfoil tip and the rotor blade tip. Results are shown for upstream airfoil angles of attack of zero and ten degrees to attempt to separate noise due to airfoil wake ingestion from tip vortex ingestion.

In part (a) of figure 19, the airfoil tip was 15 cm outboard of the rotor tip. For zero degree angle of attack, the noise spectrum (shown dashed) was identical to that obtained with no upstream airfoil. Steady loading tones at BPF and twice BPF were observed with a broadband spectrum at higher frequency. From this it can be inferred that the airfoil wake, in this case, was not ingested by the rotor. The dashed curve also applied to a noise measurement with a tip vortex but at a separation distance of 23 cm. At this larger separation distance, not only did the airfoil wake not interact with the rotor but neither did the tip vortex.

With the upstream airfoil at the angle of attack at the 15 cm separation distance, however, the resultant noise spectrum (shown as a solid curve in part (a)) displayed additional tones at frequencies between 3 and 13 times blade passage frequency. This increase in noise can be attributed to the interaction of the airfoil tip vortex with the rotor.

In figure 19, part (b), the airfoil tip-to-rotor tip separation distance was decreased to 7.5 cm. The dashed curve obtained with no vortex, displays tones which can be attributed to interaction of the rotor with the airfoil wake. These tones were caused by a wake chopping mechanism similar to that which occurs in turbofan engines equipped with inlet guide vanes.

When the upstream airfoil was placed at angle of attack at this separation distance, figure 19, part (b) shows that a significant increase in rotor tone noise occurred. Levels increased by as much as 15 dB and tones were observed to persist to 37 times BPF. This persistence of tones to high frequency is indicative of an impulsive noise mechanism.

Although vortex trajectories were not measured in the present exploratory study, comparison of parts (a) and (b) of figure 19 suggests that the vortex passed near the rotor tip in part (a) but actually intersected the tip in part (b).

The tones observed here were much narrower in bandwidth than those obtained during turbulence ingestion experiments due to the lack of randomness in the inflow field; that is, multiple blade interaction with a

discrete and fixed inlet disturbance provided highly coherent blade-to-blade unsteady pressures. The origin of the unsteady pressures was the effective angle of attack excursion sensed by the rotor blades as the blades (at 15 deg pitch) interacted with a vortex field possessing circulation in the plane normal to the tunnel axis.

This interaction process could be treated by the compressible, unsteady airfoil theory used in the present study to predict turbulence ingestion noise. Absolute level spectrum prediction could be accomplished if vortex characteristics were known.

Parts (c) and (d) of figure 19 show that as the vortex intersection position was moved further inboard, the higher frequency tonal content of the spectra decreased. This was indicative of a less impulsive waveform. Such behavior would be anticipated since the time for a blade to chop through the vortex of fixed size varied inversely with the radius to the intersection position.

Although the vortex interaction geometry employed here was relatively simple, results indicated that some of the known characteristics of vortex interaction were preserved. Since the vortex trajectory and the spatial extent and velocity field of the tip vortex were not measured in the present experiment, prediction of far-field noise was not possible.

Vortex Interaction Noise Time Histories - Figure 20 shows noise signal time histories for three of the airfoil tip-to-rotor tip separation distances of figure 19. In part (a), the waveform for the most outboard vortex position shows no indication of impulsive noise as would have been anticipated from the noise spectrum discussed previously. Part (b), corresponding to the strong vortex interaction noise spectrum of figure 19, part (b), however, clearly shows an impulsive component in the waveform. As anticipated from spectrum results, part (c) shows that at the most inboard vortex interaction position, the impulsive nature of the noise decreased.

The impulsive noise obtained here was perceptible as a high frequency whine rather than the bang usually associated with vortex interaction blade slap.

Effect of Vortex Strength - Figure 21 shows the effect of tip vortex strength on the interaction noise. In part (a), the vortex strength was zero and the tonal noise at low frequency was due to blade chopping of the airfoil wake velocity defect. As vortex strength was increased, parts (b) and (c) show noise increases on the order of 10 dB and a persistence of tones to higher frequency.

In figure 21, part (d), the upstream airfoil was stalled. Low frequency tone noise was observed to increase an additional 10 dB and the high frequency portion of the spectrum changed from tonal to broadband in nature. This high frequency broadband noise was probably caused by increased turbulence levels in the vortex and airfoil wake.

The conclusion drawn from this limited vortex strength investigation and the previously discussed vortex intersection position study is that the interaction noise is highly sensitive to details of the vortex interaction process. Prediction of such noise would appear to require either accurate measurement or prediction of vortex interaction positions, vortex strengths (circulation), vortex core sizes, airfoil wake defects and turbulence levels in the vortex and wake.

Vortex Interaction Noise Directivity - The upper portion of figure 22 shows vortex interaction noise spectra at two directivity angles of 80 and 130 deg from the axis. The tone noise is much diminished at the 80 deg position near the plane of rotation. The lower portion of the figure shows directivity patterns at four frequencies. Minimum noise levels at each frequency were observed to occur near the plane of rotation.

The directivity patter was qualitatively similar to that obtained as a result of the ingestion of turbulence. This would have been expected since noise in both cases was associated with unsteady lift forces which produced a dipole directivity pattern with the dipoles oriented perpendicular to the chord.

Summary of Tip Vortex Ingestion Results - Ingestion of a tip vortex by the rotor caused harmonic noise which extended to high frequency and displayed an impulsive waveform. Results were sensitive to vortex interaction position and strength.

Predition of such noise on an absolute level basis appears possible using unsteady airfoil theory such as employed here to treat turbulence ingestion; knowledge of vortex characteristics, however, would be required for such prediction. Simple interactions of the type considered here, while unrepresentative of the type which occur in vertical descent, appear to be relevant to the case of main rotor-tail rotor interaction noise.

CONCLUSIONS

Conclusions resulting from this research program are presented below and are grouped in terms of the different rotor inflow conditions employed in the various phases of the study.

A. Noise and Turbulence Inflow Characteristics in Hover

The following conclusions concerning hover noise and atmospheric turbulence are based upon noise and rotor inflow turbulence measurements conducted during outdoor hover experimentation.

A.1. Ingestion of atmospheric turbulence and steady blade loading were the dominant model rotor noise mechanisms in outdoor tests simulating hover. While steady blade loading was the primary cause of tone noise at blade passage frequency and one or two higher harmonics, turbulence ingestion noise dominated the remainder of the hover noise spectrum. This mechanism caused quasi-tonal (narrowband random) noise to extend to approximately twenty-five harmonics of blade passage frequency.

A.2. Based on fundamental concepts such as the effect of inflow streamline contraction on the distortion and intensification of atmospheric turbulent eddies, the above conclusion regarding the dominant role of turbulence ingestion in the generation of model rotor hover noise would be expected to apply equally well to full-scale helicopter main rotors (except possibly in those circumstances where the tail rotor wake was ingested by the main rotor or transonic tip speeds caused blade thickness noise). On a perceived noise level basis, atmospheric turbulence ingestion would be expected to be the dominant main rotor noise mechanism in hover.

A.3. A theory capable of absolute level prediction of rotor turbulence ingestion noise spectra and directivity, without use of empirical or adjustable constants, provided reasonable prediction of outdoor hover noise data acquired in the present study (except for the steady loading tones not accounted for by theory and turbulence ingestion noise near the plane of rotation). Low frequency narrowband random noise was overpredicted and high frequency broadband noise was underpredicted.

A.4 Knowledge of inflow turbulence intensity, axial length scale, transverse length scale and mean velocity near the rotor disk was required to obtain the level of prediction accuracy of outdoor hover turbulence ingestion noise reported here. Failure to account for the anisotropic nature of the inflow turbulence field in a noise prediction method resulted in poor agreement between theory and experiment.

A.5. Statistics of the atmospheric turbulence field ingested by the model rotor in hover were observed to be nonstationary in the present study and would be expected to be so in full-scale experimentation. This results in a requirement to measure inflow statistics and far-field noise simultaneously in studies directed toward prediction of far-field noise from measured inflow statistics.

A.6. The turbulence field ingested by the model rotor in outdoor hover was characterized by large eddies, elongated in the axial direction. Multiple chopping of these eddies by successive blades caused quasi-tonal noise at low-to-mid frequencies while individual blade interaction with smaller eddies was the source of high frequency broadband noise.

B. Rotor Noise for Low Turbulence Inflow Conditions

The following conclusions concerning rotor noise under clean inflow conditions are based upon noise measurements obtained in an anechoic wind tunnel with no turbulence generating grids installed in the tunnel inlet.

B.1. Model rotor noise data acquired with a spatially uniform and low turbulence level incident velocity field showed several low frequency tones that were attributed to loading. The remainder of the spectrum was broadband and relatively flat. This noise was tentatively attributed to a turbulent boundary layer trailing edge noise mechanism.

B.2. Laminar boundary layer tone noise was observed to occur in a frequency range predicted both theoretically and empirically. This mechanism is not important for full-scale rotors since boundary layers are generally turbulent at the blade trailing edge. The mechansim can, in any event, be eliminated by a boundary layer trip as demonstrated in the study.

C. Rotor Noise Due to Ingestion of Grid Generated Turbulence

The following conclusions concerning rotor turbulence ingestion noise are based upon noise measurements obtained in an anechoic wind tunnel with turbulence generating grids installed in the tunnel inlet.

C.1. Prediction of rotor noise spectra due to ingestion of isotropic, homogeneous turbulence in a wind tunnel can be accomplished with greater accuracy than prediction of outdoor hover turbulence ingestion noise. In the wind tunnel phase of this study, quasi-tonal noise at low frequency was overpredicted whereas mid-frequency tonal noise and high frequency

broadband noise were, in general, accurately predicted. This degree of prediction accuracy held for both simulated forward flight and vertical ascent configurations, as well as for a range of rotor tip Mach numbers and inflow turbulence intensities.

C.2. Ingestion of turbulence in simulated forward flight was both predicted and observed to cause less quasi-tonal noise than ingestion in a simulated vertical ascent condition.

C.3. For a fixed inflow turbulence field, the amplitude of high frequency, broadband noise due to turbulence ingestion was predicted and observed to be directly proportional to the number of blades. For low frequency quasi-tonal noise, theory predicted a stronger dependence that was not observed.

C.4. For a fixed inflow turbulence field, the effect of a change in rotor pitch was predicted and observed to be negligibly small. Instances where larger effects were observed were attributed to changes in the inflow turbulence field caused by the pitch change.

C.5. In forward flight, both theory and experiment indicated that the center frequencies of narrowband random tones were shifted away from multiples of blade passage frequency (BPF). This was attributed to the non-axial convection of large turbulent eddies in forward flight. In vertical ascent, both theory and experiment showed that narrowband random tones occurred at BPF multiples.

D. Rotor Noise Due to Tip Vortex Ingestion

The following conclusion concerning vortex ingestion noise is based upon noise measurements obtained in an anechoic wind tunnel with a stationary blade located upstream of the model rotor.

D.1. Ingestion of a tip vortex caused harmonic noise which extended to high frequency and which displayed an impulsive waveform. Such ingestion appears to be a relevant main rotor-tail rotor interaction noise mechanism.

REFERENCES

1. George, A. R.: Helicopter Noise - State of the Art. Paper 77-1337, AIAA, 1977.

2. Paterson, R. W. and Amiet, R. K: Acoustic Radiation and Surface Pressure Characteristics of an Airfoil due to Incident Turbulence. NASA CR-2733, 1976.

3. Sharland, I. J.: Sources of Noise in Axial Flow Fans. J. Sound Vibration, vol. I, 1964, pp. 302-322.

4. Sofrin, T. G. and McCann, J. C.: Pratt and Whitney Experience in Compressor Noise Reduction. Paper presented at the 72nd Meeting of the Acoustical Society of America, Los Angeles, Cal., Nov. 2-5, 1966.

5. Hanson, D. B.: Spectrum of Rotor Noise Caused by Atmospheric Turbulence. J. Acoustical Soc. Amer., vol. 56, no. 1, July 1974, pp. 110-126.

6. Pegg, R. J., Magliozzi, B. and Farassat, F.: Some Measured and Calculated Effects of Forward Velocity on Propeller Noise. Paper 77-GT-70, ASME, 1977.

7. Feiler, C. E. and Groeneweg, J. F.: Summary of Forward Velocity Effects on Fan Noise. NASA TM 73722, 1977. (Also published as Paper 77-1319, AIAA, 1977).

8. Amiet, R. K.: Noise Produced by Turbulent Flow into a Propeller or Helicopter Rotor. Paper 76-560, AIAA, 1976. (Also published in synoptic form in AIAA Journal, vol. 15, no. 3, March 1977, pp. 307-308).

9. Homicz, G. F. and George, A. R.: Broadband and Discrete Frequency Radiation from Subsonic Rotors. J. Sound Vibration, vol. 36, 1974, pp. 151-177.

10. Hawkings, D. L.: Theoretical Models of Helicopter Rotor Noise. In Helicopter Acoustics, NASA Conference Publication 2052, Part I, 1978, pp. 89-108.

11. Amiet, R. K.: Acoustic Radiation from an Airfoil in a Turbulent Stream. J. Sound Vibration, vol. 41, 1975, pp. 407-420.

12. Paterson, R. W. and Amiet, R. K.: Noise and Surface Pressure Response of an Airfoil to Incident Turbulence. J. Aircraft, vol. 14, 1977, pp. 729-736.

13. Lowson, M. V.: The Sound Field for Singularities in Motion. Proc. Roy, Soc., vol. A286, 1965, pp. 559-572.

14. Bendat, J. S. and Piersol, A. G.: Measurement and Analysis of Random Data . John Wiley and Sons, Inc., 1965.

15. Amiet, R. K.: Noise Due to Rotor-Turbulence Interaction. NASA Conference Publication 2052, 1978, pp. 109-126.

16. Hinze, J. O.: Turbulence. McGraw-Hill, Inc. 1959.

17. Paterson, R. W., Vogt, P. G. and Foley, W. M.: Design and Development of the United Aircraft Research Laboratories Acoustic Research Tunnel. J. Aircraft, vol. 10, no. 7, 1973, pp. 427-433.

18. Paterson, R.W., Vogt, P. G., Amiet, R. K. and Fink, M. R.: Vortex Shedding Noise of an Isolated Airfoil. Proceedings of the Helicopter Noise Symposium, U. S. Army Research Office, Durham and American Helicopter Society Inc., Sept. 28-30, 1971, Durham, N.C., pp. 73-83.

19. Paterson, R. W., Vogt, P. G., Fink, M. R. and Munch, C. L.: Vortex Noise of Isolated Airfoils. J. Aircraft, vol. 10, no. 5, May 1973, pp. 296-302.

20. Fink, M. R.: Prediction of Airfoil Tone Frequencies. J. Aircraft, vol. 12, no. 2, Feb. 1975, pp. 118-120.

21. Hama, F. R.: An Efficient Tripping Device. J. Aeronautical Sci., vol. 24, Mar. 1957, pp. 236-237.

22. Horlock, J. H.: Fluctuating Lift Forces on Airfoils Moving Through Transverse and Chordwise Gusts. Trans ASME, J. Basic Eng., vol. 90, 1969, pp. 494-500.

23. Pegg, R. J. and Shidler, P. A.: Exploratory Wind-Tunnel Investigation of the Effect of the Main Rotor Wake on Tail Rotor Noise. NASA Conference Publication 2052, 1978, pp. 205-219.

24. Prandtl, L.: Attaining a Steady Air Stream in Wind Tunnels, NACA TM 726, 1933.

25. Filleul, N. S.: An Investigation of Axial Flow Fan Noise. J. Sound Vibration, vol. 3, 1966, p. 147.

26. Griffith, E. D. and Revell, J. D.: Low Noise Propeller Technology. Report AFAPL-TR-73-115, Wright-Patterson AFB, Dec. 1973.

27. Lowson, M. V., Watmore, A. R. and Whitfield, C. E.: Source Mechanisms for Rotor Noise Prediction. NASA CR-2077, Aug. 1973.

28. Robbins, B. and Lakshminarayana: Effect of Inlet Turbulence on Compressor Noise. J. Aircraft, vol. 11, no. 5, May 1974, pp. 273-281.

29. Mani, R.: Noise Due to Interaction of Inlet Turbulence with Isolated Stators and Rotors. J. Sound Vibration, vol. 17, no. 2, 1971, pp. 251-260.

30. Sevik, M.: Sound Radiation from a Subsonic Rotor Subjected to Turbulence. Proceedings of the International Symposium on Fluid Mechanics and Design of Turbomachinery, Penn. State Univ., 1970.

31. Magliozzi, B.: The Influence of Forward Flight on Propeller Noise. NASA CR-145105, 1977.

32. Aravamudan, K. S., Lee, A. and Harris, W. L.: Wind Tunnel Investigations of Model Rotor Noise at Low Tip Speeds. NASA Conference Publication 2052, Part I, 1978, pp. 221-261.

33. Lowson, M. V. and Ollerhead, J. B.: A Theoretical Study of Helicopter Rotor Noise. J. Sound Vibration, vol. 9, 1969, pp. 197-222.

34. Morfey, C. L. and Tanna, H. K.: Sound Radiation from a Point Force in Circular Motion. J. Sound Vibration, vol. 15, 1971, pp. 325-351.

35. Osborne, C.: Unsteady Thin Airfoil Theory for Subsonic Flow. American Institute of Aeronautics and Astronautics Journal, vol. 11, 1973, pp. 205-209.

36. Amiet, R. K.: Compressibility Effects in Unsteady Thin Airfoil Theory. AIAA Journal, vol. 12, 1974, pp. 253-255.

37. George, A. R. and Kim, Y. N.: High-Frequency Broadband Rotor Noise. AIAA Journal, vol. 15, 1977, pp. 538-545.

38. Pickett, G. F.: Effects of Non-Uniform Inflow on Fan Noise. Paper presented at Spring Meeting of Acoustical Society of America, April 23-26, 1974.

39. Amiet, R. K.: Frame of Reference Considerations for the Forward Flight Noise Problem. Report N2127751-1, United Technologies Research Center, 1974.

40. Amiet, R. K.: Effects of Compressibility in Unsteady Airfoil Lift Theories. Unsteady Aerodynamics, University of Arizona/AFOSR Symposium, March 18-20, 1975, Tucson, Arizona (ed. R. B. Kinney), pp. 631-653.

41. Amiet, R. K.: Low Frequency Approximations in Unsteady Small-Pertubation Subsonic Flows. J. Fluid Mech., vol. 75, 1976, pp. 545-552.

42. Amiet, R. K.: High Frequency Thin-Airfoil Theory for Subsonic Flow. AIAA Journal, vol. 14, 1976, pp. 1076-1082.

TABLE I

WIND TUNNEL TEST CONDITIONS

Test Designation	Configuration	Grid	Rotational Speed, rev/sec	Tip Mach Number (absolute)	Pitch, deg	Shaft angle, deg	Number Blades
FF-L-1	Forward flight	L	65.8	0.47	9.5	-2.8	4
FF-L-2	Forward flight	L	52.1	0.37	9.5	-2.8	4
FF-L-3	Forward flight	L	65.8	0.47	9.5	-2.8	2
FF-L-4	Forward flight	L	65.8	0.47	9.5	-2.8	4
FF-M-1	Forward flight	M	73.5	0.52	9.5	-2.8	4
VA-M-1	Vertical ascent	M	73.5	0.52	3.7	----	4
VA-M-2	Vertical ascent	M	52.1	0.37	3.7	----	4
VA-M-3	Vertical ascent	M	52.1	0.37	15.7	----	4
VA-M-4	Vertical ascent	M	73.5	0.52	3.7	----	2
VA-L-1	Vertical ascent	L	65.8	0.47	3.0	----	4
VA-L-2	Vertical ascent	L	65.8	0.47	9.0	----	4
VA-L-3	Vertical ascent	L	65.8	0.47	3.7	----	4
VA-C-1	Vertical ascent	None	58.5	0.42	15	----	4

TABLE I (Concluded)

Test Designation	Temperature deg C	Tunnel speed, m/sec.	Turbulence length scale, cm	Root-mean-square turbulence velocity, m/sec.	Turbulence intensity, percent
FF-L-1	7	22.9	6.0	4.2	18.5
FF-L-2	7	22.9	6.0	4.2	18.5
FF-L-3	7	22.9	6.0	4.2	18.5
FF-L-4	7	9.1	6.0	1.6	17.3
FF-M-1	16	22.9	12.5	1.6	6.9
VA-M-1	11	9.1	7.3	.80	8.8
VA-M-2	11	9.1	7.3	.80	8.8
VA-M-3	11	9.1	7.3	.80	8.8
VA-M-4	11	9.1	7.3	.80	8.8
VA-L-1	8	9.1	7.3	1.3	14.0
VA-L-2	8	9.1	7.3	1.3	14.0
VA-L-3	11	9.1	7.3	1.3	14.0
VA-C-1	0	9.1	4.9	.041	0.45

TABLE II

OUTDOOR HOVER TEST CONDITIONS[a]

Test Designation	Rotational Speed, rev/sec (b)	Microphone Position, θ, deg (c)	Inflow Mean Velocity, U, m/sec (d)	Inflow Turbulence Level, % (e)
HOVER- 1	58.5	0	7.6	3.0
HOVER- 2	58.5	60	7.7	2.8
HOVER- 3	58.5	70	8.0	2.7
HOVER- 4	58.5	80	8.0	2.7
HOVER- 5	58.5	90	7.9	2.7
HOVER- 6	58.5	100	7.9	2.4
HOVER- 7	58.5	110	7.8	2.4
HOVER- 8	58.5	120	7.8	2.0
HOVER- 9	58.5	130	7.9	2.4
HOVER-10	52.1	0	7.0	2.7
HOVER-11	52.1	60	7.0	2.3
HOVER-12	52.1	80	6.8	2.3
HOVER-13	52.1	110	6.8	3.0
HOVER-14	52.1	120	6.8	2.6
HOVER-15	52.1	130	6.9	2.4

[a]For all tests temperature was 12°C, collective pitch was 15 deg, far-field microphone position on 2.44m radius

[b]Corresponding tip Mach numbers were 0.413 for 58.5 rps and 0.368 for 52.1 rps

[c]Zero degrees refers to rotor axis

[d]Mean velocity as measured by fixed (upper) probe at location shown in figure 13

[e]Axial (longitudinal) turbulence component level given by (u'/U) x 100

TABLE II - CONCLUDED

Test Designation	Turbulence Length Scale Λ_f, cm. (f)	Turbulence Length Scale Ratio, Λ_f/Λ_g (g)	Average Wind Speed, Knots	Maximum Wind Speed During Run, Knots
41 HOVER- 1	113	31	2.2	2.9
39 HOVER- 2	105	29	1.6	2.2
38 HOVER- 3	85	23	1.6	2.4
37 HOVER- 4	66	18	1.3	2.1
36 HOVER- 5	117	32	1.2	1.8
35 HOVER- 6	61	17	1.2	1.8
34 HOVER- 7	66	18	0.1	0.4
33 HOVER- 8	140	38	0.1	0.1
32 HOVER- 9	215	59	0.2	0.8
43 HOVER-10	183	50	0.4	1.1
44 HOVER-11	93	26	0.1	0.1
46 HOVER-12	109	30	0.9	1.6
49 HOVER-13	87	24	1.4	1.9
50 HOVER-14	121	33	1.6	1.8
52 HOVER-15	163	44	0.1	0.1

[f]Axial length scale of axial turbulence component as measured by fixed (upper) probe (figure 13)

[g]Transverse length scale, Λ_g, taken as 3.65 cm for all test runs

TABLE III

EFFECT OF VARIATIONS IN ASSUMED TURBULENCE INFLOW PARAMETERS ON HOVER NOISE PREDICTION[a] (HOVER CASE-2, θ = 60 DEG)

	CHANGE IN BPF LEVEL, dB	CHANGE IN 5X BPF LEVEL, dB	CHANGE IN 20X BPF LEVEL, dB
25% INCREASE IN u'	1.94	1.94	1.94
25% DECREASE IN u'	-1.94	-1.94	-1.94
25% INCREASE IN Λ_f	0.97	0.97	0.80
25% DECREASE IN Λ_f	-0.96	-0.97	-0.75
25% INCREASE IN Λ_g	1.84	-0.91	-1.37
25% DECREASE IN Λ_g	-2.25	0.61	2.06

[a]Noise prediction using anisotropic inflow noise theory

TABLE IV

COMPARISON OF MEASURED AND PREDICTED
OVERALL SOUND PRESSURE LEVEL FOR
OUTDOOR HOVER CASES

TEST DESIGNATION	M_{tip}	θ, deg	MEASURED OVERALL SPL, dB	THEORETICALLY PREDICTED OVERALL SPL, dB	THEORY RELATIVE TO MEASUREMENT, dB
HOVER-1	0.41	0	81.2	83.3	HIGH 2.1
HOVER-10	0.37	0	72.9	82.0	HIGH 9.1
HOVER- 2	0.41	60	76.2	77.4	LOW 1.2
HOVER-11	0.37	60	73.3	72.3	LOW 1.0
HOVER- 3	0.41	70	74.6	73.1	LOW 1.5
HOVER- 4	0.41	80	73.9	66.2	LOW 7.7
HOVER-12	0.37	80	70.1	64.3	LOW 5.8
HOVER- 5	0.41	90	71.7	26.1	LOW 45.6
HOVER- 6	0.41	100	69.1	64.9	LOW 4.2
HOVER- 7	0.41	110	71.8	71.0	LOW 0.8
HOVER-13	0.37	110	68.1	71.4	HIGH 3.3
HOVER- 8	0.41	120	75.4	75.7	HIGH 0.3
HOVER-14	0.37	120	70.0	74.5	HIGH 4.5
HOVER- 9	0.41	130	76.1	80.9	HIGH 4.8
HOVER-15	0.37	130	75.0	77.1	HIGH 2.1

APPENDIX A

Discussion of Previous Investigations

Experimental Studies - Sharland (reference 3) conducted one of the first investigations of rotating blade turbulence induced noise. He demonstrated that ingested turbulence can have a significant effect on fan broadband noise.

By placing a 1 cm diameter circular rod bent into a ring, 20 rod diameters upstream of a model fan rotor, he found broadband noise sound power increases of 1 to 7 dB (depending on blade tip speed) relative to measurements with the rod removed. Using a simple theoretical model with many approximations, Sharland predicted overall sound power level from turbulence intensity measurements showing reasonable agreement with data. Turbulence length scale was neither measured nor accounted for in the theoretical formulation. Sharland incorrectly concluded that the inflow to a rotor in a static test environment is smooth in the absence of turbulence generators in the inlet or inlet guide vanes. He therefore did not identify inflow turbulence as a possible source of noise at blade passage frequency and higher harmonics.

Based on compressor rig tests, Sofrin and McCann in 1966 (reference 4) indicated that ingestion of turbulence was a potentially important source of discrete frequency noise. From the dependence of blade passage frequency sound level on inlet guide vane - rotor spacing and tests conducted with vanes removed, they concluded that ingestion of patches of turbulence produce random bursts of blade passage tones. In the same time period Filleul (reference 25) also concluded that blade passage frequency noise observed in isolated rotor axial flow fan tests was associated with inflow turbulence. These early investigators were not specific as to the origin or nature of the inflow turbulence field and inflow turbulence measurements were not obtained.

In a study of propeller noise reported by Griffith and Revell (reference 28) in 1973, large discrepancies between static and flyover noise data were noted for several propellers. They observed that harmonics of blade passage frequency decayed much more slowly in the static case and therefore concluded static data could not be used in the development of a propeller noise prediction procedure. The authors did not identify the probable cause for this disagreement between flight and static results. Lowson, Whatmore and Whitfield (reference 27) tested an axial fan in a sealed anechoic chamber and concluded that turbulent flow into the rotor was responsible for low frequency broadband noise. Using a theoretical model similar to Sharland's, overall broadband noise was predicted from turbulence intensity measurements showing good agreement with data. As in Sharland's study, turbulence length scale effects were neglected.

A significant advance in understanding was made in 1974 with Hanson's (reference 5) publication of measurements of both turbulence in a static inlet and unsteady blade pressures on a fan rotor. The inflow was found to contain long, narrow eddies with an integral length scale on the order of 30 m. Hanson concluded that the spectrum peaks of propellers, helicopter rotors and fans that had previously been considered harmonics due to fixed inflow distortion were likely narrow-band random noise associated with ingestion of atmospheric turbulence. This conclusion was supported by a theoretical formulation that predicted turbulence noise spectra given unsteady blade pressures as experimental input.

In the same time period Robbins and Lakshminarayana (reference 28) reported the results of a study of the effect of grid generated turbulence on the noise of an axial inflow fan rotor. Inflow turbulence intensities and length scales were measured and the theories of Mani (reference 29) and Sevik (reference 30) used to predict noise spectra. Limited agreement between theory and experiment was obtained. This was attributed to assumptions made in the theories and measured variations of turbulence integral length scale with blade spanwise position.

A study of propeller noise forward flight effects was reported by Magliozzi (reference 31) and Pegg, Magliozzi and Farassat (reference 6) in 1977. Using measurements of both unsteady blade surface pressures and far-field noise it was shown that ingestion of atmospheric turbulence caused significant harmonic and broadband noise during static operation. In flight, steady loading and blade thickness mechanisms were dominant. From this it can be concluded that static testing of propellers for the purpose of noise research is not viable unless some form of atmospheric turbulence control is employed at the inlet to the propeller.

In 1978, Aravamudan et al. (reference 32) reported the results of a wind tunnel model rotor study conducted with turbulence generating grids in the tunnel inlet. This study was similar in concept to that phase of the present wind tunnel study in which grids were installed upstream of the rotor. One difference was that the reference 32 study was conducted at low tip Mach numbers (0.2 and lower). Another difference, in terms of results, was that turbulence ingestion was observed to cause only broad-band noise. This was due to the combination of turbulence eddy sizes, convection velocities and rotor blade passage periods employed in this study.

Also in 1978, Amiet (reference 15) presented one comparison of predicted and measured propeller turbulence ingestion noise spectra obtained with upstream grids in the tunnel employed in the present study. Both peaking of noise at BPF multiples and the broadband noise level were well predicted.

In addition to the above experimental studies, turbulence ingestion has recently become an active turbofan engine fan noise research area. A summary of recent fan noise research is given in reference 7.

Theoretical Studies - Until recently, most theoretical studies of rotor broadband noise concentrated on the relation of the blade forces to noise. This was the approach followed by Lowson and Ollerhead (reference 33) and Morfey and Tanna (reference 34). These analyses are useful for studying the properties of rotating point sources, but they are restricted in scope in the sense that they do not include certain important physical effects such as source noncompactness and the relation of the turbulent inflow to the magnitude of the blade loading.

While empirically deriving a factor that yields an observed roll-off in harmonic noise levels with frequency can be considered a description of an unsteady loads effects, it provides no insight into how this factor should be calculated in various turbulent inflow situations. In presenting experimental rotor noise data, a common practice has been to consider this harmonic roll-off factor a theoretical noise prediction method. Good agreement with data can give the incorrect impression that the problem is understood on a first-principles basis.

Hanson (reference 5) avoided the problem of relating inflow turbulence to blade loading by using blade mounted pressure transducers to estimate unsteady blade loading. Assuming source compactness and using incompressible flow airfoil theory, far-field noise was predicted. Although these assumptions were not rigorous, this approach provided insight into the operative mechanism. From a diagnostic standpoint, blade pressure data such as Hanson's can sometimes be more instructive than an inflow turbulence measurement. This is because the blade transducer samples the complete inflow field each revolution. Conversely, high blade pressures, which are uncorrelated, may not cause significant noise. Although instructive, Hanson's approach does not provide a generally applicable prediction system since the inflow turbulence field rather than blade pressure is the ultimate cause of turbulence ingestion noise.

Some of the limitations of previous studies were removed by Homicz and George (reference 9). In their study, blade forces and turbulence were related by the airfoil theory of Osborne (reference 35) and Amiet (reference 36) both of which include the effects of compressibility but which are limited to acoustic wavelengths longer than several airfoil chordlengths. As noted below, the subsequently published noise theory of Amiet eliminated the long wavelength assumption. Chordwise noncompactness effects were included through the use of an estimated correction factor, but spanwise noncompactness effects were neglected. One limitation of the approach of

reference 9 was that a significant amount of computer time was needed to calculate noise at high frequency. This limitation was removed by George and Kim (reference 37) who obtained a simpler expression for the high frequency limit.

Most of the above mentioned limitations were eliminated in the theoretical approach developed by Amiet (reference 8). In this analysis, blade forces were related to the inflow turbulence by compressible flow airfoil theory, valid for both low and high frequency. Noncompactness of the blade forces was allowed in both the chordwise and spanwise directions. The analysis then determined, fairly rigorously, the acoustic spectrum and directivity of the noise. Furthermore, as in the theory of Homicz and George, there were no adjustable constants in the theory. A comparison between the theories of Amiet and Homicz and George for one test case (reference 8) showed good agreement. The ability of two related, but independently derived prediction methods, to predict the same noise spectrum in a test case minimizes the possibility of an error in either method.

A similar, but less rigorous approach was used by Aravamudan and Harris (reference 32). This was intended to be less a comprehensive prediction scheme, but more a means of correlating the data presented in the paper. Chordwise and spanwise compactness of blade forces was assumed. Also, the effect of blade-blade correlation, although discussed in the paper, was not included in the theory. Thus, the narrow-band random character of turbulence ingestion noise that occurs in many situations, would not be predicted.

In addition to the above, theoretical studies that have been directed toward the propeller or rotor application, various treatments of fan and compressor turbulence ingestion noise have been developed (eg. references 29 and 38). This problem, however, is much more complicated than the open rotor case due to the generation of duct modes, the occurrance of singularities near cut-off and the need to predict radiation patterns from the duct inlet and annular fan exhaust. Treatments of the ducted rotor case will probably, therefore, continue to be more approximate than those for open rotors where the possibility of accurate, absolute level noise prediction appears reasonably near at hand.

APPENDIX B

Extension of Turbulence Ingestion Noise Theory to Helicopter Rotor Forward Flight

The purpose of this Appendix is to extend previously published theory for turbulence ingestion noise of propellers and helicopter rotors with axial inflow to the case of helicopter rotor forward flight.

A general discussion of the theoretical approach employed in this study is given in the main text section entitled "Theoretical Formulation". A detailed derivation of turbulence ingestion noise theory for propellers and helicopter rotors with axial inflow was previously published by Amiet (Reference 8). This forms the basis for the extension derived here. In addition to this extension of theory, a minor error in equation (6) of reference 8 regarding retarded source position is corrected. Since this error is proportional to axial flow Mach number and the results calculated in reference 8 were for a hovering rotor ($M_z = 0.027$), this error had a negligibly small effect on results presented.

Figure 23 shows the geometry of the problem. The x, y, z axis is fixed to the rotor hub with z being the rotor axis. The axial component of flow is in the negative z direction. The observer is assumed to be in the x-z plane at a distance r from the hub and at an angle θ' with the z axis. The non-axial component of flow M_f, is at an angle ϕ' to the y axis, pointing inward as shown.

The principles employed here are the same as in reference 8. Results for the sound produced by rectilinear motion of an airfoil through turbulence are used to give an "instantaneous" noise spectrum due to a single rotor segment. This spectrum is then averaged around the azimuth, together with a weighting factor which accounts for retarded time effects.

The blade segment is assumed to be a flat plate and unloaded so that it makes an angle α' with the x-y plane where

$$\alpha' = \cot^{-1} \frac{M_f + M_f \cos(\gamma + \phi')}{M_z} \tag{B1}$$

where M_z is the azimuthal Mach number of the blade segment. The flow onto the rotor segment is skewed; i.e., there is a spanwise Mach number M_a

$$M_a = M_f \sin(\gamma + \phi') \tag{B2}$$

For $\gamma + \phi'$ values in the first quadrant, M_a is a flow inward toward the axis.

The retarded position of the source must be calculated. If at time $t = 0$ a marker is placed in the fluid at the rotor hub, when at time $t = T_r$ the observer hears the sound emitted at time $t = 0$, the marker will have moved to position $\underline{x}_s = (x_s, y_s, z_s)$. This point must lie in the plane formed by M_f and M_z. Thus

$$y_s = x_s \cot \phi' \tag{B3}$$

The observer is at $(r \sin \theta', 0, r \cos \theta')$ so that the distance r_e from observer to retarded source point $\underline{x}_s$ is

$$r_e^2 = (r \sin \theta' - x_s)^2 + y_s^2 + (r \cos \theta' - z_s)^2 \tag{B4}$$

Since the observer is in the far field, the distance from observer to the blade segment source is, to lowest order, the same as the distance from observer to rotor hub. Thus,

$$T_r = r_e / c_o \tag{B5}$$

Then

$$x_s = - M_f r_e \sin \phi' \tag{B6a}$$

$$y_s = - M_f r_e \cos \phi' \tag{B6b}$$

$$z_s = - M_z r_e \tag{B6c}$$

Substitution of equations (A6) in equation (B4) leads to the following result for r_e:

$$r_e = \frac{r}{1 - M_f^2 - M_z^2} \left[\sqrt{M_f^2 + M_z^2} \cos \textcircled{H} + \sqrt{1 - (M_f^2 + M_z^2) \sin^2 \textcircled{H}} \right] \tag{B7}$$

This can be substituted in equation (B6) to give results for x_s, y_s and z_s. The angle Θ was introduced above through the equation

$$\sqrt{M_f^2 + M_z^2} \cos \Theta = M_f \sin \phi' \sin \theta' + M_z \cos \theta' \tag{B8}$$

By taking the dot product $(\underline{M}_z + \underline{M}_f) \cdot (-\hat{i} \sin \theta' - \hat{k} \cos \theta')$, Θ is shown to be the angle between the convection Mach number and a unit vector from observer to source. Equation (B7) can be shown to agree with equations (3), (5) and (6) of reference 39.

The results of reference 11 for the sound produced by an airfoil in rectilinear motion are expressed in terms of present airfoil coordinates rather than retarded coordinates. Thus, it is necessary to calculate the "present" position of the rotor. This is the position the rotor would occupy if it had continued in rectilinear motion from the time t = 0 when the sound was emitted until the time $t = T_r$ when the observer hears the sound. (Alternatively, the results of reference 11 could be cast in terms of the retarded source position.)

Since reference 8 does not include a spanwise Mach number component, the spanwise Mach number component M_a should be ignored when calculating the "present" source position. Note that M_a does not affect the noise generation since the airfoil in reference 11 is effectively infinite in span and M_a could be eliminated by a coordinate transform.

Ignoring the spanwise Mach number component M_a, the chordwise Mach number $\underline{M}_c$ of the rotor segment relative to the fluid is

$$\underline{M}_c = \left[M_t + M_f \cos (\gamma + \phi)\right] \left[-\hat{i} \sin \gamma + \hat{j} \cos \gamma\right] + \hat{k} M_z \tag{B9}$$

The "present" source position $\underline{x}_p$ is then

$$\underline{X}_p = \underline{X}_s + T_r \underline{M}_c c_o \tag{B10}$$

Introducing equations (A6) and equations (B7, B8 and B9) into equation (B10) gives

$$\underline{x}_p/r_e = -\hat{i}\left[M_t \sin\gamma + M_f \cos\gamma \sin(\gamma+\phi')\right] \qquad \text{(B11)}$$

$$+\hat{j}\left[M_t \cos\gamma - M_f \sin\gamma \sin(\gamma+\phi')\right]$$

For a coordinate system located at this "present" source position the observer has coordinates $\underline{x}'''$

$$\underline{x}''' = \underline{x} + \underline{x}_p \qquad \text{(B12)}$$

The results of reference 11 are given in a coordinate system in which the flat plate airfoil lies in the x-y plane with the span along y. A similar coordinate system must be defined here. The $\underline{x}''$ coordinate system is defined by rotation of the $\underline{x}'''$ system about the z' axis by γ so that y'' lies along the span. Then

$$x'' = x'''\sin\gamma - y'''\cos\gamma \qquad \text{(B13a)}$$

$$y'' = x'''\cos\gamma + y'''\sin\gamma \qquad \text{(B13b)}$$

$$z'' = z''' \qquad \text{(B13c)}$$

The $\underline{x}'$ system is defined by rotation of the $\underline{x}''$ system about the y axis by α' so that the x' axis lies along the chord pointing from leading to trailing edge. Then

$$x' = x''\cos\alpha' - z''\sin\alpha' \qquad \text{(B14a)}$$

$$y' = y'' \qquad \text{(B14b)}$$

$$z' = x''\sin\alpha' + z''\cos\alpha' \qquad \text{(B14c)}$$

Combining equations (B11, B12, B13 and B14) gives for the observer coordinates in the primed system with y along the rotor span and x' along the chord

$$x' = r_e M_t \cos \alpha' - r \cos \Phi \tag{B15a}$$

$$y' = x \cos \gamma + M_s c_o T_r \tag{B15b}$$

$$z' = (x \sin \gamma + r_e M_t) \sin \alpha' + z \cos \alpha' \tag{B15c}$$

where

$$\cos \Phi = \cos \theta' \sin \alpha' - \sin \theta' \sin \gamma \cos \alpha' \tag{B15d}$$

Here Φ is the angle between the x' axis and a line from observer to the rotor blade segment. These primed observer coordinates are the values to use for (x, y, z) in the noise prediction equations given in reference 11.

Except for the fact that blade-to-blade correlations exist in the turbulence induced blade loading, the above results combined with those of reference 11 and averaged around the aximuth, would lead to a prediction for the far-field spectrum. The blade-to-blade correlations will be accounted for here in the same manner as in reference 8.

The time T_1 will be used to represent the time from when a blade chops an eddy until the next blade reaches its closest approach to the same eddy. This is illustrated in figure 24 which shows the assumed paths that successive blades take relative to the fluid. The description "assumed path" is used since the paths are assumed to be rectilinear when in actual fact they are circular. This should not be a serious fault unless the eddy moves a significant distance between eddy chops so that the effect of rotor path curvature becomes significant.

Consideration of figure 24 shows that value of T_1 is needed which will minimize the distance Z between the eddy and the succeeding blade. The expression for Z is

$$Z^2 = T_1^2 V_z^2 + \left[\ell - T_1 V_f \cos (\gamma + \phi')\right]^2 \tag{B16}$$

Also

$$\ell = V_t (T - T_1) \tag{B17}$$

Setting the derivative $dZ/dT_1 = 0$ gives

$$T_1 = T\,(M_t/M_c)\cos\alpha' \tag{B18}$$

$$Z = c_o\,T\,M_t\,M_z/M_c$$

Note that the z' axis is aligned with the line Z. Also, M_r represents the Mach number of the blade relative to the fluid, neglecting the spanwise component of Mach number given by equation (B2); i.e.,

$$M_c^2 = M_z^2 + \left[M_t + M_f \cos\,(\gamma + \phi')\right]^2 \tag{B19}$$

If M_t is significantly greater than M_z and M_f, the eddy chopping time T_1 will be approximately equal to the blade passing time, T.

The autocorrelation function of the far-field noise can be written

$$R_{pp}\,(\tau) = E\left[P\,(t)\,P(t+\tau)\right] \tag{B20}$$

where E denotes an expected value is to be taken. The autocorrelation function has a maximum for $\tau = 0$. As τ deviates from zero, R_{pp} decays rapidly until τ begins to approach T_1. For τ near $\pm nT_1$, R_{pp} reaches local maxima, as sketched in figure 25, since the eddy that was chopped at $\tau = 0$ is being chopped again. Each of those peaks represents the cross-correlation of the sound from one blade passage with the sound from a different blade passage; for example, the n^{th} peak represents the cross-correlation of the sound from the zeroth passage with that from the n^{th} blade passage. Thus, R_{pp} can be written

$$R_{pp}\,(\tau, \gamma, \underline{x}) = \sum_{n=-\infty}^{\infty} R_{pp}^{(n)}\,(\tau - nT_1, \gamma, \underline{x}) \tag{B21}$$

where $R_{pp}^{(n)}(\tau)$ represents the cross-correlation of the far-field sound from the zeroth blade passage with that from the n^{th} blade passage.

Since correlation functions R_{pp} and spectrum functions S_{pp} are Fourier transforms of one another, equation (B21) gives

$$S_{pp}(\omega_o, \gamma, \underline{x}) = \frac{1}{2\pi}\int_{-\infty}^{\infty} R_{pp}(\tau, \gamma, \underline{x}) e^{-in\omega_o \tau} d\tau \quad = \sum_{n=-\infty}^{\infty} S_{pp}^{(n)}(\omega_o, \gamma, \underline{x})\, e^{in\omega_o T_1} \qquad \text{(B22)}$$

The subscript, o, on ω_o is to differentiate the observed frequency from ω which will later be used to represent the frequency in a coordinate system fixed to the rotor blade.

The spectrum $S_{pp}^{(o)}(\omega)$ for an airfoil encountering turbulence was given in reference 11. This must be generalized here to the case $n \neq 0$. The coordinate system is unprimed here for comparison with the previous derivation in reference 11. For an airfoil in a plane z = constant encountering a gust of the form

$$w(k_x, k_y, k_z) = w_o e^{i\left[k_x(x - v_c t) + k_y y + k_z z\right]} \qquad \text{(B23)}$$

the airfoil pressure jump can be written

$$\Delta P = 2\pi \rho_o b V_c w_o g(x, k_x, k_y) e^{i(k_y y + k_z z - k_x v_r t)} \qquad \text{(B24)}$$

This defines the airfoil response function g. The pressure jump due to all gusts is then

$$\Delta P = 2\pi \rho_o b V_r \int_{-\infty}^{\infty}\int\int w(k_x, k_y, k_z)\, g(x, k_x, k_y) e^{i(k_y y + k_z z - k_x v_c t)} dk_x dk_y dk_z \qquad \text{(B25)}$$

The cross correlation $R_{qq}^{(n)}$ of the surface pressure on the zeroth blade passage with that on the n^{th} passage is found by taking the expected value of the product $\Delta P(0)\Delta P^*(nZ)$

$$R_{qq}^{(n)}(\tau) = (2\pi\rho_o b V_c)^2 \iiint_{-\infty}^{\infty} \Phi_{ww}(\underline{k})\, g^*(x_1,k_x,k_y)\, g(x_2,k_x,k_y)$$
$$e^{i\left[k_y\eta + k_x\tau V_c + nZk_z\right]} dk_x\, dk_y\, dk_z \qquad \text{(B26)}$$

where $\tau = t_1 - t_2$, $\eta = y_1 - y_2$, Z is given by equation (A18) and where the relation

$$E\left[w(k_x,k_y,k_z)\, w^*(k_x',k_y',k_z')\right] = \Phi_{ww}(k_x,k_y,k_z)\quad \delta(k_x-k_x')\,\delta(k_y-k_y')\,\delta(k_z-k_z') \qquad \text{(B27)}$$

was used. The symbol E denotes the expected value and Φ_{ww} is the spectrum of the turbulence. Taking the Fourier transform of equation (B26) with respect to τ gives the frequency spectrum

$$S_{qq}^{(n)}(\omega) = (2\pi\rho_o b)^2\, V_c \int_{-\infty}^{\infty} \tilde{\Phi}_{ww}(K_x,k_y,nZ)\, g^*(x_1,K_x,k_y)\, g(x_2,K_x,k_y)\, e^{ik_y\eta} dk_y \qquad \text{(B28)}$$

where
$$K_x = \omega/V_c$$
$$\tilde{\Phi}_{ww}(k_x,k_y,nZ) = \int_{-\infty}^{\infty} \Phi_{ww}(k_x,k_y,k_z)\, e^{inZk_z} dk_z \qquad \text{(B29)}$$

Equation (B28) is the same as equation (11) of reference 11, the only difference being that $n \neq 0$ in equation (B29) above.

Introducing this generalization into equation (15) of reference 11 gives for $S_{pp}^{(n)}$

$$S_{pp}^{(n)}(\omega,\underline{x}') = \left(\frac{\omega z'\rho_o b}{C_o\sigma'^2}\right)^2 \pi V_c d \left|\mathcal{L}(x',K_x,K_y)\right|^2 \tilde{\Phi}(K_x,K_y,nZ) \qquad \text{(B30)}$$

where
$$K_y = \omega y'/(C_o\sigma')$$
$$\mathcal{L} = \int_{-b}^{b} g(\xi,K_x,K_y,M_c)\, e^{i\xi K_y x'/y'} d\xi \qquad \text{(B31)}$$
$$\sigma'^2 = x'^2 + \beta^2(y'^2 + z'^2)$$

Equation (B30) gives the acoustic spectrum produced by an airfoil encountering turbulence as measured by an observer fixed with respect to the airfoil. A Doppler shift must now be applied to determine the spectrum in a ground fixed or direct system. Equation (12) of reference 38 gives for the ratio between observed and source frequencies, for a far-field observer

$$\frac{\omega}{\omega_o} = 1 + \frac{\underline{M}_t \cdot \hat{OS}}{1 - \underline{M}_s \cdot \hat{OS}} \tag{B32}$$

where

ω_o = observed frequency

ω = source frequency

$\underline{M}_t$ = Mach number of source relative to observer

$\underline{M}_s$ = Mach number of source relative to fluid

$\hat{OS}$ = unit vector from retarded source position to observer

In vector notation

$$\underline{M}_t = M_t(-\hat{i}\sin\gamma + \hat{j}\cos\gamma)$$

$$\underline{M}_s = \hat{i}\,(M_f \sin\phi' - M_t \sin\gamma) + \hat{j}\,(M_f \cos\phi' + M_t \cos\gamma) + \hat{K}\,M_z \tag{B33}$$

where $\hat{i}$, $\hat{j}$, $\hat{k}$ are the unit vectors in the x, y and z direction. The vector $\underline{OS}$ is

$$\underline{OS} = \hat{i}(x - x_s) + \hat{j}(y - y_s) + \hat{K}(z - z_s) \tag{B34}$$

Using equation (A6) and the fact that $|\underline{OS}| = r_e$ gives

$$\hat{OS} = \hat{i}\,(x/r_e + M_f \sin\phi') + \hat{j}\,M_f \cos\phi' + \hat{K}\,(z/r_e + M_z) \tag{B35}$$

The final result for ω/ω_o is then

$$\omega/\omega_o = 1 + M_t \left[x \sin\gamma - M_f r_e \cos(\gamma + \phi')\right] \Big/ \left[(1-M_f^2 - M_z^2) r_e + x M_f \sin\phi' - z M_z\right] \quad \text{(B36)}$$

Applying the Doppler factor to equation (B30) and substituting in equation (B22) gives for the "instantaneous spectrum"

$$S_{pp}(\omega_o, \gamma, \underline{X}) = \left(\frac{\pi\omega\rho_o b z' M_c |\mathcal{L}|}{c_o \sigma'^2}\right)^2 \frac{2d}{T M_t M_z} \frac{\omega}{\omega_o} \sum_{n=-\infty}^{\infty} \Phi(K_x, K_y, K_z^{(n)}) \quad \text{(B37)}$$

where $$K_z^{(n)} = \frac{1}{V_z}\left(\omega_o \cos\alpha' + \frac{2\pi n M_r}{T M_t}\right)$$

In the above expression, Φ must be expressed in the primed coordinate system. If the turbulence is isotropic, of course, the orientation of the coordinate system in which Φ is expressed is immaterial. For nonisotropic turbulence the coordinate system orientation must be considered.

Equation (B37) gives only the "instantaneous spectrum", i.e., the spectrum produced by an airfoil moving rectilinearly at a particular value of γ. As the blade moves around the azimuth, this "instantaneous spectrum" is averaged. Thus, to find actual spectrum an average over γ of equation (B37) must be made. However, a straight average cannot be taken. Rather a weighting factor must be introduced to account for the fact that the rotor spends different amounts of retarded time at different azimuthal locations. This factor is, in fact, the ratio of source to observed frequency ω/ω_o given by equation (B36). In effect, the source can be thought of as a kind of clock with frequency ω. The observed frequency ω_o then indicates the passage of time on the rotor as measured by the observer; i.e., ω_o indicates retarded time.

The final expression for the average far-field noise for B blade segments of semi-span d rotating at radius R is then

$$\overline{S_{pp}}\,(\omega_o, \underline{X}) = \frac{\pi d}{V_z R}\left(\frac{B\rho_o b}{\omega_o}\right)^2 \int_0^{2\pi}\left(\frac{\omega^2 z' M_r |\mathscr{L}|}{\sigma'^2}\right)^2 \sum_{n=-\infty}^{\infty} \Phi_{ww}(K_x, K_y, K_z^{(n)})\, d\gamma \tag{B38}$$

where $T = 2\pi\ R/BV_t$ was introduced. The primed coordinates are given by equation (A15), ω by equation (B36) and $\mathscr{L}$ by equation (B31). A review of the airfoil response function g for a skewed gust in compressible flow is given, for example, in references 40-42.

The summation and integral in equation (B38) are carried out numerically. However, when the change in $K_z^{(n)}$ is small compared with K_x ($K_z^{(n)} - K_z^{(n-1)} << K_x$) the summation can be approximated by an integral. This can be carried out in closed form for certain analytical expressions for the turbulence spectrum Φ, among them being the isotropic turbulence spectrum of von Kármán.

APPENDIX C

Grid Turbulence Spectra and Correlations

The upper portion of figure 26 compares measured axial correlations of the axial turbulence velocity component for various grids at a tunnel speed of 9 m/sec. with the von Kármán correlation for isotropic turbulence (reference 16). The spatial longitudinal correlation coefficient, f(x), was obtained from autocorrelation measurements by using Taylor's frozen-flow hypothesis (reference 16) to convert from a temporal to spatial frame.

The lower portion of figure 26 compares measured wavenumber spectra of the axial turbulence velocity component with the isotropic spectrum derived from the von Kármán interpolation formula (reference 16). Both the measured correlations and spectra displayed good agreement with the von Kármán formulation. Based on these results, the von Kármán formulation was used in the theoretical noise prediction method.

APPENDIX D

Data Acquisition and Processing for Outdoor Hover Experimentation

Experimental Arrangement - The hot film probe arrangement employed during hover testing is shown schematically in the upper portion of figure 27 (photographs are shown in figure 13). The upper probe was fixed at a 59 percent radius (span) position, 2.2 chords in front of the plane of rotation. A second probe, capable of traverse in the vertical direction, was located in the same axial plane but at variable distances, ξ, below the fixed probe.

Lacking previous rotor inflow turbulence data to offer guidance, the radial position of the fixed probe and the direction of traverse of the moveable probe were selected on the basis of convenience. Since the tip region would be expected to be the dominant noise producing region, determination of inflow properties near the tip was desirable. Conversely, the transverse turbulence length scale was not known in advance of testing. If it were large and the fixed probe were positioned near the tip, the traversing probe would pass out of the projection of the rotor disk on the measurement plane while significant correlation existed. It was therefore decided to locate the fixed probe inboard from the tip.

A vertical traverse of the moveable probe was used because it was not considered critical to generate transverse cross-correlation data along coordinate lines (radial or azimuthal).

The measurement plane selected was the closest to the disk that avoided probe-blade interference. A blade restraining disk was installed on the hub to prevent such interference during rig start-up and shutdown; prior to installation, a blade was damaged when wind blew the blade into the plane of the probe. This restraining disk was visually observed not to interfere with coning during operation.

Data Acquisition System - The lower portion of figure 27 shows the data acquisition system employed for outdoor hover testing. Signals from the two hot-film probes, the far-field microphone, cup anemometer and a once-per-revolution shaft pickup were tape recorded simultaneously.

Linearizers were employed in the anemometer circuitry for convenience rather than necessity. On the other hand, a D.C. coupled system was required due to the low frequency nature of the atmospheric turbulence. This in turn required a calibrated D.C. suppression capability at the linearizer output. If the D.C. voltage were not suppressed at the recorder input, the high ratio of D.C. to A.C. signal level (order of 50) would have placed A.C. information near the noise floor of the recorder.

Data Reduction System - Figure 28, part (a) shows the instrumentation arrangement for outdoor hover data reduction. The tape-recorded hot-film probe signals were processed through 30 Hz low-pass filters, operated in either a D.C.-pass or attenuate (high pass) mode. The reasons for these filtering arrangements are discussed subsequently. The filter signal was input to a D.C. coupled, 100 line, real-time correlator. The correlator computation was started at the same tape record position used to analyze microphone data and averaged for approximately the same time.

Far-field noise was spectrum analyzed using a 500 line, real-time, narrowband analyzer and ensemble averager. Wind speed was recorded on a printer at one second intervals.

Figure 28, part (b), shows the measured attenuation characteristics of the filters at low frequency when operated in a D.C. attenuate (high pass) mode. While suppressing D.C., there was only a small loss of low frequency signal content associated with use of the filters.

Low Pass Filtering - Low pass filtering of the hot-film signals was required to prevent the contribution of the particle velocity of the rotor acoustic near field at shaft and blade passage frequencies from contaminating the inflow turbulent velocity signal. The need for this is apparent in figure 29, part (a).

The upper spectrum shows the unfiltered hot-film signal. Without filtering, measured overall root-mean-square (rms) inflow turbulence level would be high due to the strong BPF tone and weaker 1-p tone. In addition to causing an overestimate of rms turbulence levels, part (b) shows that calculation of a turbulence autocorrelation function from the unfiltered hot-film would be impossible. Aliasing of the BPF noise signal caused an apparent 34 Hz pure tone which resulted in a periodic autocorrelation function; Eulerian time scale and hence turbulence axial length scale could not be calculated from this distorted function.

By low-pass filtering at 120 Hz, the second curve in figure 29, part (b) shows the distortion caused by BPF noise was removed although shaft frequency noise continued to cause some oscillations in the function. The third curve shows that use of a low pass filter, set at a cut-off frequency of 30 Hz, eliminated acoustic field contamination. Such filtering of the hot-film signal was used in the determination of overall rms turbulence levels and autocorrelation functions in the outdoor hover phase of the present study.

The effect of this filtering on the hot-film spectrum is shown in the lower curve of figure 29, part (a). The only concern would be whether this filtering caused significant error in the measured rms level of turbulence or affected determination of the Eulerian length scale. The spectrum level was down 13 dB from the zero-frequency peak level at the frequency where

the filter began to attenuate the signal. Based on the shape of the spectrum, it is estimated that the resultant error in overall rms level due to filtering was less than 10 percent. Since a 10 percent error would cause an error of only 0.8 dB in the prediction of hover noise levels, this was not considered significant.

Relative to Eulerian time scale determination, figure 29 shows that a change in low pass cutoff frequency from 120 to 30 Hz had only a small influence on the autocorrelation function, primarily an elimination of the 1-p oscillation. Since the spectrum level at 120 Hz was down over 20 dB from the zero frequency level (a factor of 10 on a linear voltage basis) and the autocorrelation function weights contributions on a linear basis, negligible error would be expected from suppression of frequencies about 120 Hz (and by the previous argument, 30 Hz).

High Pass Filtering - High pass filtering (using the filter characteristic shown in figure 28, part (b)) was employed in the computation of autocorrelation functions. These functions in turn were used to calculate overall rms levels of turbulence and the Eulerian time scales.

Overall rms level was calculated from the zero time delay value of the autocorrelation function. This was used in lieu of a true rms meter because these meters cause a greater attenuation of low frequencies when operated with a time constant (averaging time) consistent with the available tape record length (one minute).

The reason for high pass filtering is evident from a consideration of figure 30. The upper portion shows an autocorrelation function computed from a high pass filtered signal whereas the lower portion shows a typical function computed from a D.C. coupled signal. In the filtered case, the overall rms level was the square root of the zero time delay value; at long delay time the function approached an asymptote of zero.

In the unfiltered case, the function asymptotes to an unknown D.C. level at long delay time. An estimate must be made of this level and then rms level computed from the square-root of the difference between the zero time delay and D.C. level. As shown by the sample calculations in the figure, computed rms levels vary by 17 percent depending on the assumed D.C. asymptote.

The problem cannot be solved simply by using larger sample increments and thereby calculating the value of the autocorrelation function at long delay time; this is because the number of averages performed by the correlator per unit record length decreases directly with sample increment. For a tape record of fixed length, the longer sample increment will therefore result in a correlation function with lower statistical confidence level. It was not

obvious that this problem could be eliminated by simply recording for a longer period of time since the inflow statistics were nonstationary. In addition, a wind gust can cause rotor noise to be generated by the additional mechanism of tip vortex interaction. By recording for relatively short time periods, which were free of wind gusts, this additional contribution to noise could be avoided.

While determination of the rms level of turbulence was difficult using an autocorrelation function derived from a hot film signal containing a D.C. component, calculation of Eulerian time scale, J_u, was more difficult. The upper portion of figure 30 shows the uncertainty in selecting a value of J_u corresponding to a 1/e decrease in the value of the function. In the lower portion of the figure this uncertainty is seen to be greater for the D.C. coupled signal. In Case 1, a value of approximately 200 msec. would be estimated whereas in Case 2 (corresponding to a different assumed D.C. asymptote), the value could range from 500 to 800 msec.

Summary - In outdoor hover turbulence ingestion studies it is necessary to measure inflow turbulence statistics in the presence of the acoustic field of the rotor. This requires the contribution of the acoustic field to be suppressed either by low pass filtering the analog signal or band reject filtering at shaft and blade passage frequencies. Furthermore, the non-stationary nature of the inflow requires that some time scale be selected for analysis purposes. This time scale is to some extent arbitrary, however, it is essential that averaging of noise and inflow statistics be performed for the same time period.

In the present study, this time scale was selected to be approximately one minute so as to minimize the effect of wind speed changes. Recording of data was suspended during wind gusts. This in turn required high pass filtering of the hot film signal. Averaging for significantly shorter time periods would have resulted in low spectrum and autocorrelation function confidence levels even if the inflow had been stationary. On the other hand, averaging for significantly longer time periods may have produced good results. The only concern with this latter approach is that the results of wind gusts, which occur intermittently, would be included in the data. Such gusts can blow the rotor tip vortex field into the rotor and thereby generate noise by an additional mechanism.

APPENDIX E

Clean Inflow Noise Spectra

Figure 31 shows noise spectra obtained in a vertical ascent configuration in the wind tunnel under clean inflow conditions (no grids installed in the tunnel inlet). Rotor operating conditions were identical to those employed during outdoor hover testing at a tip Mach number of 0.41 with the exception that the vertical ascent speed was 9.1 m/sec. in the tunnel whereas in outdoor hover the rotor ingested the ambient air. Test conditions for the clean inflow study are given in Table I under Test Condition VA-C-1.

The spectra shown in figure 31 are significantly different from the outdoor hover spectra given in figure 16. Instead of a persistence of high intensity quasi-tonal noise to high frequency, figure 31 shows tones only at BPF and twice BPF. These are attributed to steady blade loading. At higher frequencies, the observed spectra are broadband in nature with a nearly constant level. Although flat spectra of the type observed here are often associated with instrumentation noise, measurements discussed below indicate that this broadband noise was produced by the rotor.

The dashed curves in figure 31 show noise spectra obtained with the rig and wind tunnel operating but with the rotor removed from the hub. The tonal nature of this background noise was caused by bearing and shaft noise in the operating rig. At microphone positions of 70 and 140 deg, microphones of 1.27 cm. dia were employed whereas at the other angles, lower sensitivity 0.635 cm. dia microphones were used. This accounts for the better definition of rig tone noise at 70 and 140 deg; at the other positions, the noise floor of the smaller dynamic range microphones raised the apparent tunnel background noise.

Of importance was that the measured background noise was generally lower than that obtained with the rotor although background noise tones caused some small spikes in the rotor noise spectra. For both the background and rotor noise tests, microphone amplifier settings were held constant. From this it can be concluded that instrumentation noise was not responsible for the higher levels obtained during rotor testing.

The origin of the clean inflow rotor broad band noise shown here has not yet been established. It is believed to be caused by the interaction of the rotor blade turbulent boundary with the trailing edge. The fact that broadband noise appears to show no preferred frequency may be due to the Doppler shift effects which occur at off-axis positions.

APPENDIX F

Scattering of Sound Energy from Harmonic Peaks into Half-Harmonic Troughs

As discussed in the main text relative to hover noise results, turbulence ingestion noise theory predicted large ratios of harmonic peak noise level to half-harmonic noise level. The purpose of this appendix is to estimate the amount of sound energy transfer from the peaks to the troughs that would account for the lower observed ratios. Possible mechanisms for such frequency shifting in the turbulent inflow problem are non-frozen turbulent inflow fields and non-axial inflow velocities. This frequency shifting will be referred to here as scattering.

An estimate of the amount of scattering needed to account for the observed results can be made by comparing the energy in a peak to the energy in a broadband spectrum at the level of the troughs. A simple exponential is chosen to model the spectrum, S, around a harmonic peak. Thus,

$$S = \sum_{n=-\infty}^{\infty} A(\omega)\, e^{-(\omega-\omega_n)^2/\omega_1^2} \qquad \text{(F1)}$$

where $\omega_n = n\omega_o$, ω_o is the radian blade passing frequency, A is a slowly varying function of ω and ω_1 is a constant which determines the rate of decay of a peak as frequency deviates from the center frequency. Denoting by X the difference in dB between a peak and a trough, then

$$X = 10 \log_{10}(S_p/S_t) = 4.34 \left(\frac{\omega_o}{2\omega_1}\right)^2 - 3 \qquad \text{(F2)}$$

where S_p is the spectrum level at a peak and S_t is that at a trough. The -3 is to account for the adjacent peak which also contributes to the level in the trough.

The total energy, E, in the nth peak

$$E_p = 2 \int_{\omega_n}^{\infty} S\, d\omega \simeq A\omega_1\sqrt{\pi} \qquad \text{(F3)}$$

If there were broadband noise at the level S_t, the energy contained between two adjacent trough frequencies would be

$$E_{min} = S_t\omega_o = A\omega_o e^{-(\omega_o/2\omega_1)^2} \qquad (F4)$$

Taking the ratio of equations (F4) and (F3) and eliminating ω_o/ω_1 in favor of X gives

$$\frac{E_{min}}{E_p} = 0.54\sqrt{X+3}\,e^{-(x+3)/4.34} \qquad (F5)$$

This ratio is given in the table below for several values of X.

X (dB)	E_{min}/E_p
10	.10
20	1.3×10^{-2}
30	1.6×10^{-3}
40	1.8×10^{-4}
50	2.0×10^{-5}

This table shows that if there were a 50 dB difference between the peaks and troughs and if 2×10^{-5} of the energy in a peak were scattered to adjacent frequencies, the level in a trough would be raised by 3 dB. If 1.3×10^{-2} of the energy in a peak were scattered, the difference between peak and trough would be decreased to 20 dB.

This strong sensitivity of trough levels to a small amount of frequency shifted (scattered) noise is a possible explanation for the lack of large peak-to-trough ratios in general noise experimentation. In the present case, where wind unsteadiness was present and the rotor produced noise in response to a nonstationary turbulence field, such frequency shifting was the likely cause.

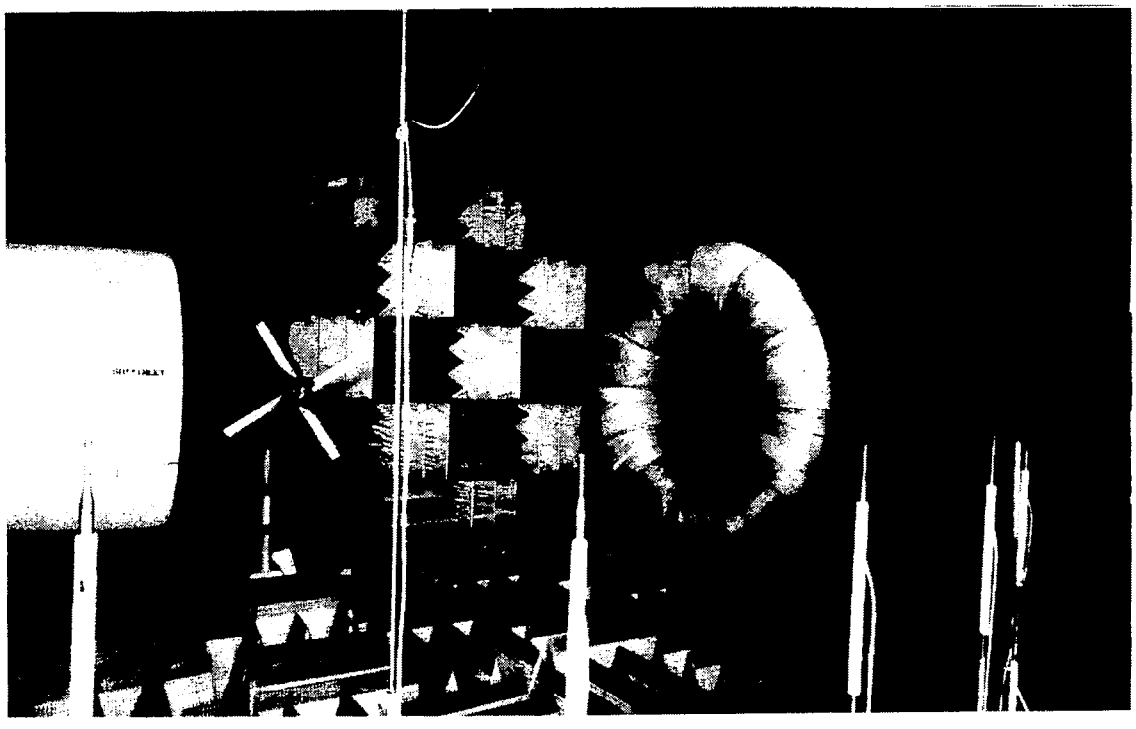

(a) Forward Flight

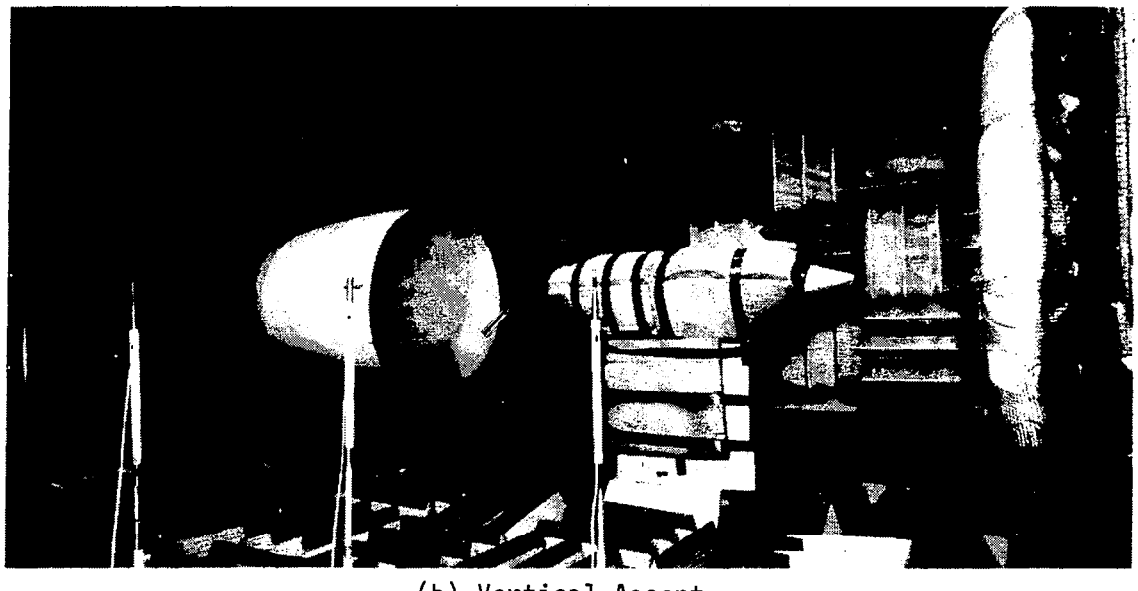

(b) Vertical Ascent

Figure 1 – Wind Tunnel Arrangement

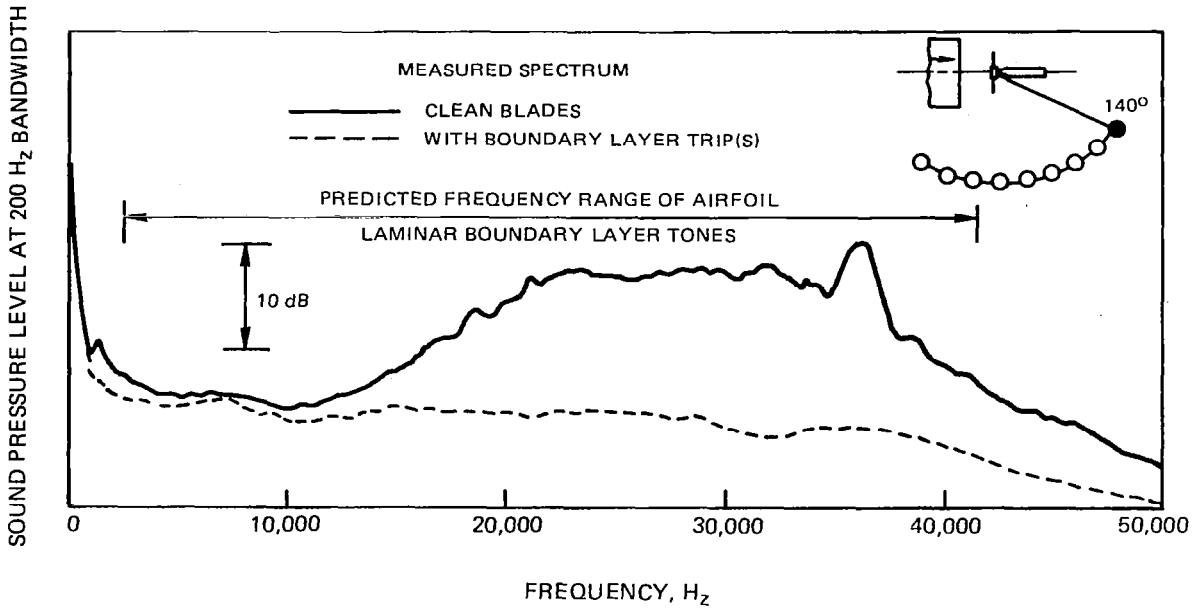

(a) ROTOR SPECTRA AT M_{TIP} = 0.47, TUNNEL SPEED = 9.1 m/SEC

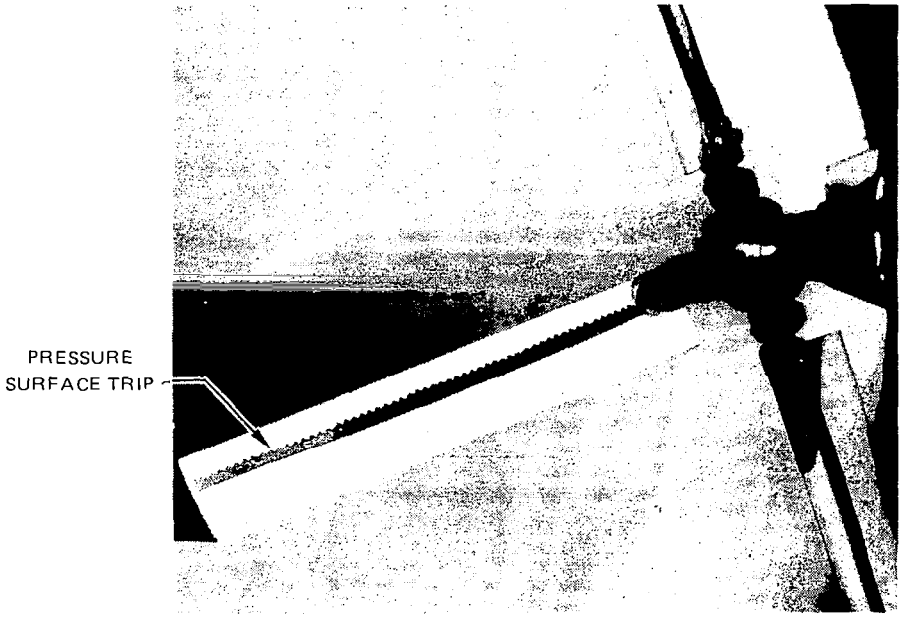

(b) BOUNDARY LAYER TRIP INSTALLATION

Figure 2 – Suppression of Laminar Boundary Layer Discrete Frequency Vortex Shedding

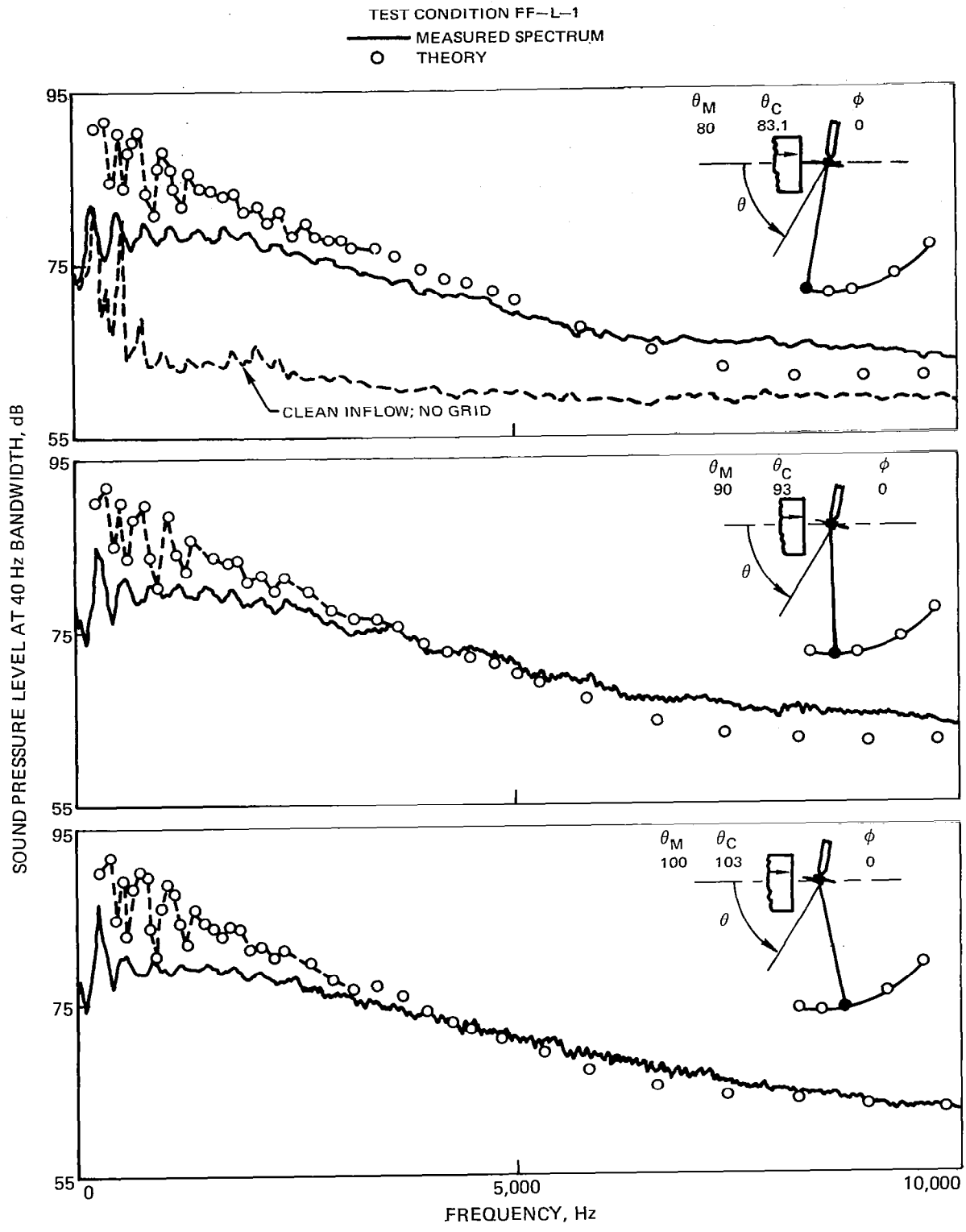

Figure 3 – Rotor Turbulence Ingestion Noise in Simulated Forward Flight (High Turbulence Level)

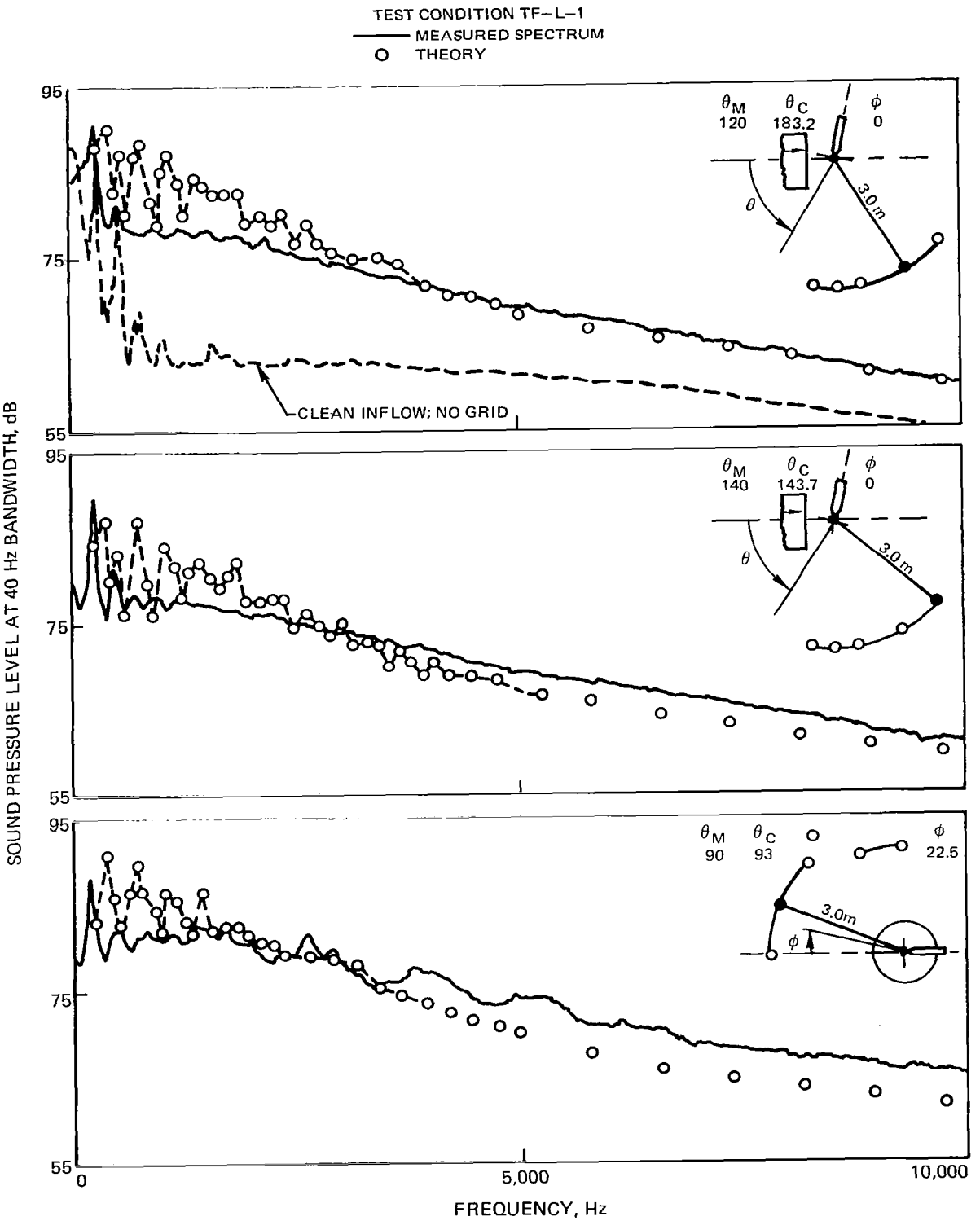

Figure 3 – Continued

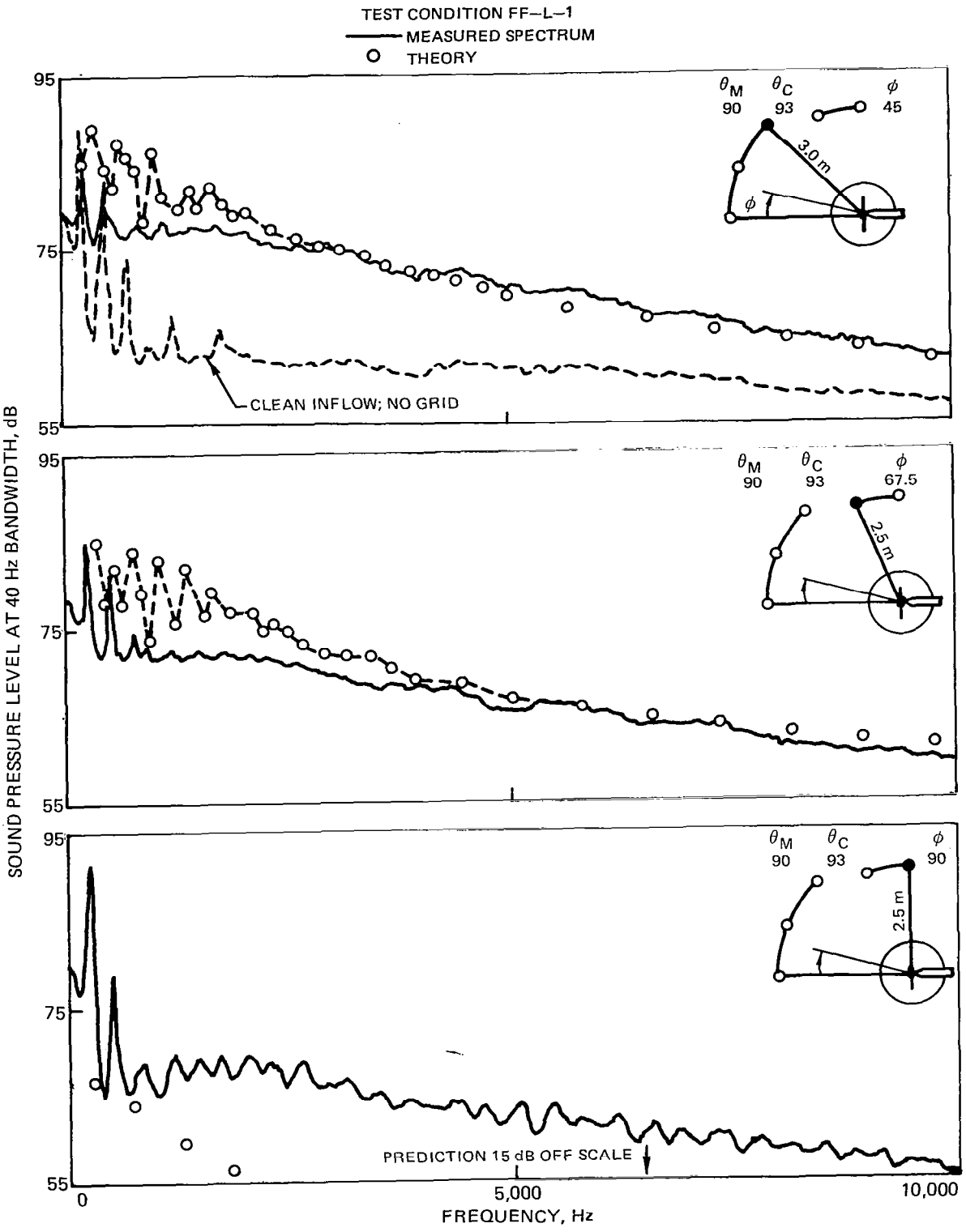

Figure 3 — Concluded

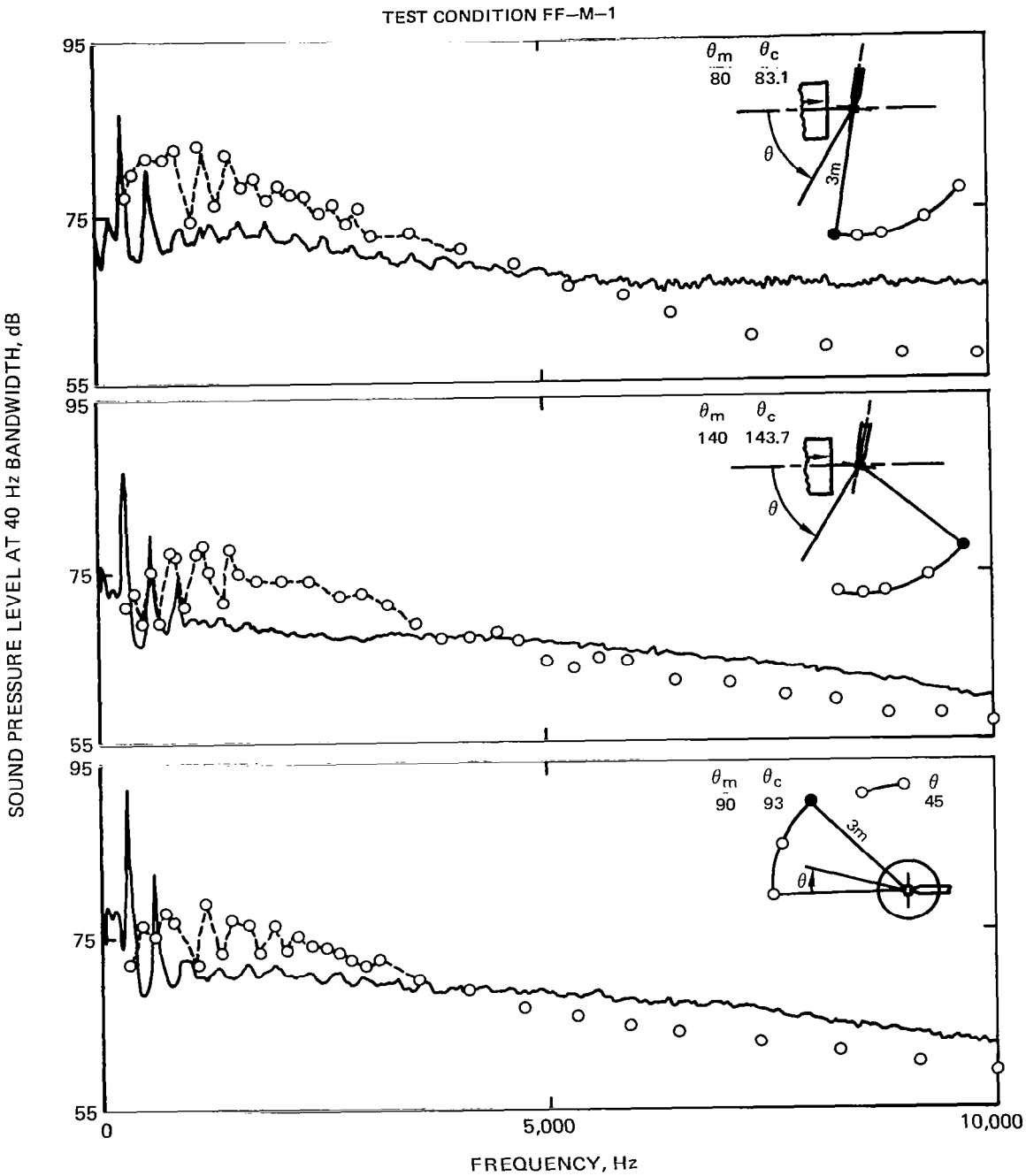

Figure 4 – Rotor Turbulence Ingestion Noise in Simulated Forward Flight (Moderate Turbulence Level)

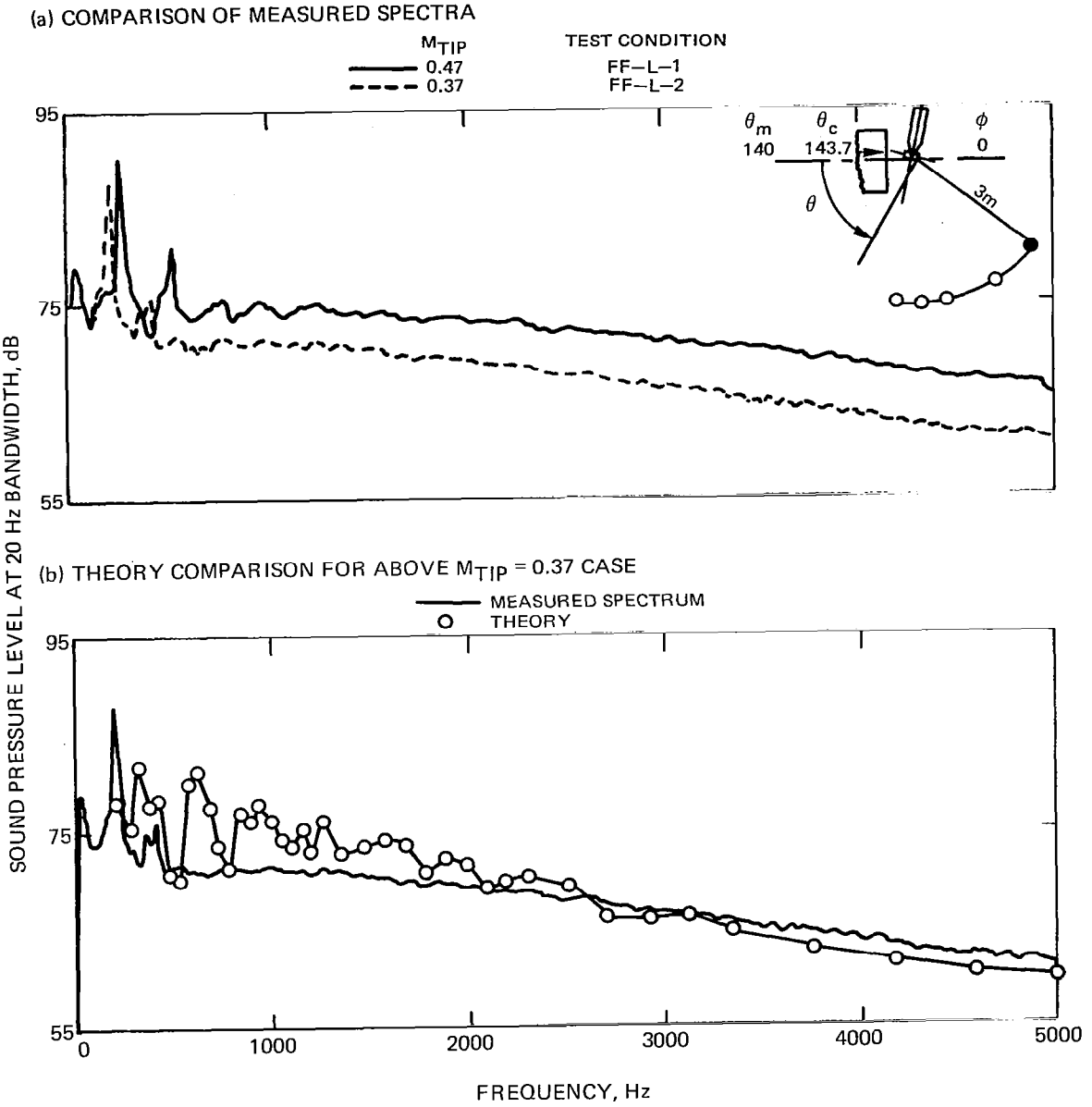

Figure 5— Effect of Rotor Tip Mach Number on Forward Flight Turbulence Ingestion Noise (High Turbulence Level)

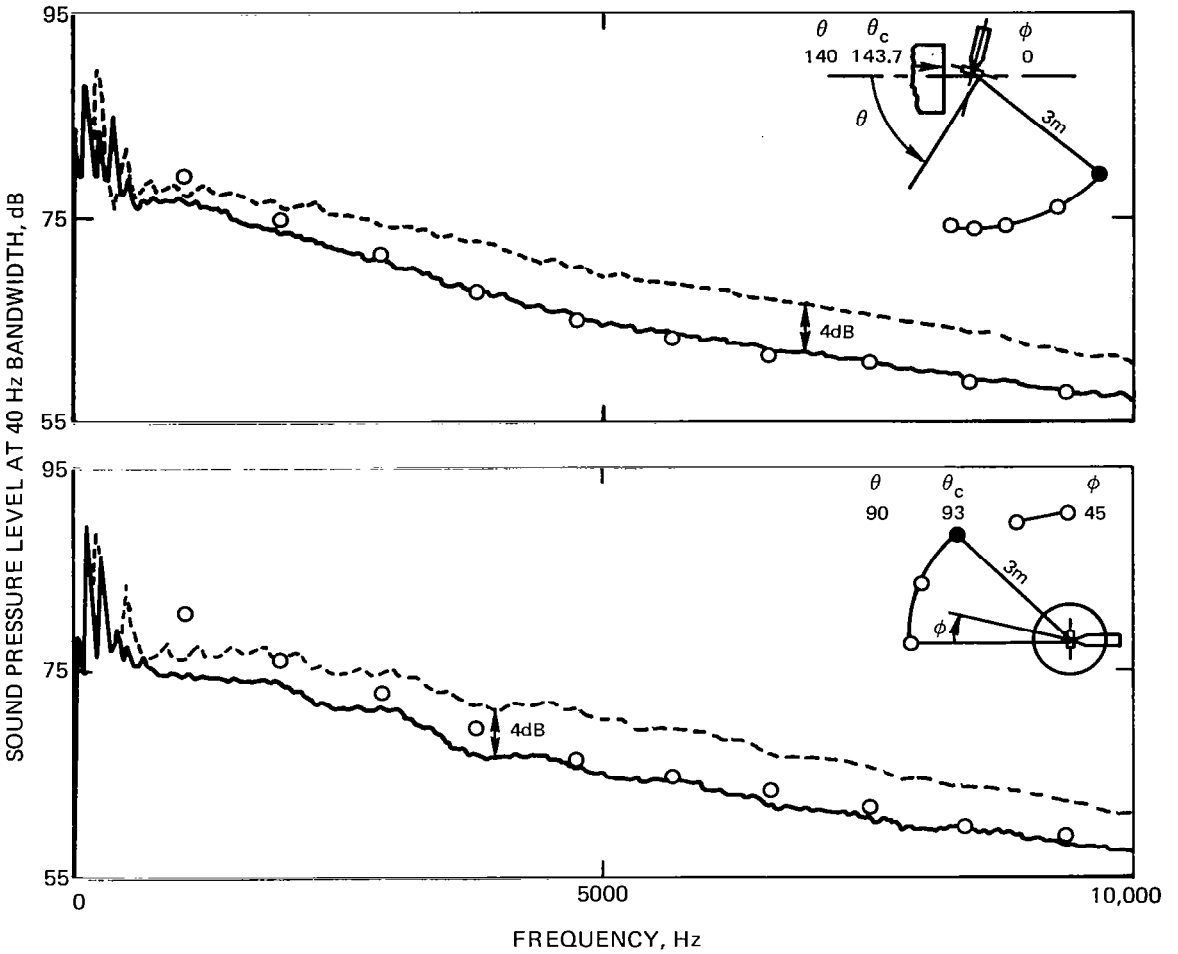

MEASURED SPECTRUM	BLADES	TEST CONDITION
———	2	FF–L–3
- - - - -	4	FF–L–1
O THEORY FOR 2 BLADED CASE		

Figure 6— Effect of Blade Number on Forward Flight Turbulence Ingestion Noise (High Turbulence Level)

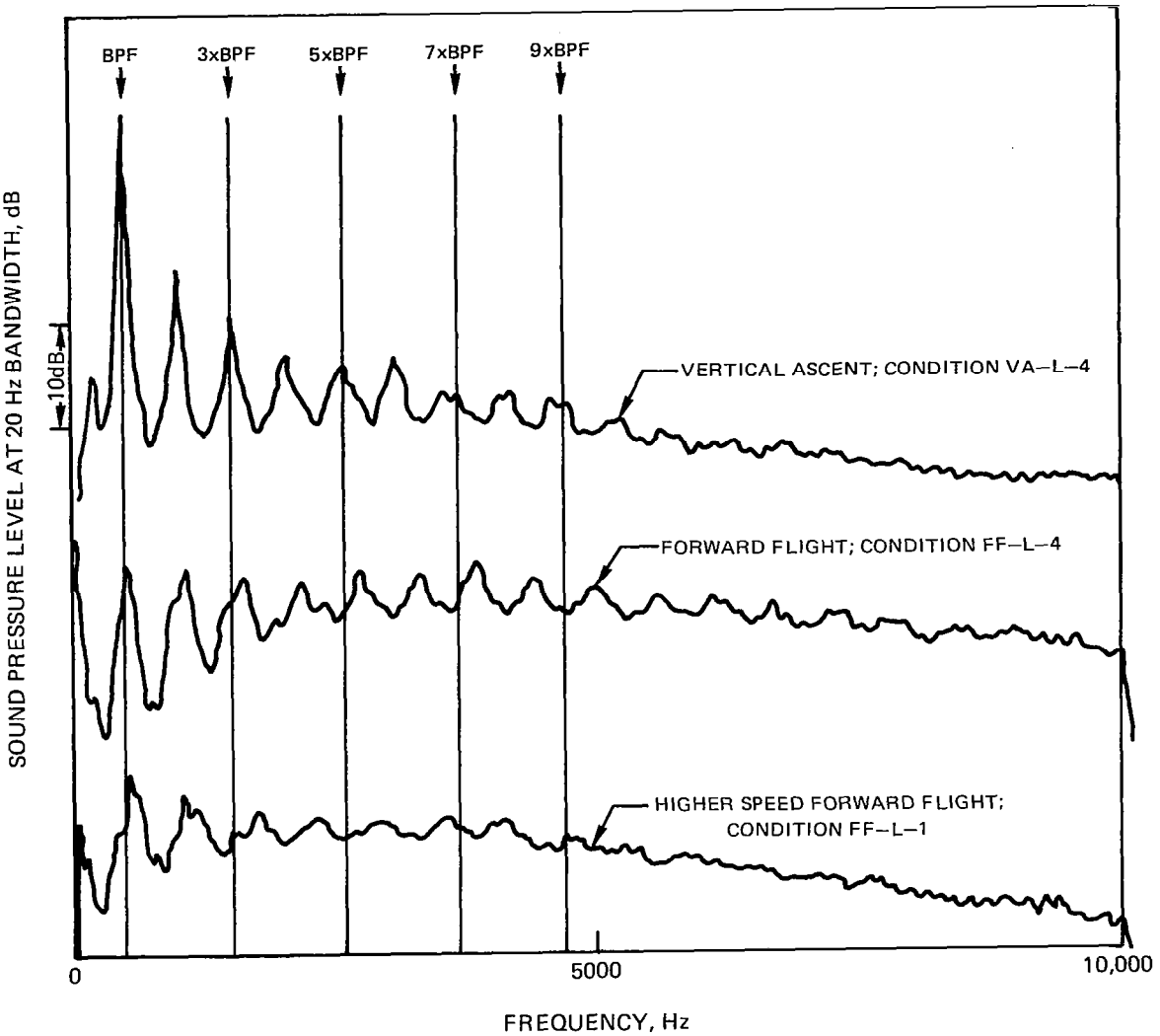

Figure 7– Effect of Skewed Inflow on Narrowband Random Noise Peak Frequencies

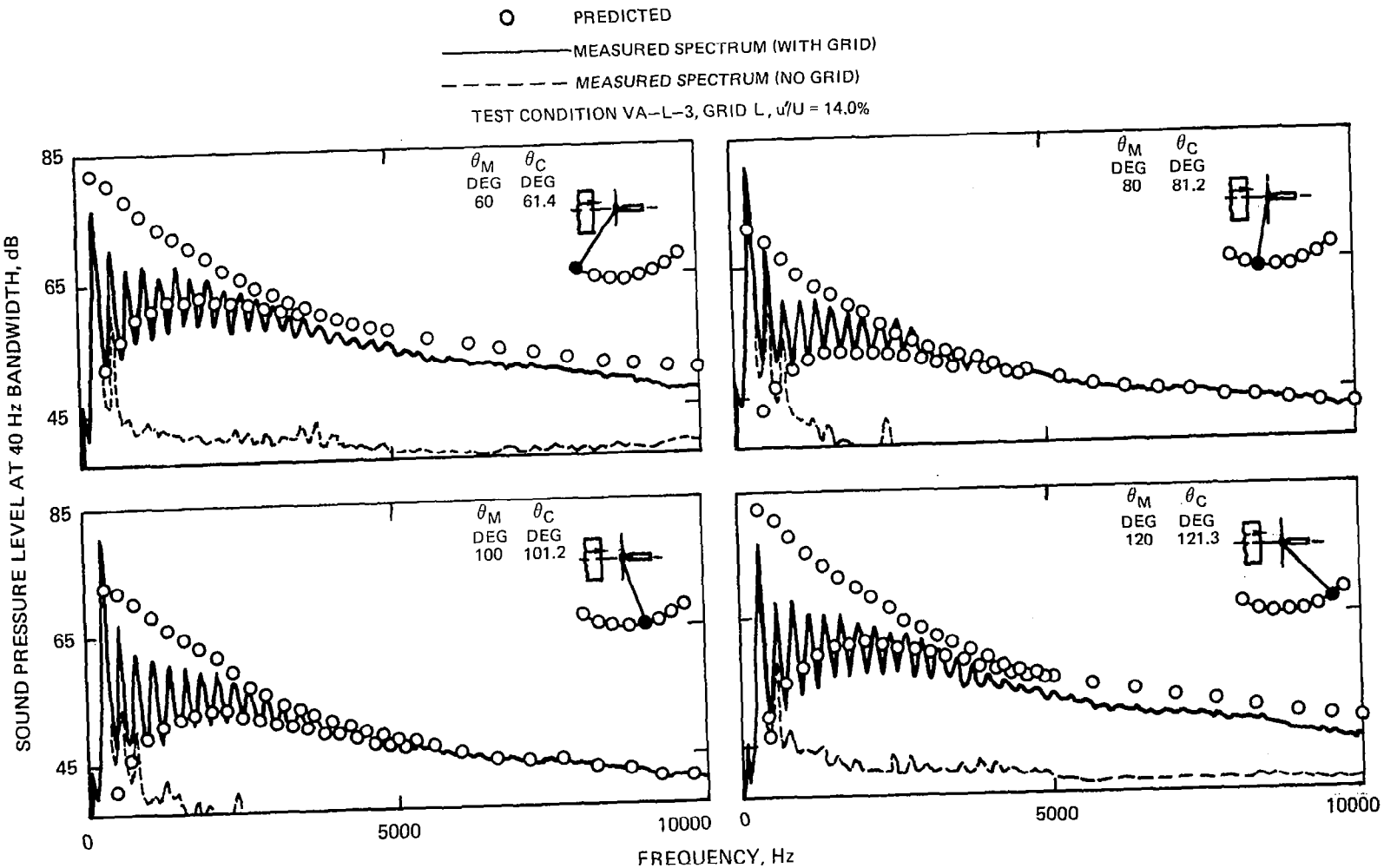

Figure 8 — Rotor Turbulence Ingestion Noise in Vertical Ascent (High Turbulence Level)

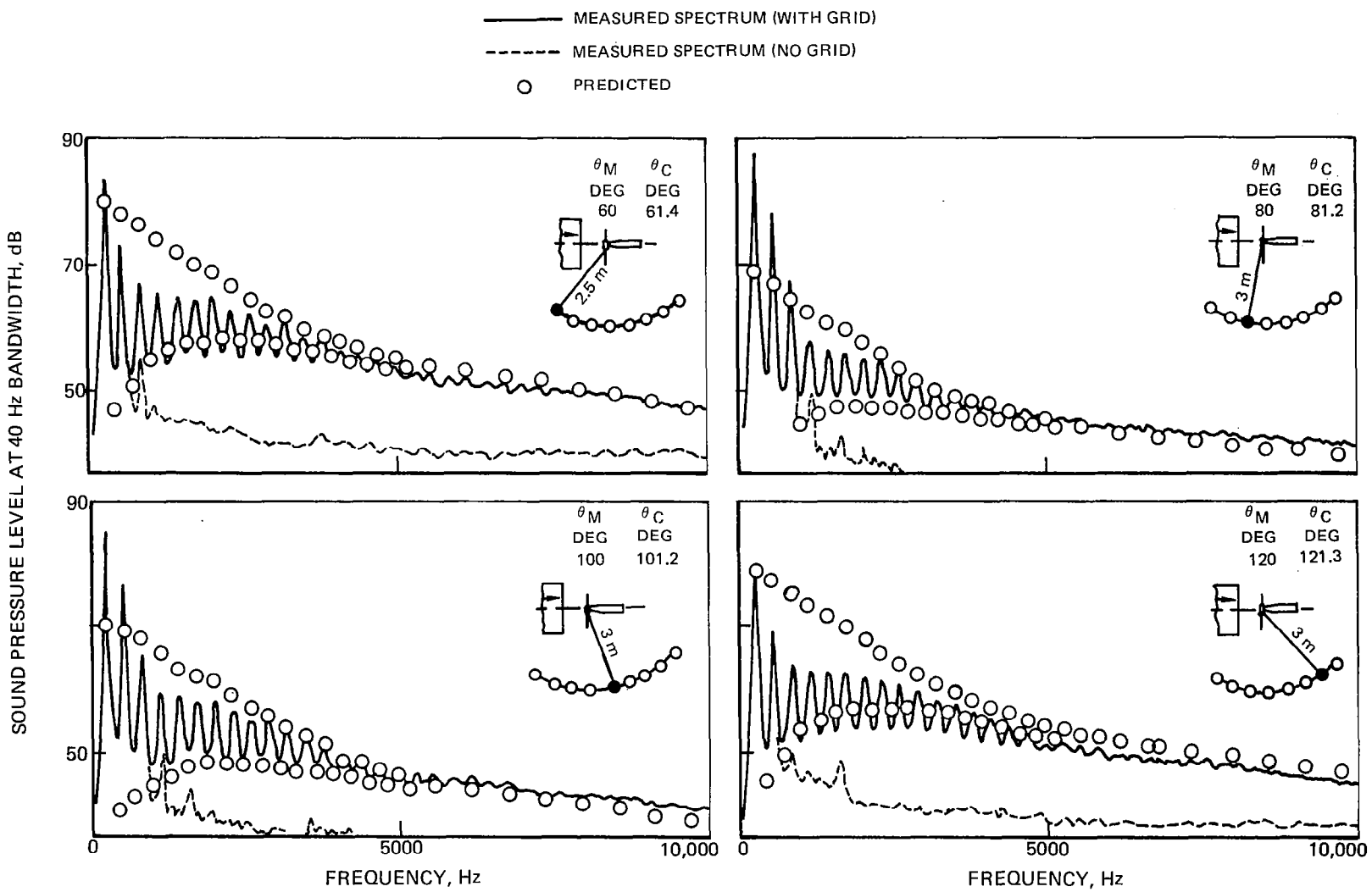

Figure 9 — Rotor Turbulence Ingestion Noise in Vertical Ascent (Moderate Turbulence Level)

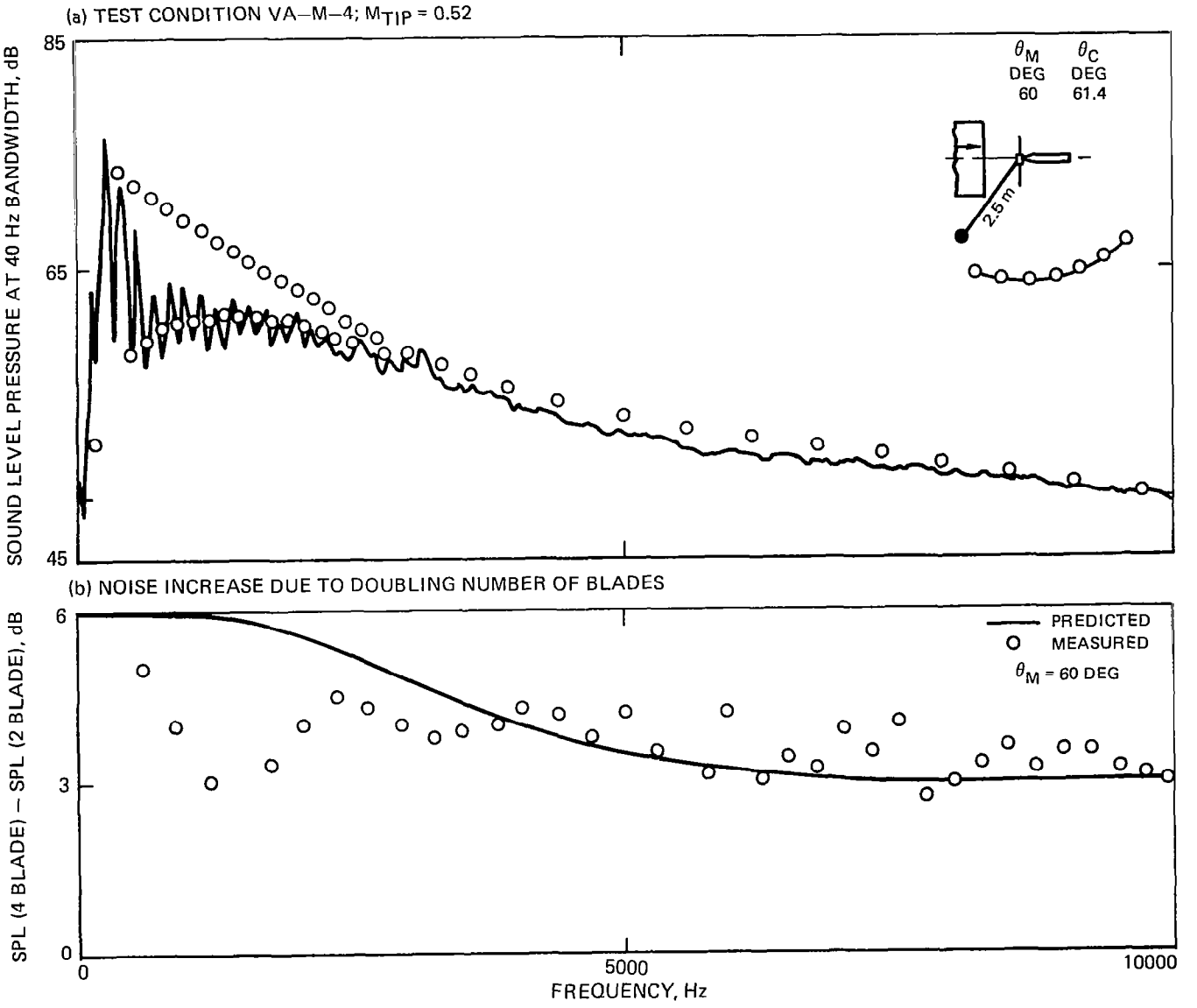

Figure 10 – Effect of Number of Blades on Turbulence Ingestion Noise

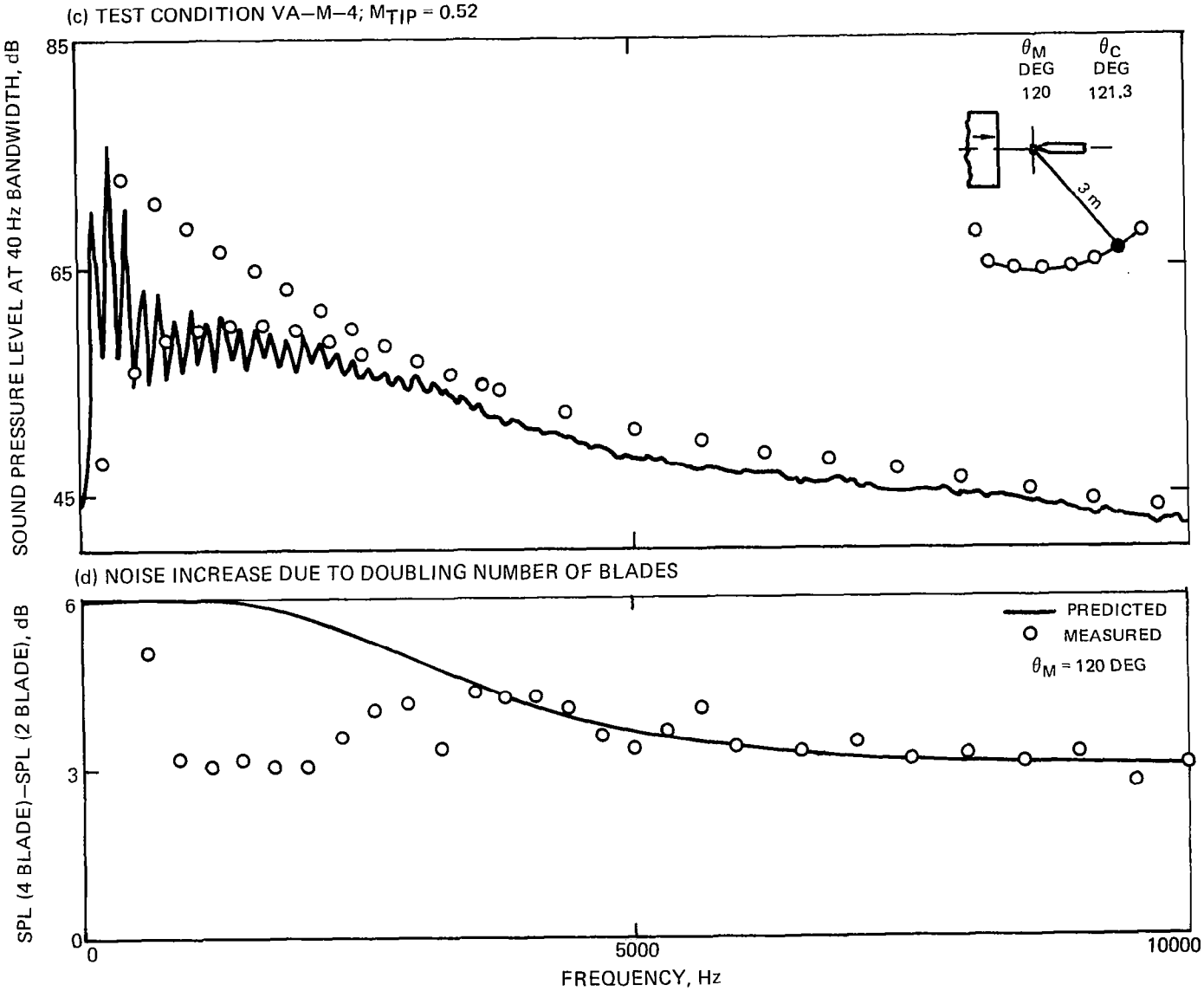

Figure 10 — Concluded

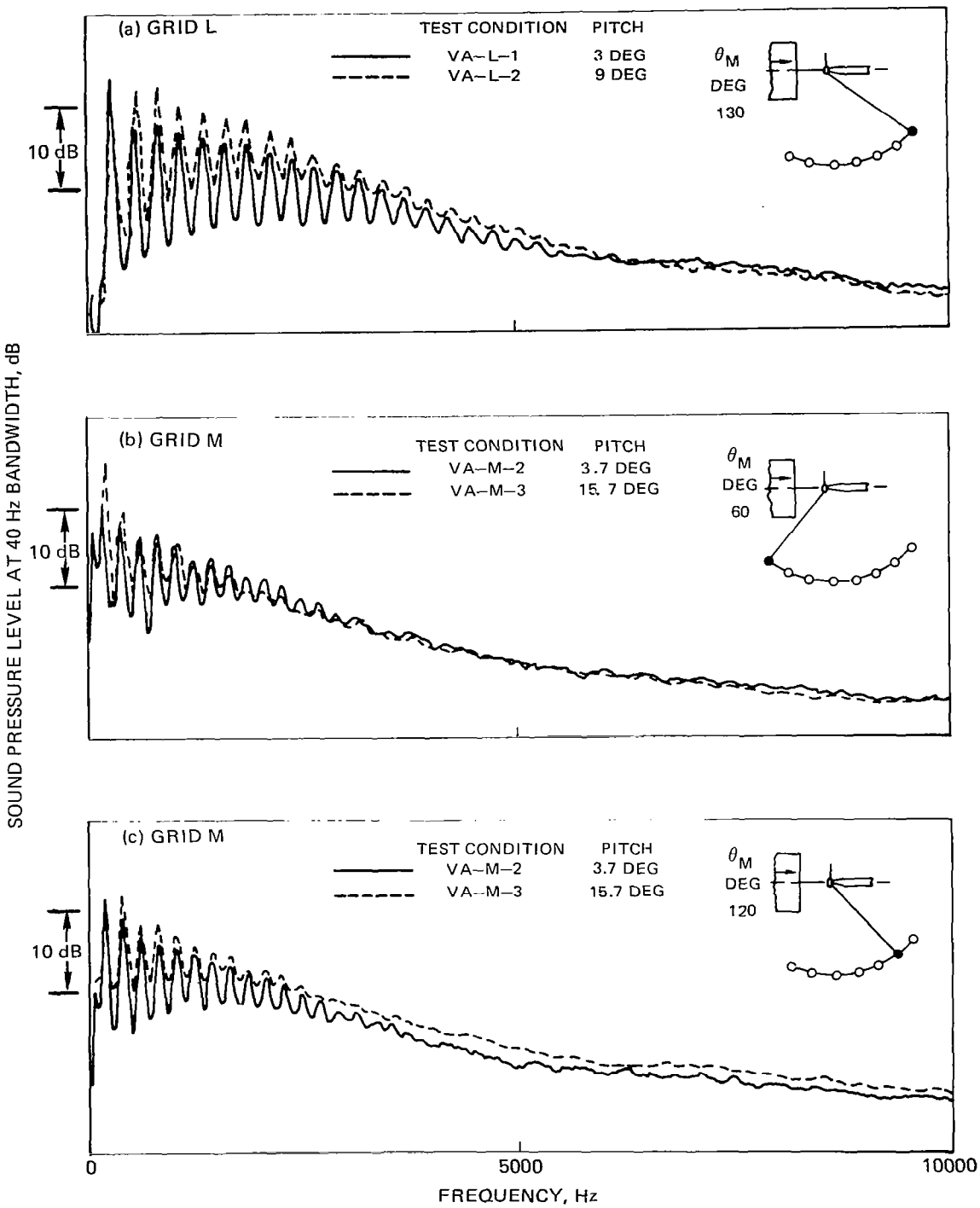

Figure 11 – Effect of Blade Pitch on Turbulence Ingestion Noise

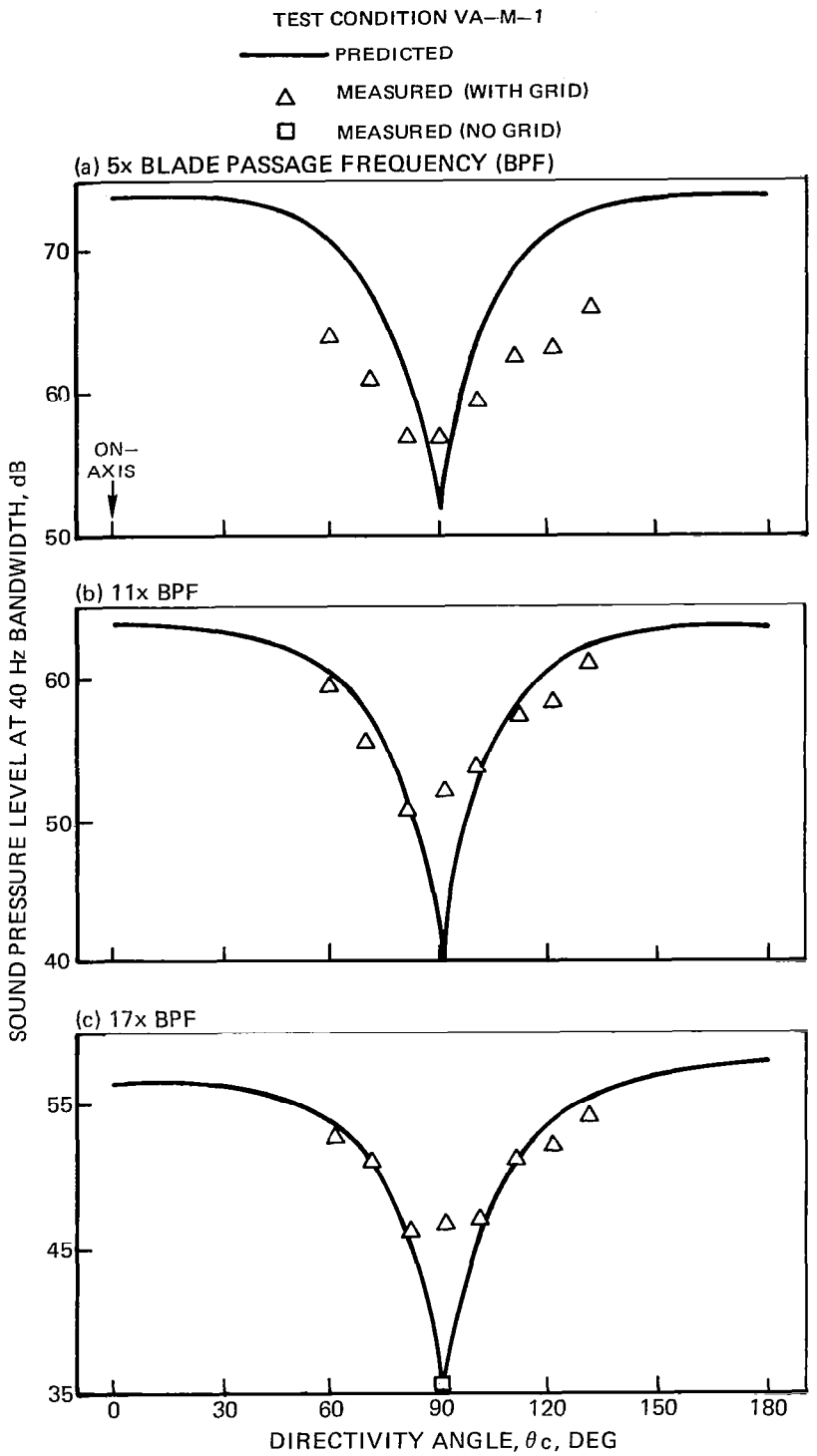

Figure 12 – Directivity of Turbulence Ingestion Noise

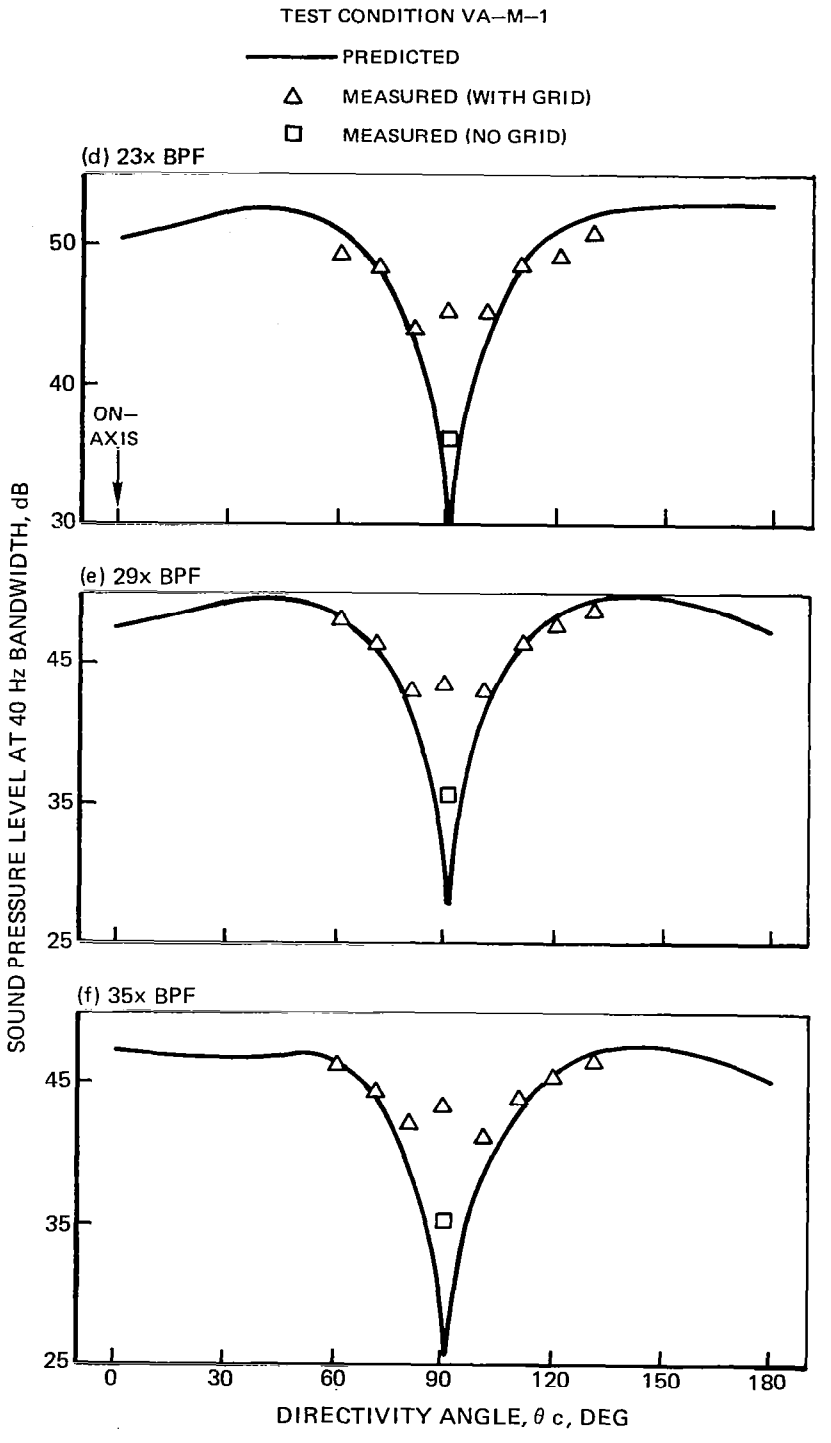

Figure 12 – Concluded

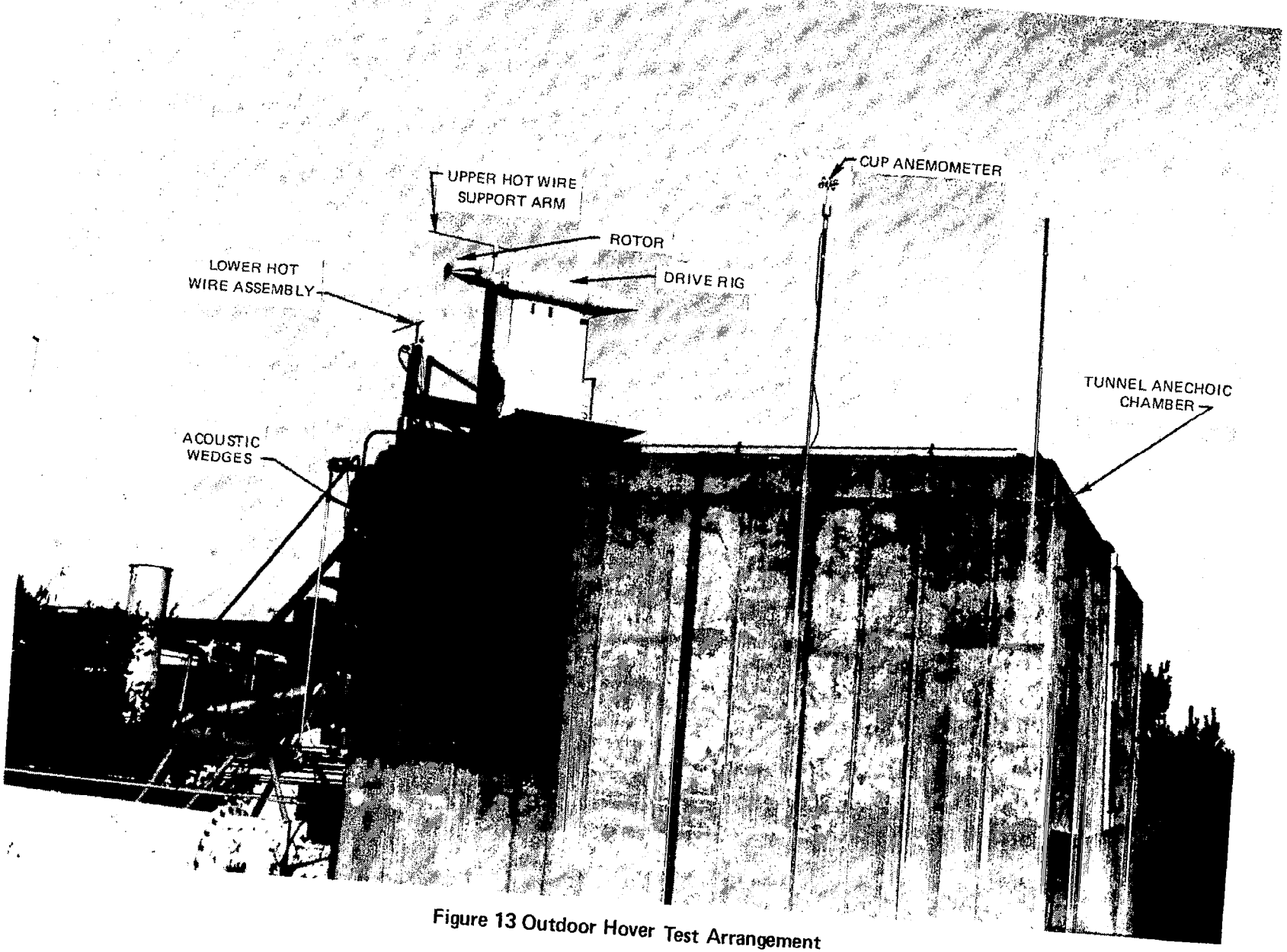

Figure 13 Outdoor Hover Test Arrangement

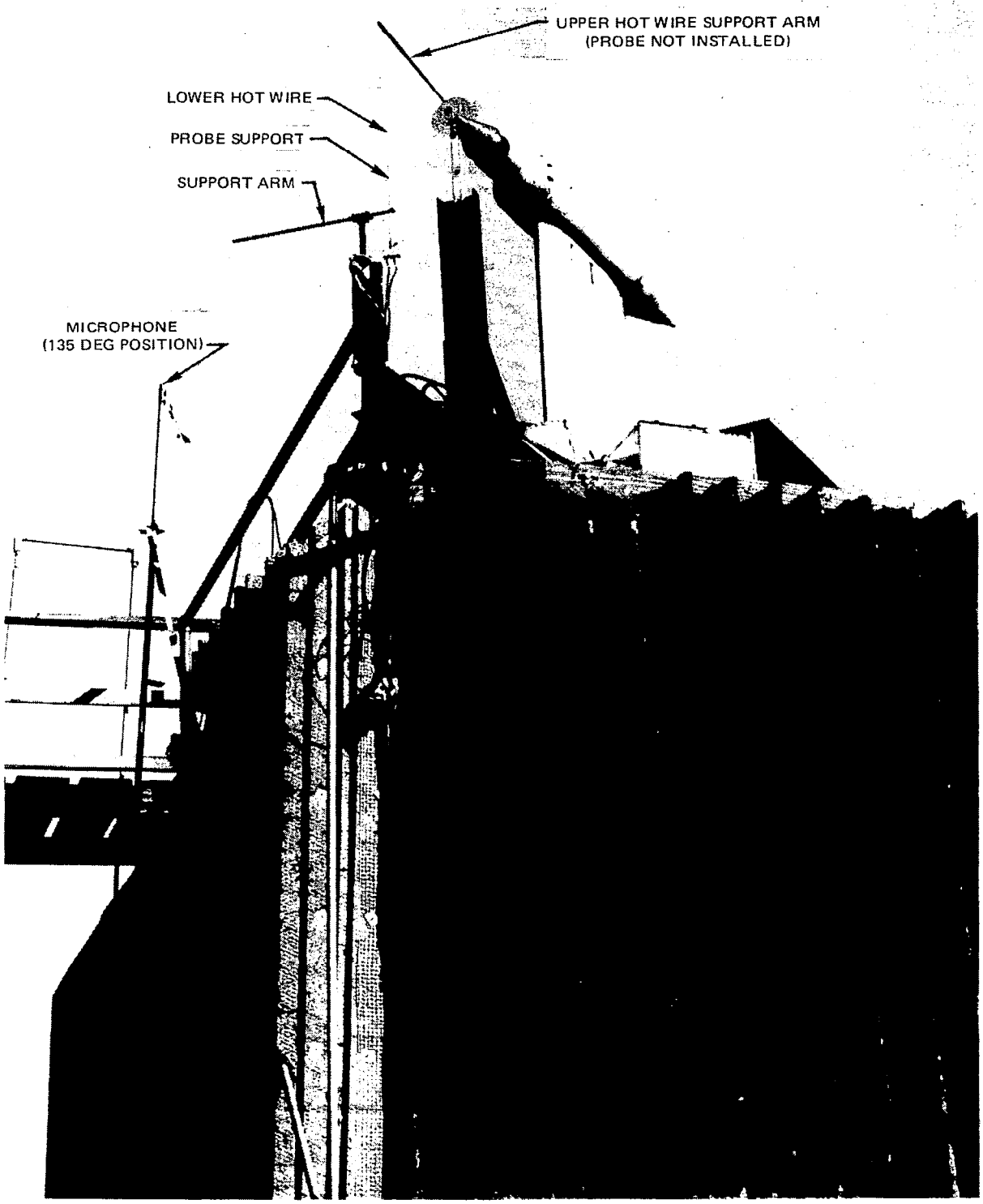

Figure 13—Concluded

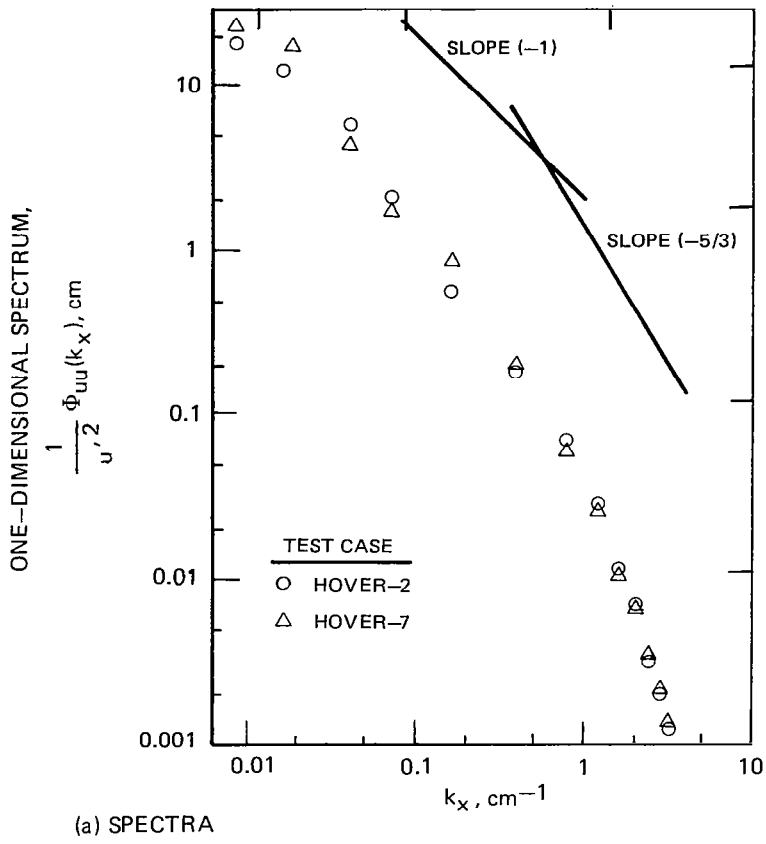

(a) SPECTRA

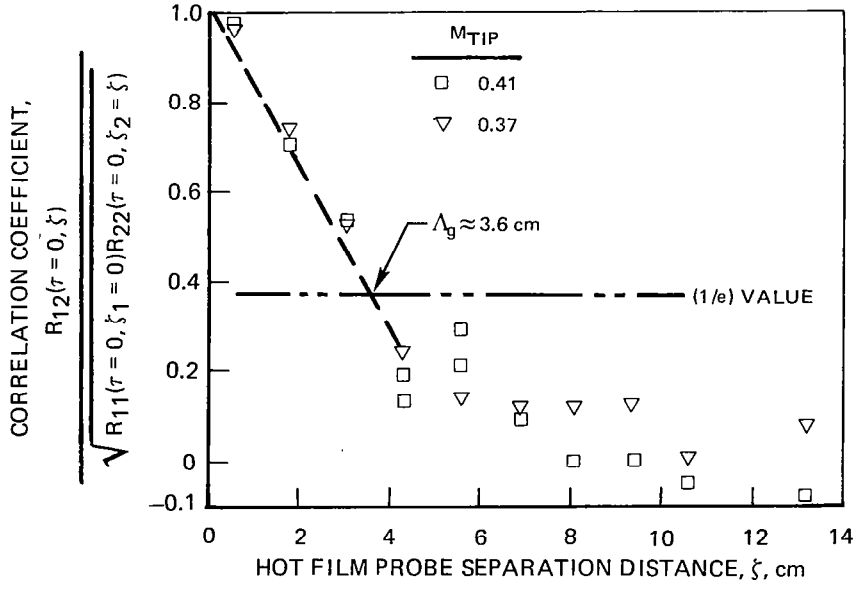

(b) TRANSVERSE CROSS–CORRELATION

Figure 14 – Spectra and Spatial Correlations of Axial Component of Inflow Turbulence in Hover

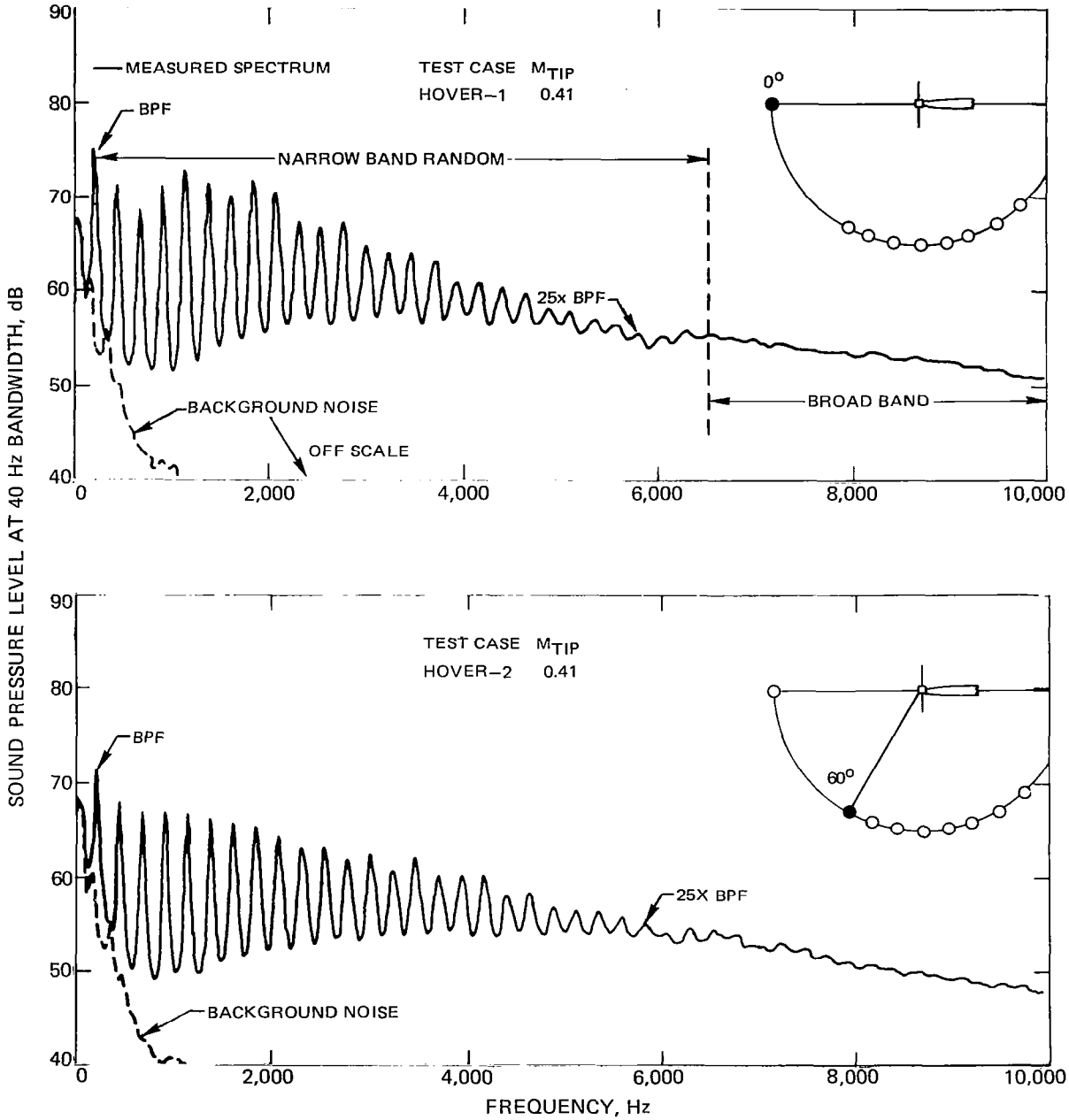

Figure 15. Typical Outdoor Hover Noise Spectra

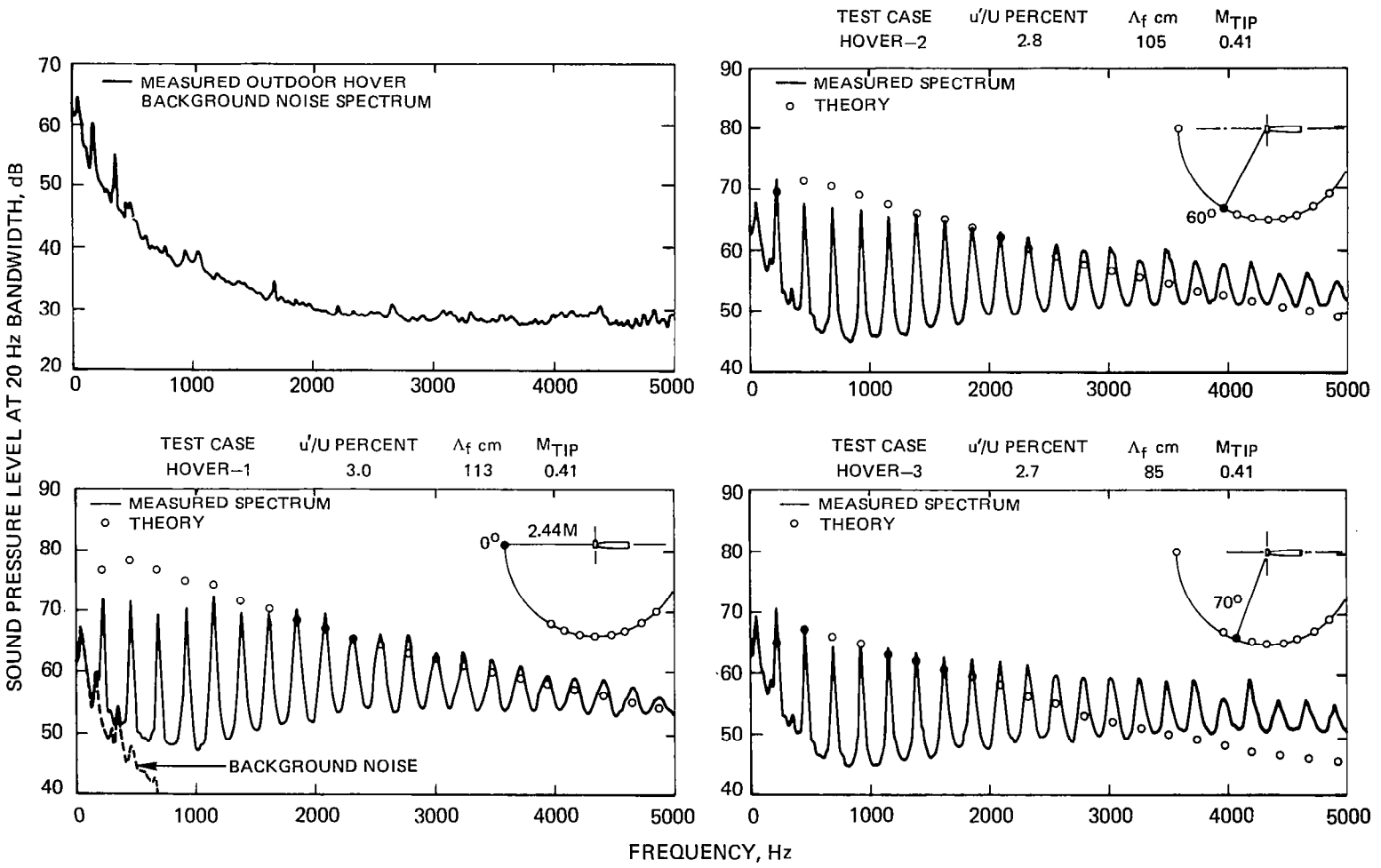

Figure 16 Comparison of Measured and Theoretically Predicted Far–Field Noise Spectra for Outdoor Hover Cases 1 to 15

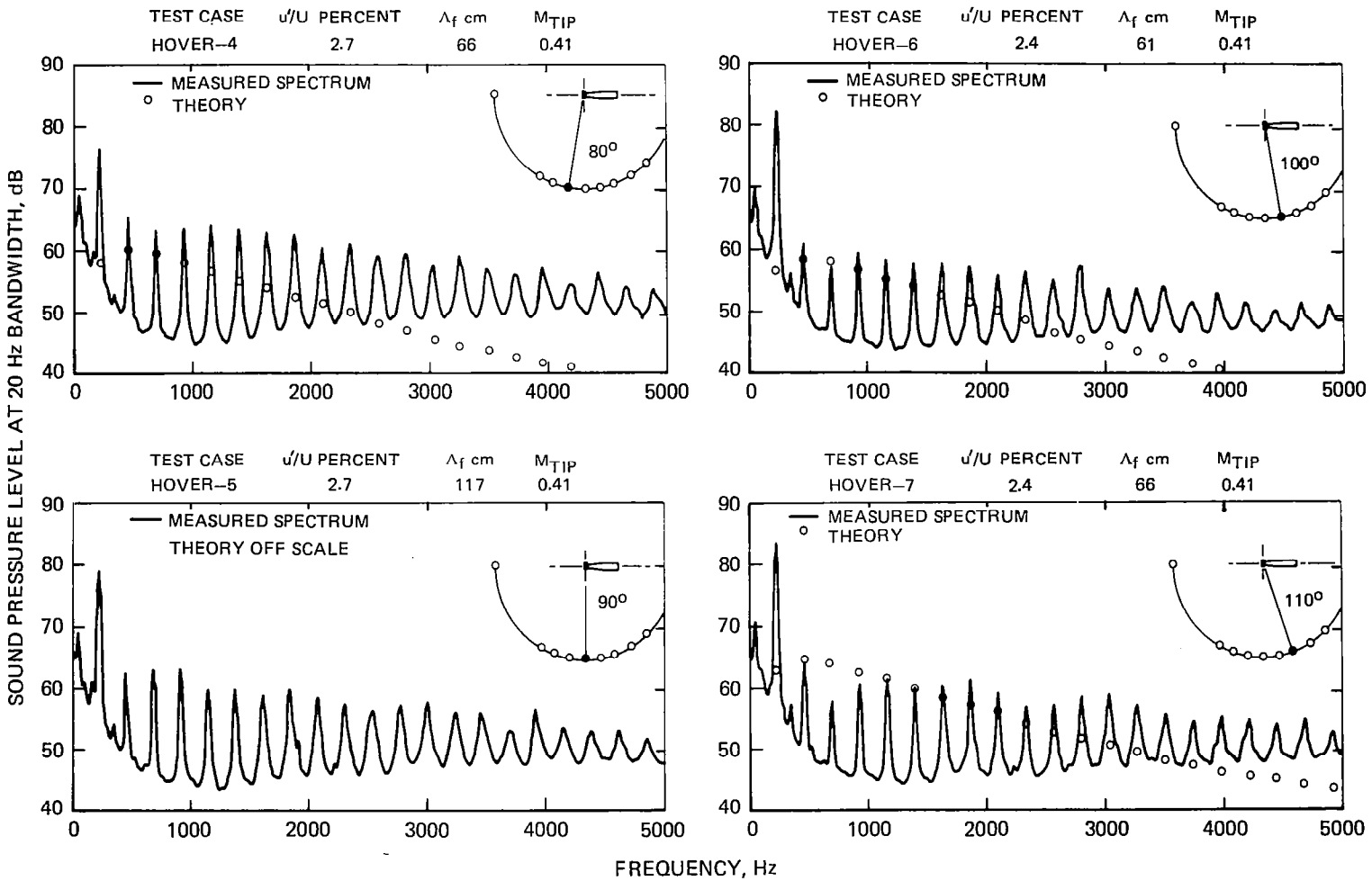

Figure 16 Continued

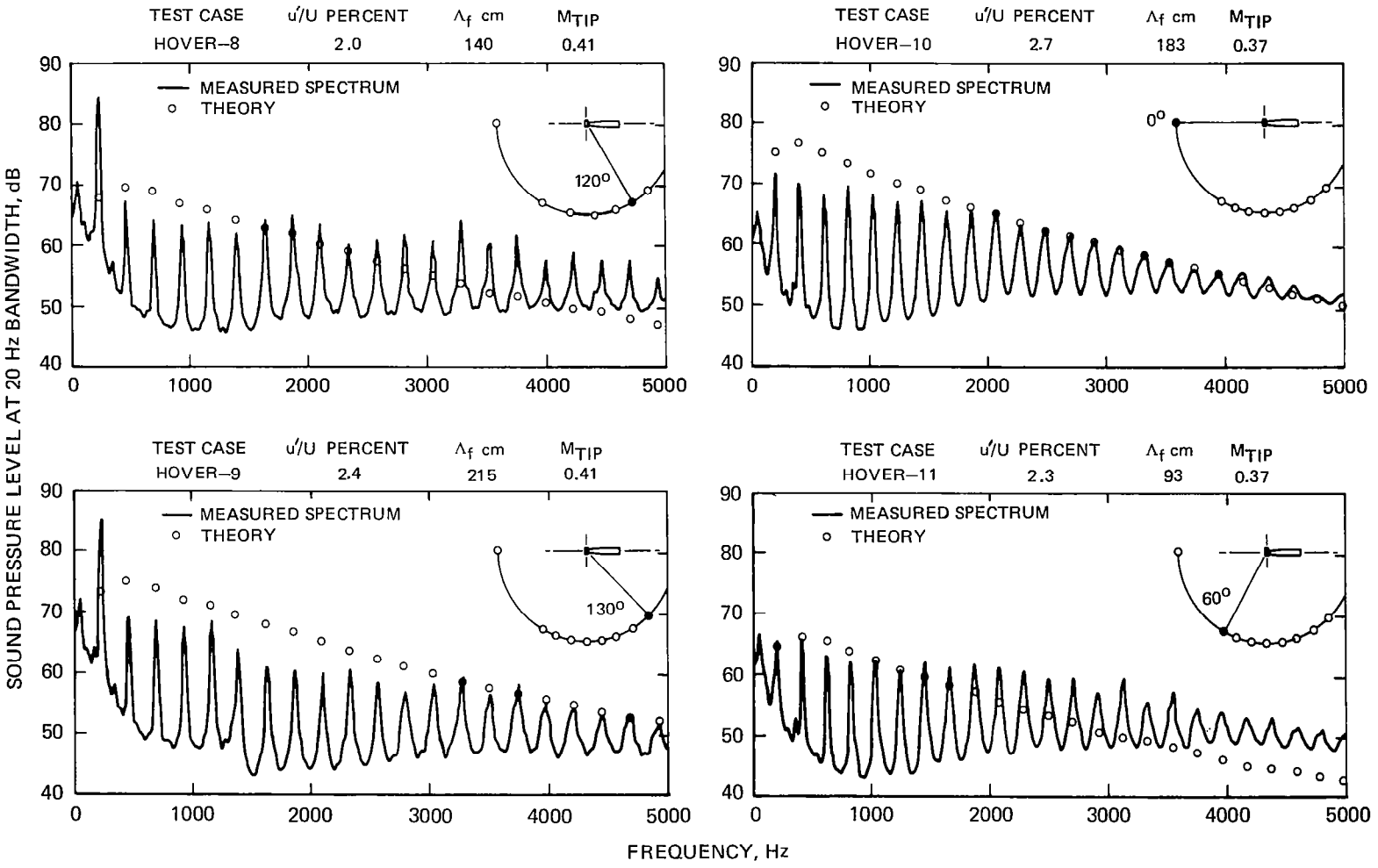

Figure 16 – Continued

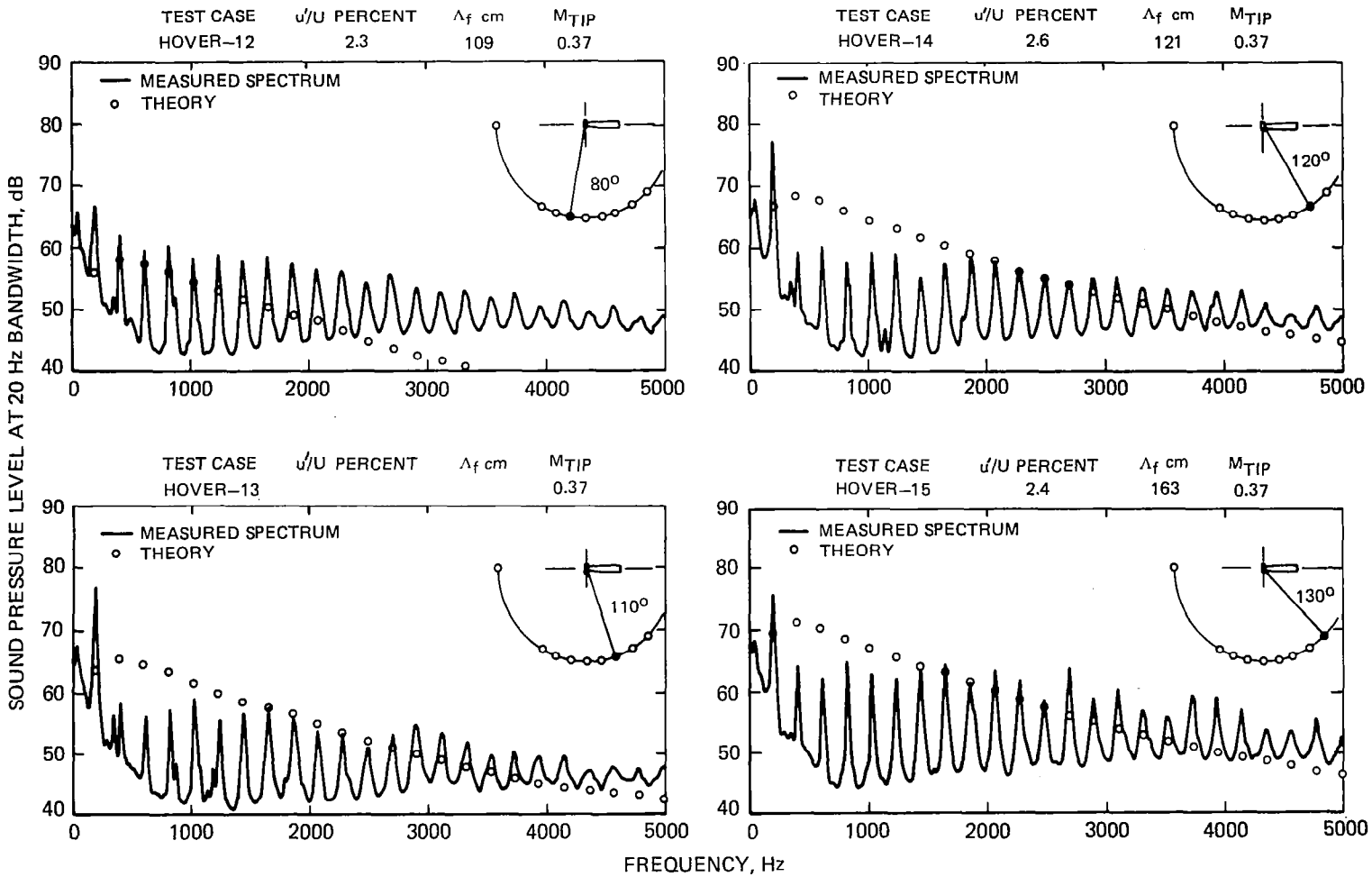

Figure 16 Concluded

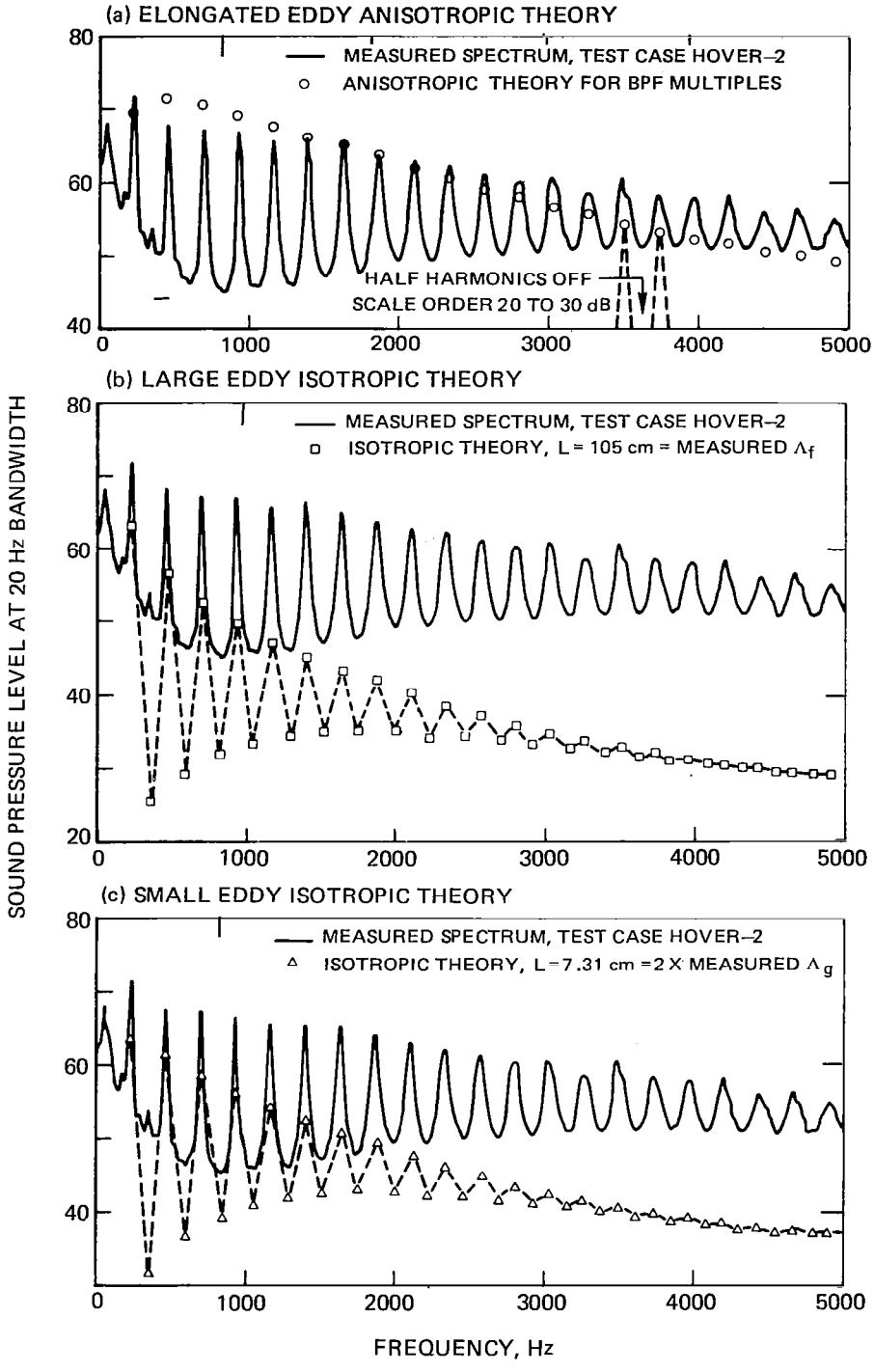

Figure 17. Comparison of Anisotropic Inflow Noise Prediction Theory and Isotropic Theories with Outdoor Hover Data

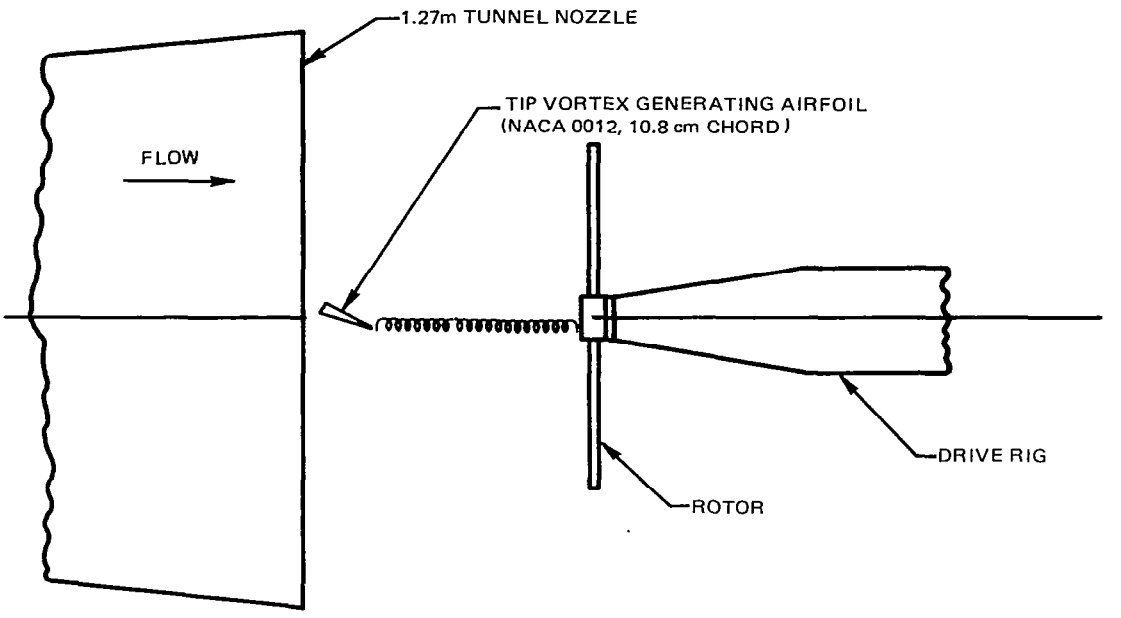

(a) PLAN VIEW; VERTICAL ASCENT

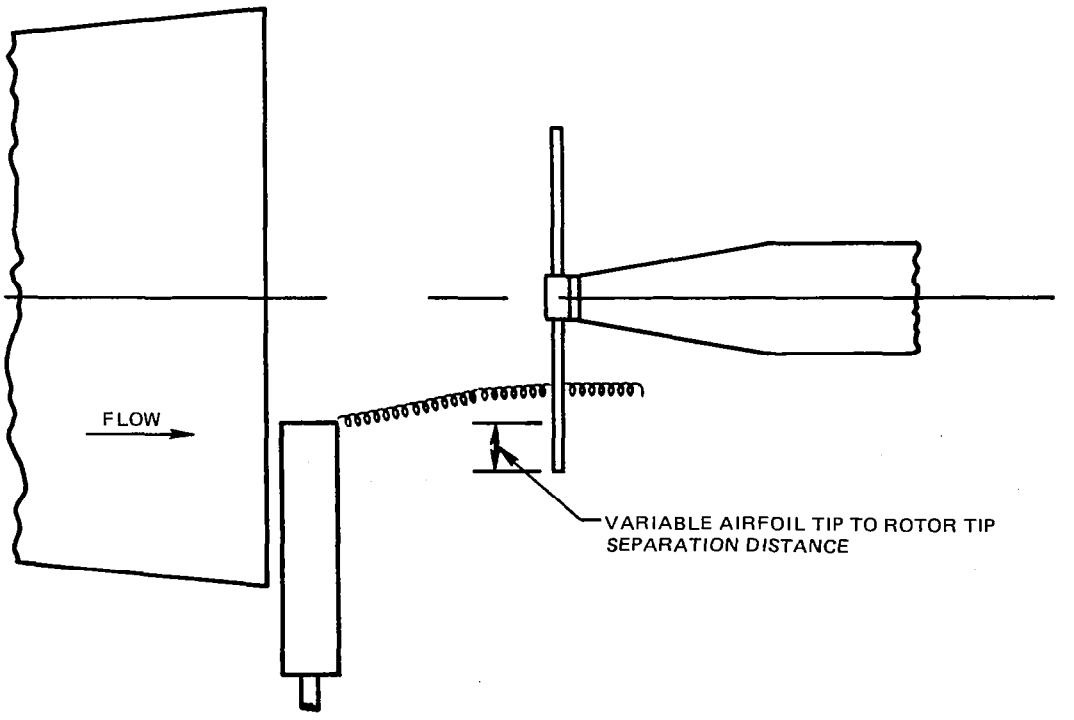

(b) SIDE ELEVATION; VERTICAL ASCENT

Figure 18 — Tip Vortex Ingestion Test Arangement

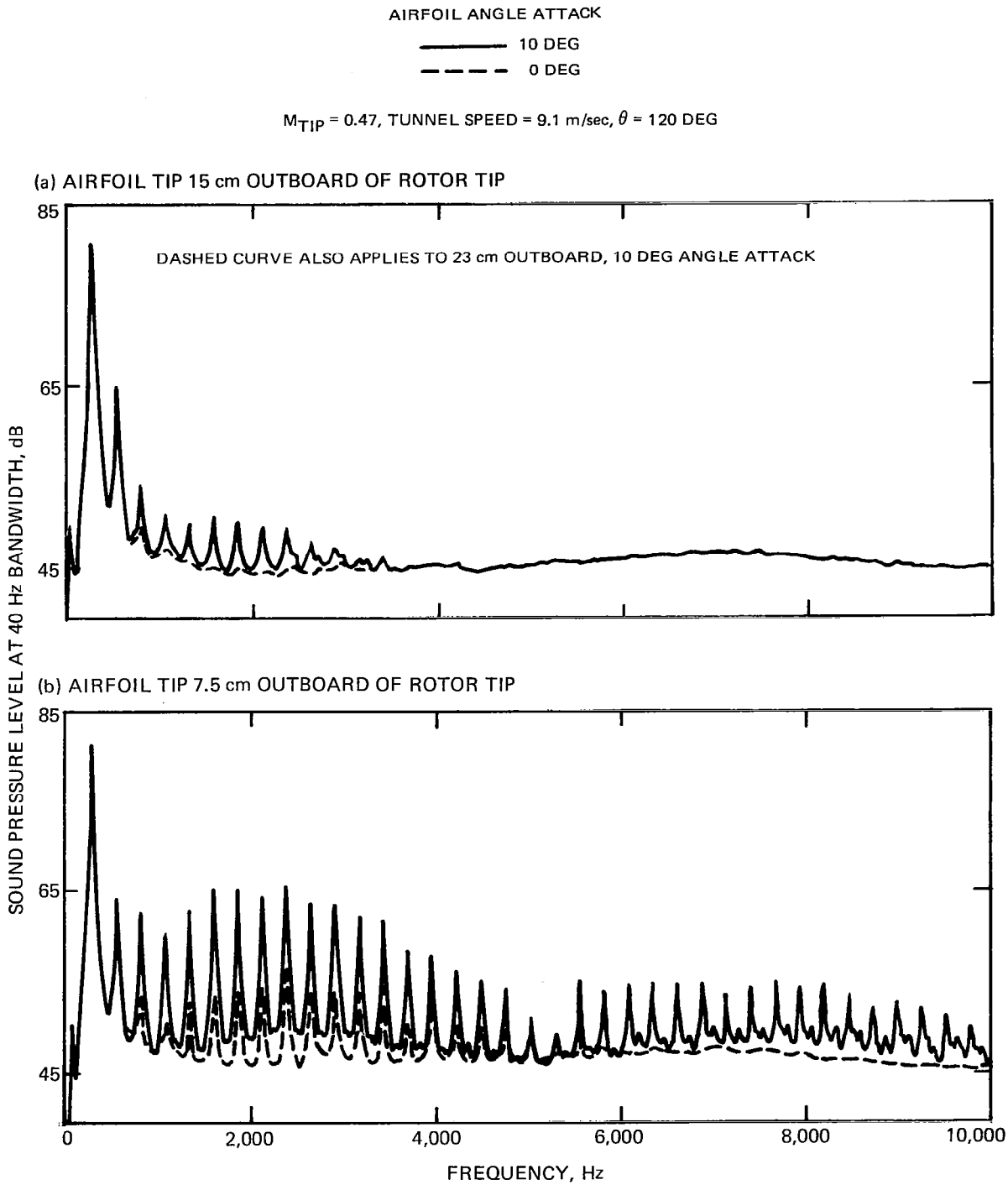

Figure 19 – Effect of Vortex Ingestion Position on Rotor Noise Spectra

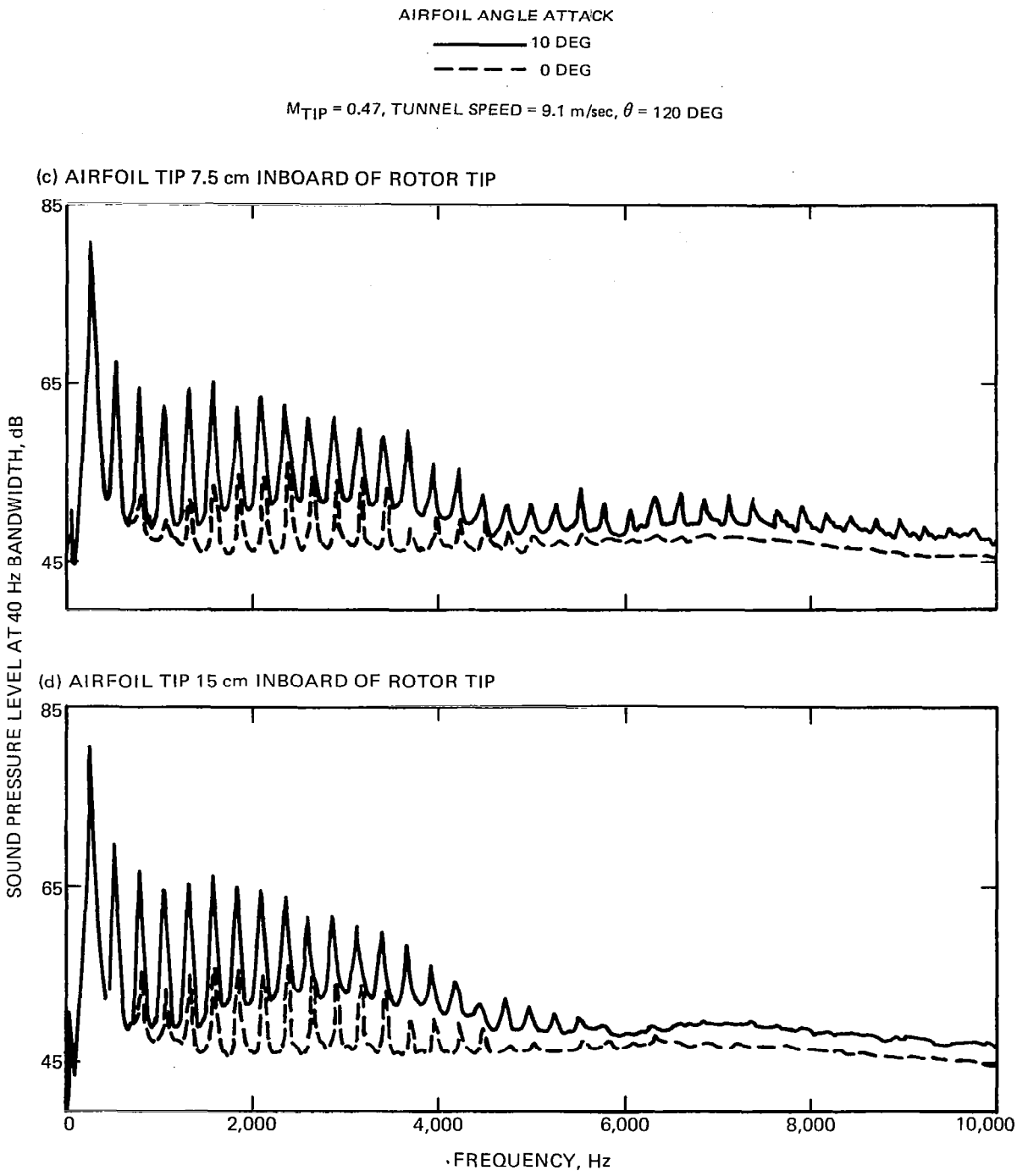

Figure 19 — Concluded

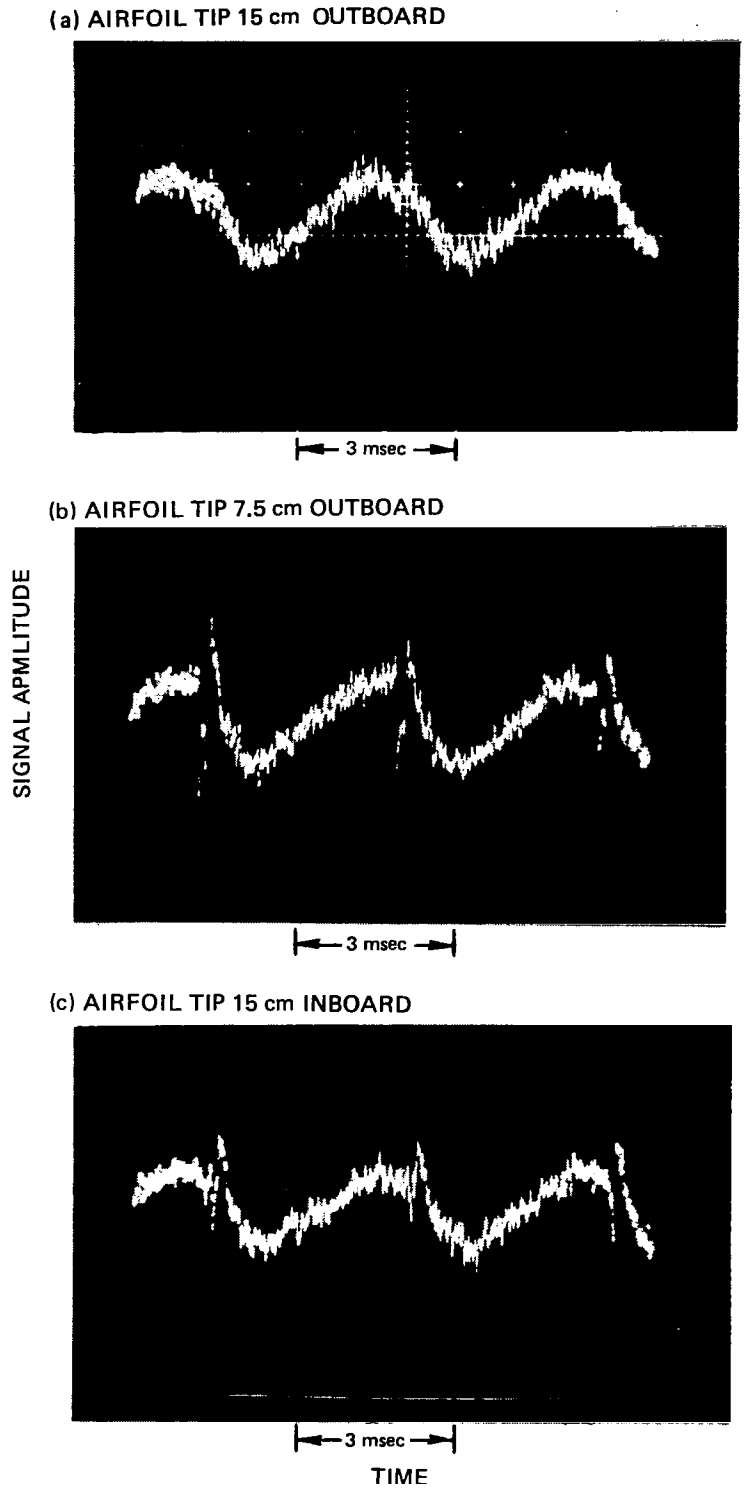

Figure 20 – Effect of Vortex Ingestion Position on Rotor Noise Time Histories (Same Conditions as Figure 19)

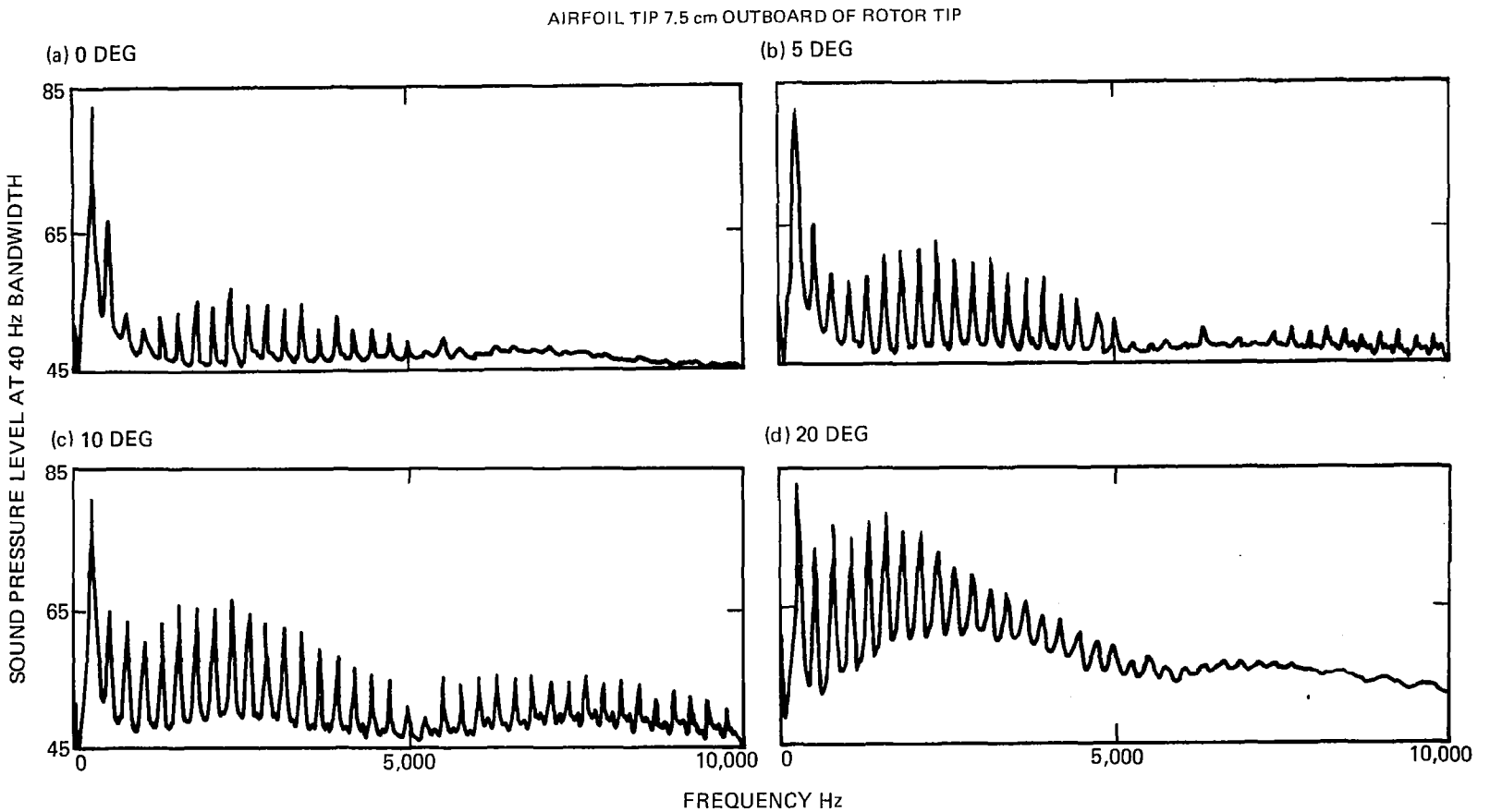

Figure 21 – Effect of Vortex Generating Airfoil Angle of Attack on Rotor Noise Spectra (Same Conditions as Figure 19)

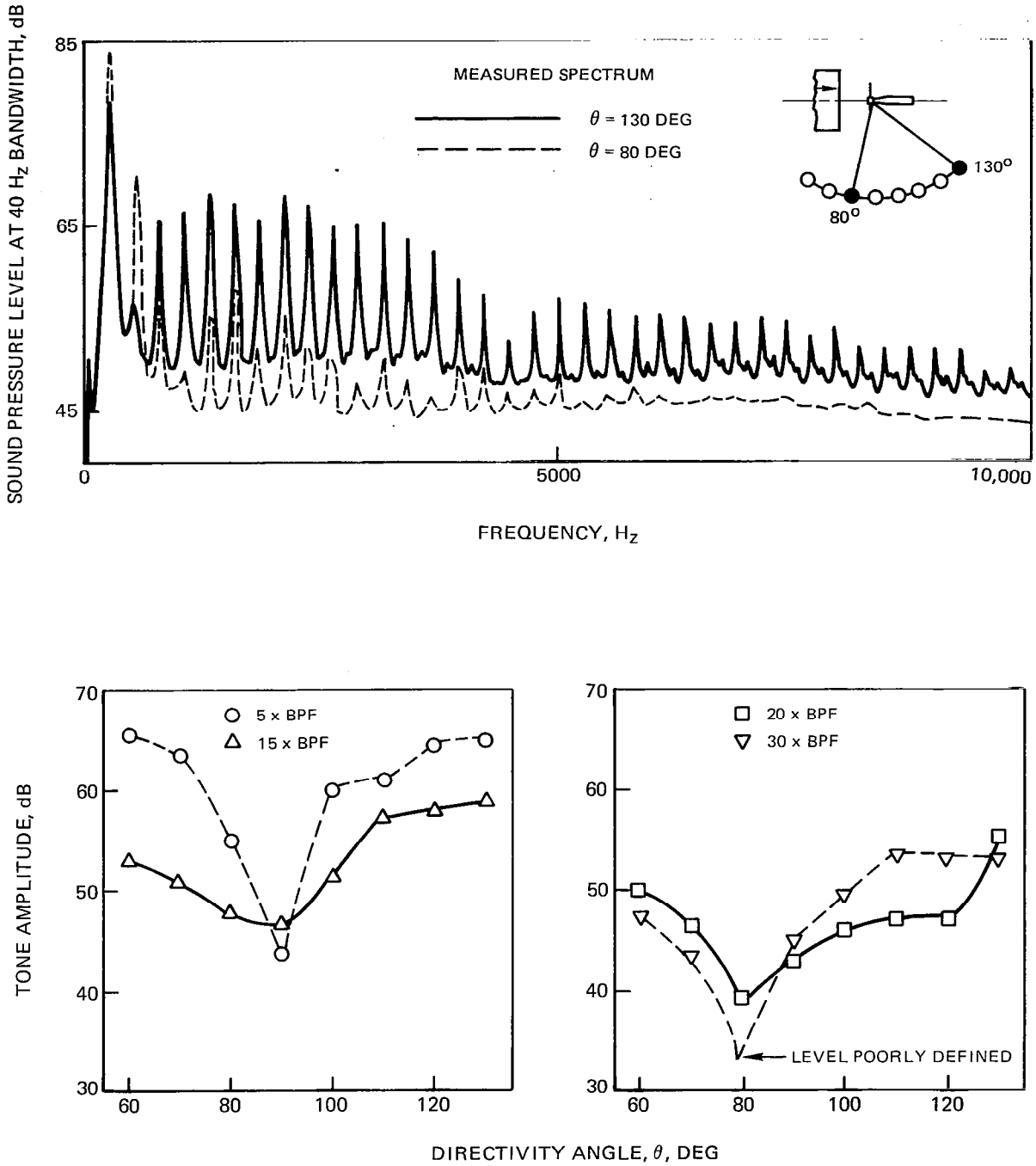

(SAME CONDITIONS AS FIGURE 19; AIRFOIL TIP 7.5 cm OUTBOARD OF ROTOR TIP)

Figure 22 – Directivity of Vortex Ingestion Noise

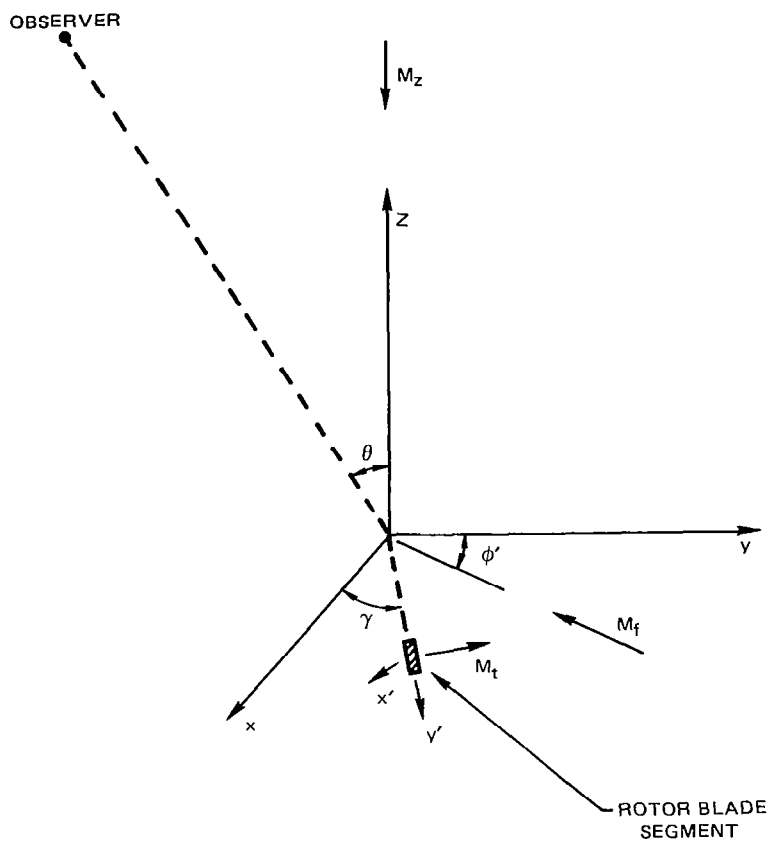

Figure 23. Rotor Blade Segment Moving in Forward Flight

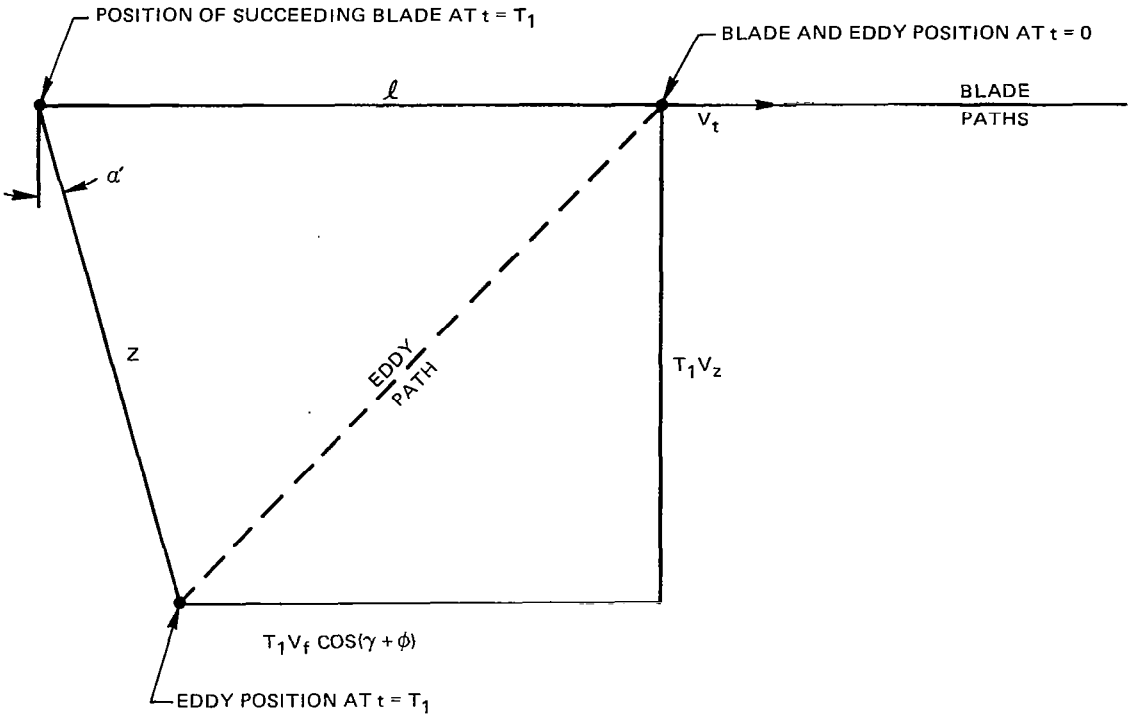

Figure 24. Trajectories of Rotor Blades and Turbulent Eddies

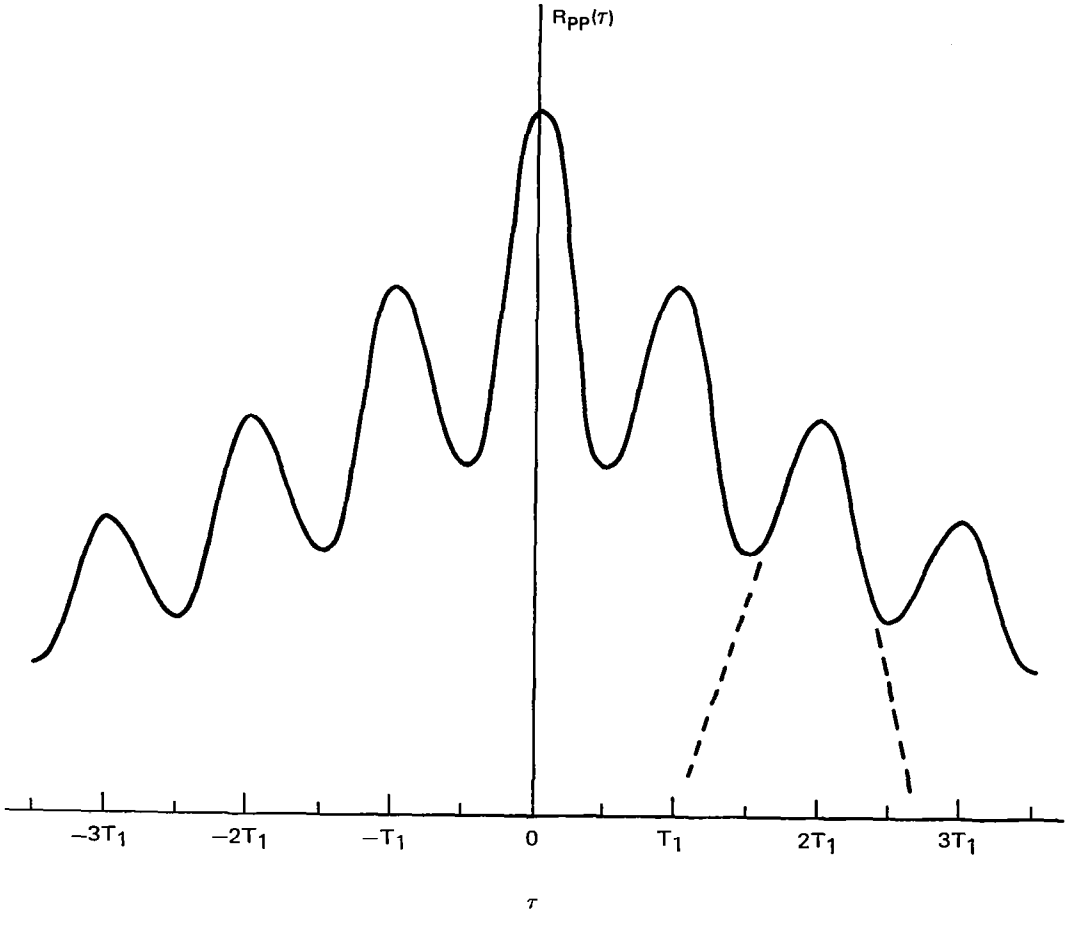

Figure 25. Cross Correlation of Far—Field Noise

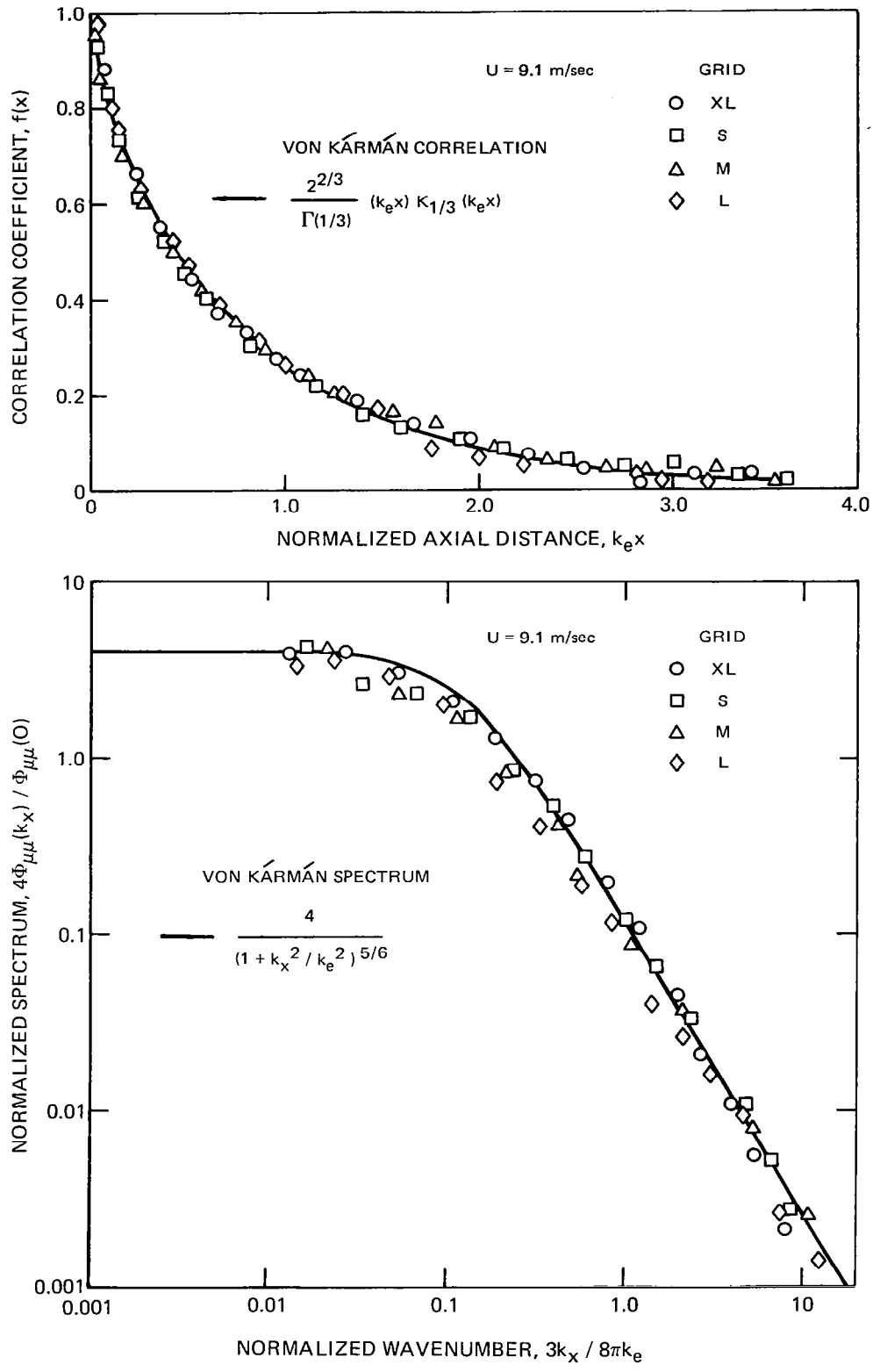

Figure 26 – Axial Correlation and One–Dimensional Spectrum of Axial Turbulence Component for Various Grids

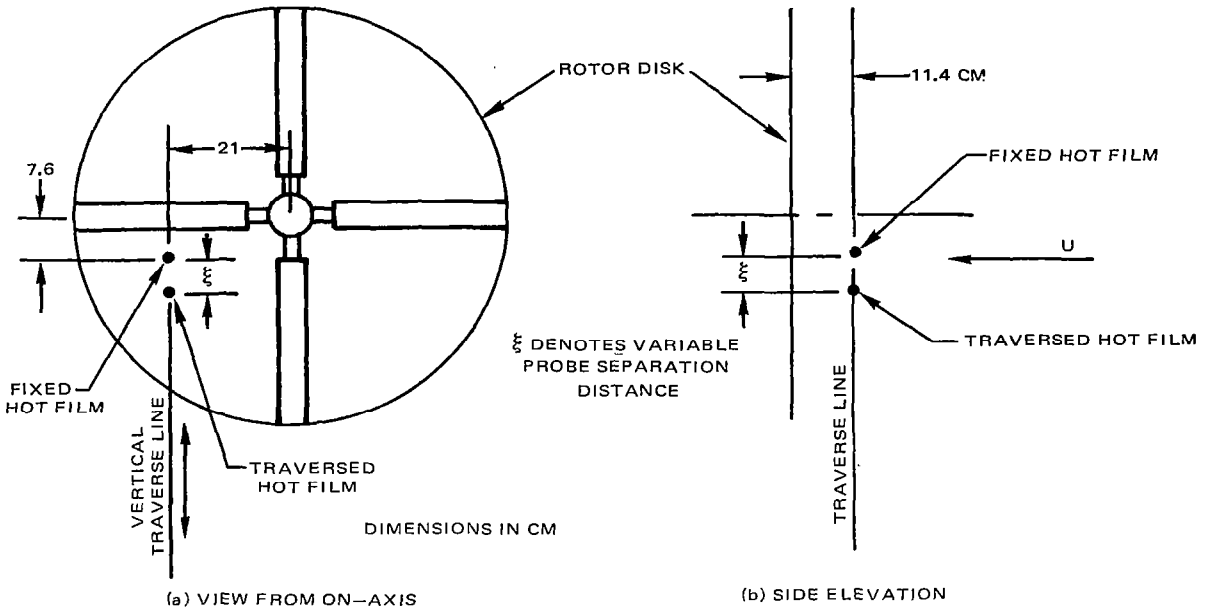

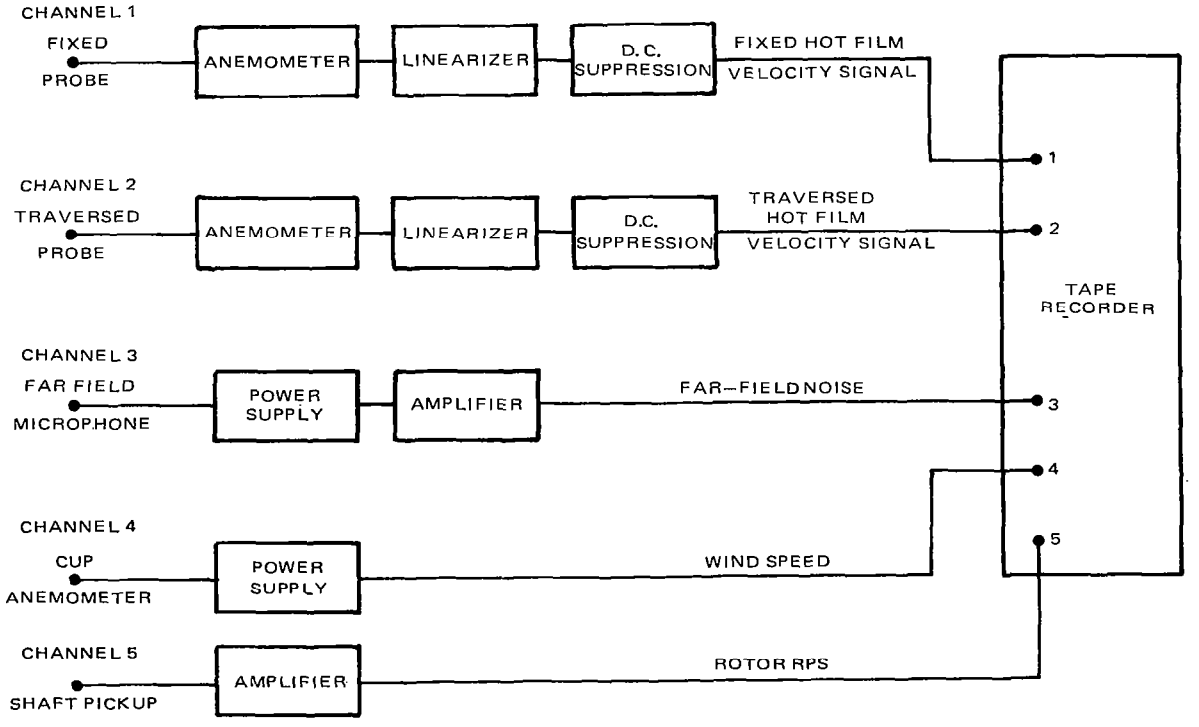

Figure 27–Outdoor Hover Data Acquisition System

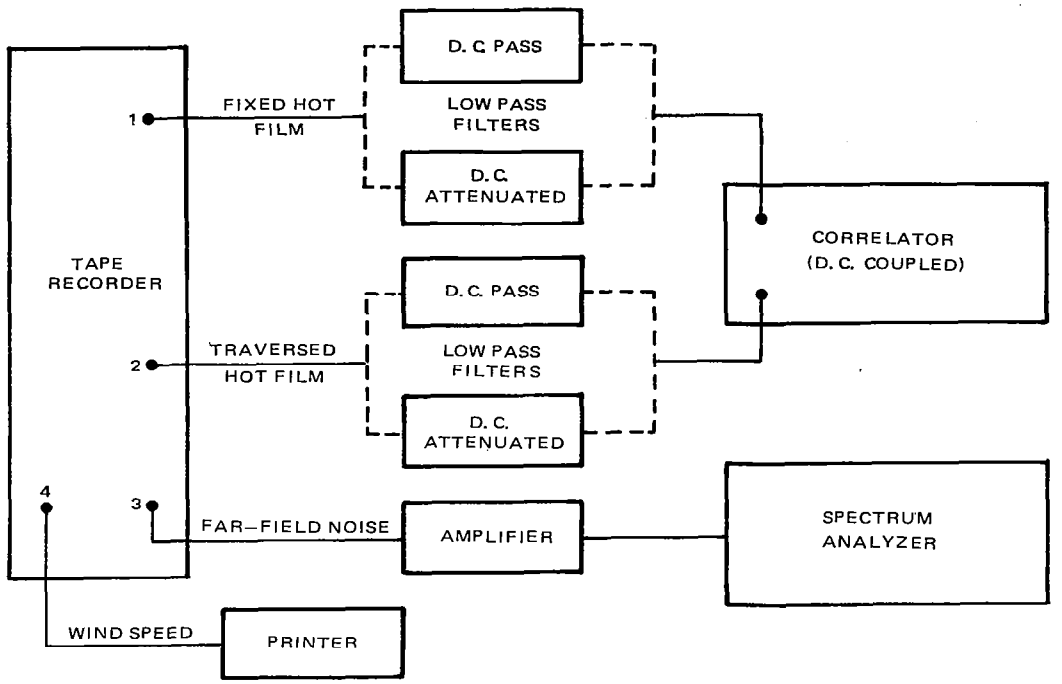

(a) INSTRUMENTATION ARRANGEMENT

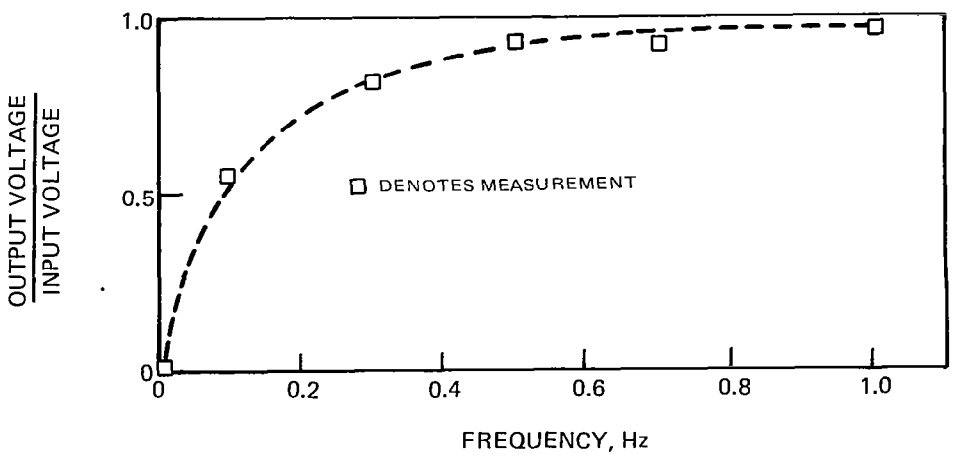

(b) LOW FREQUENCY CHARACTERISTICS OF D. C. ATTENUATION FILTER

Figure 28. Outdoor Hover Data Reduction System

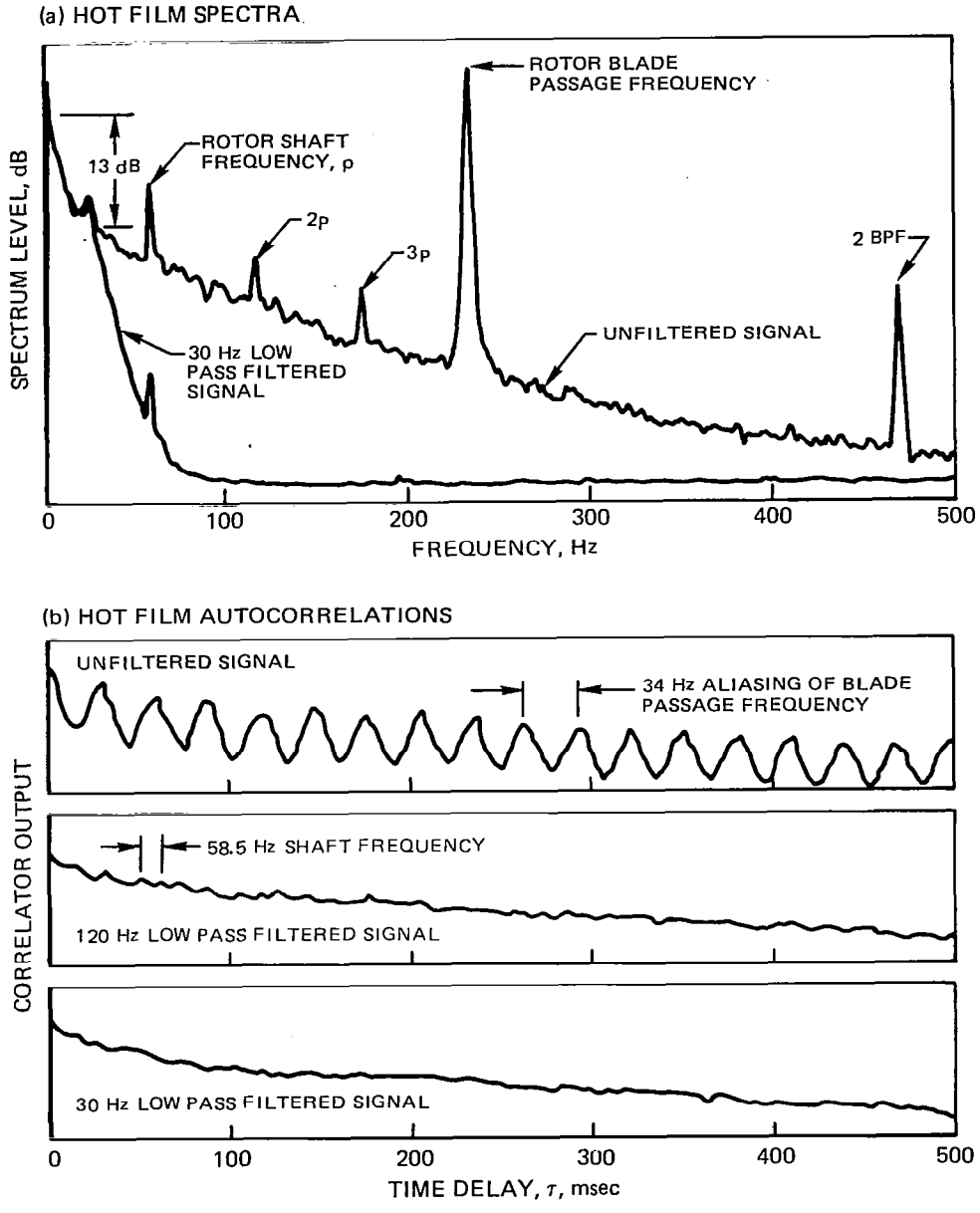

Figure 29. Effect of Low Pass Filtering on Hover Inflow Turbulence Spectra and Autocorrelations

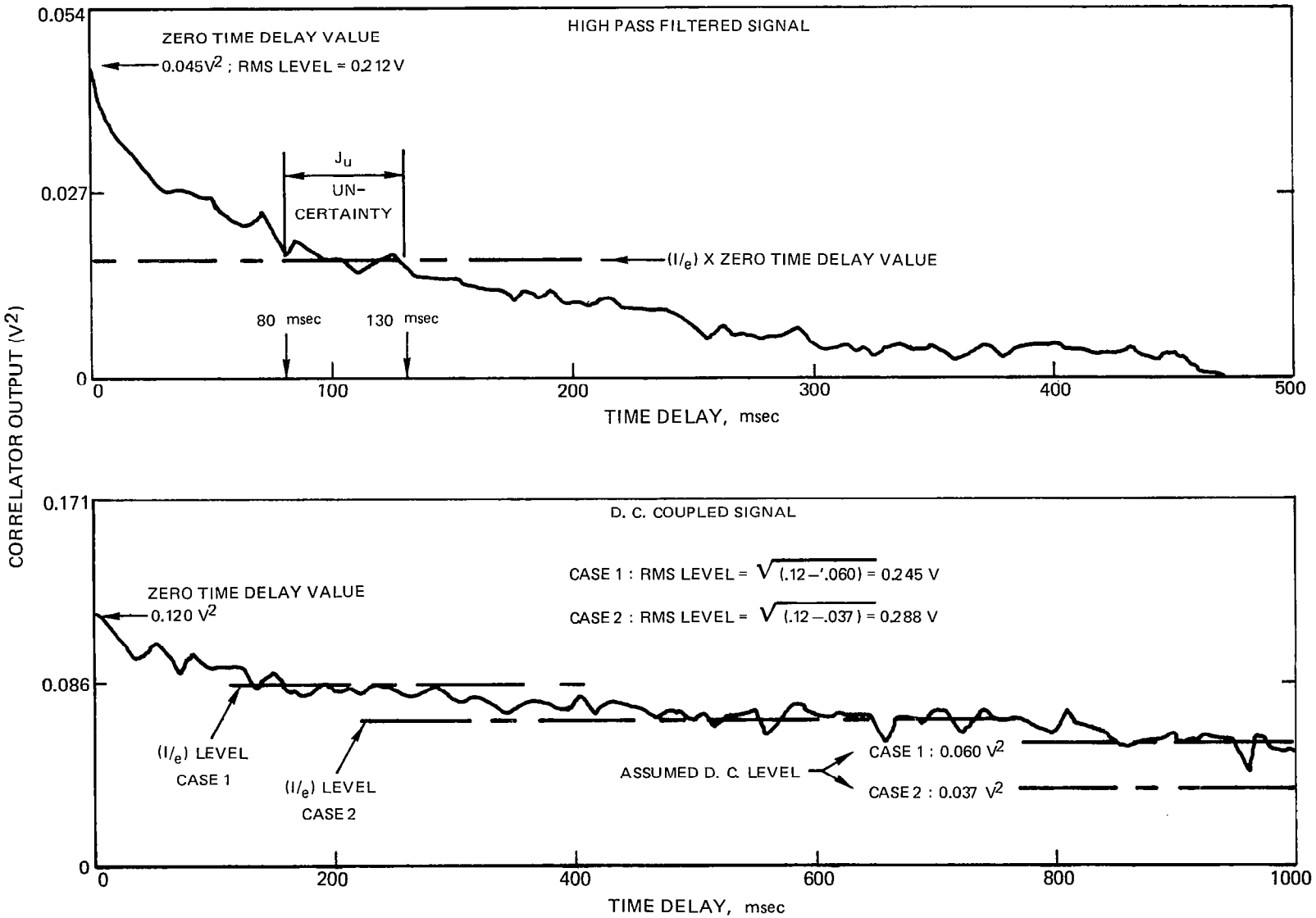

Figure 30 —Effect of High Pass Filtering On Analysis of Hover Inflow Turbulence Autocorrelation Functions

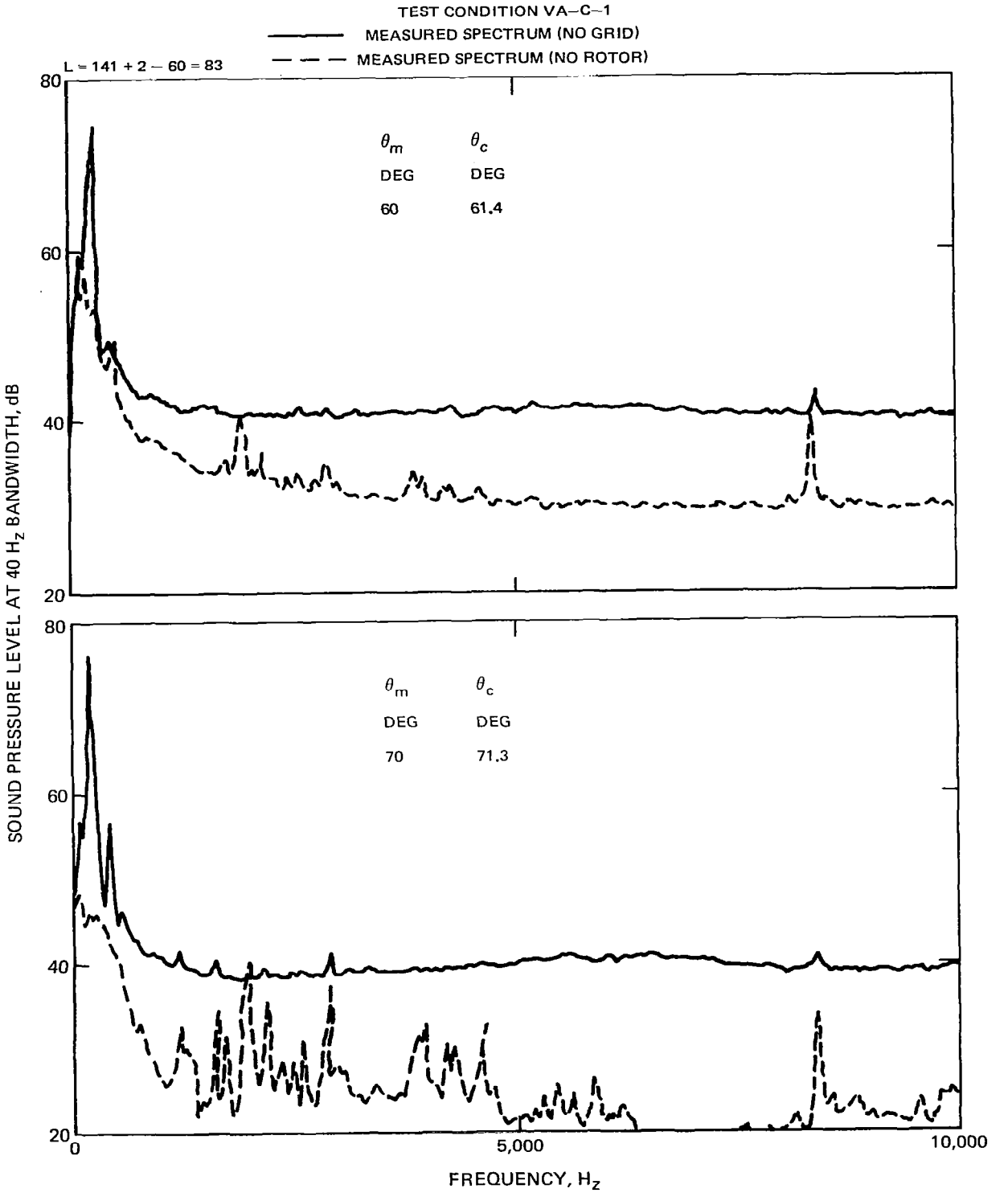

Figure 31 – Clean Inflow Noise in Tunnel at Outdoor Hover Operating Condition

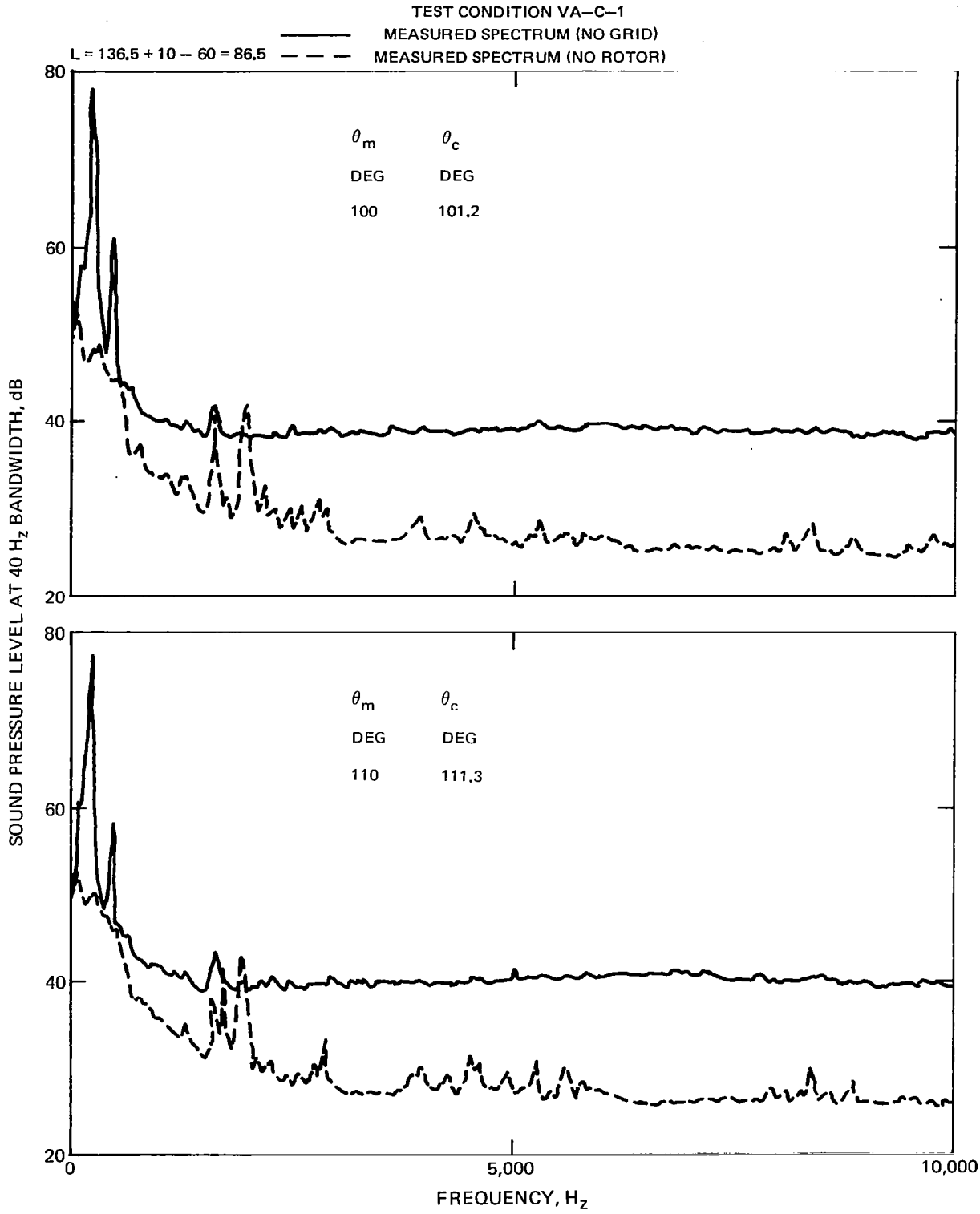

Figure 31 — Continued

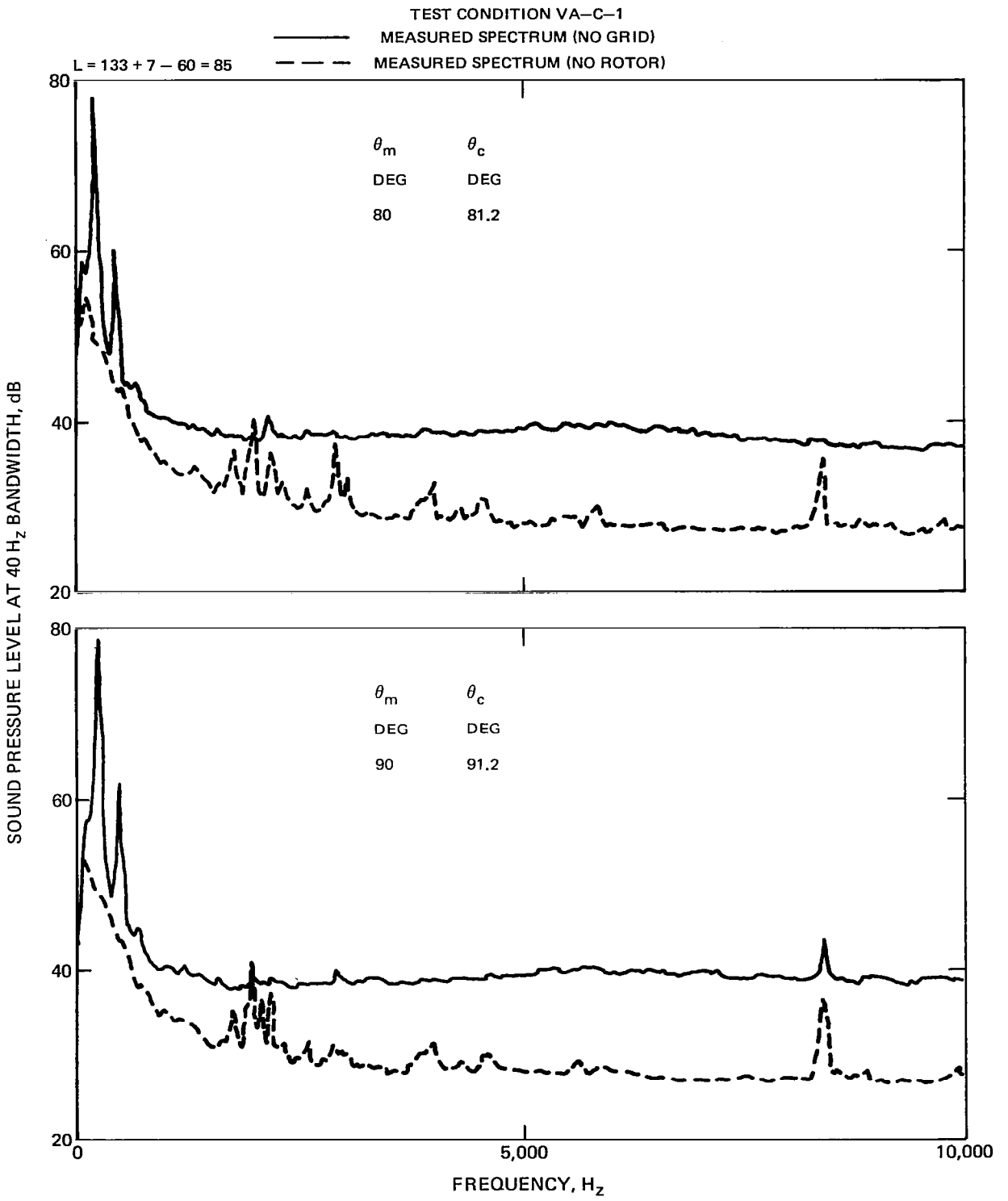

Figure 31 — Continued

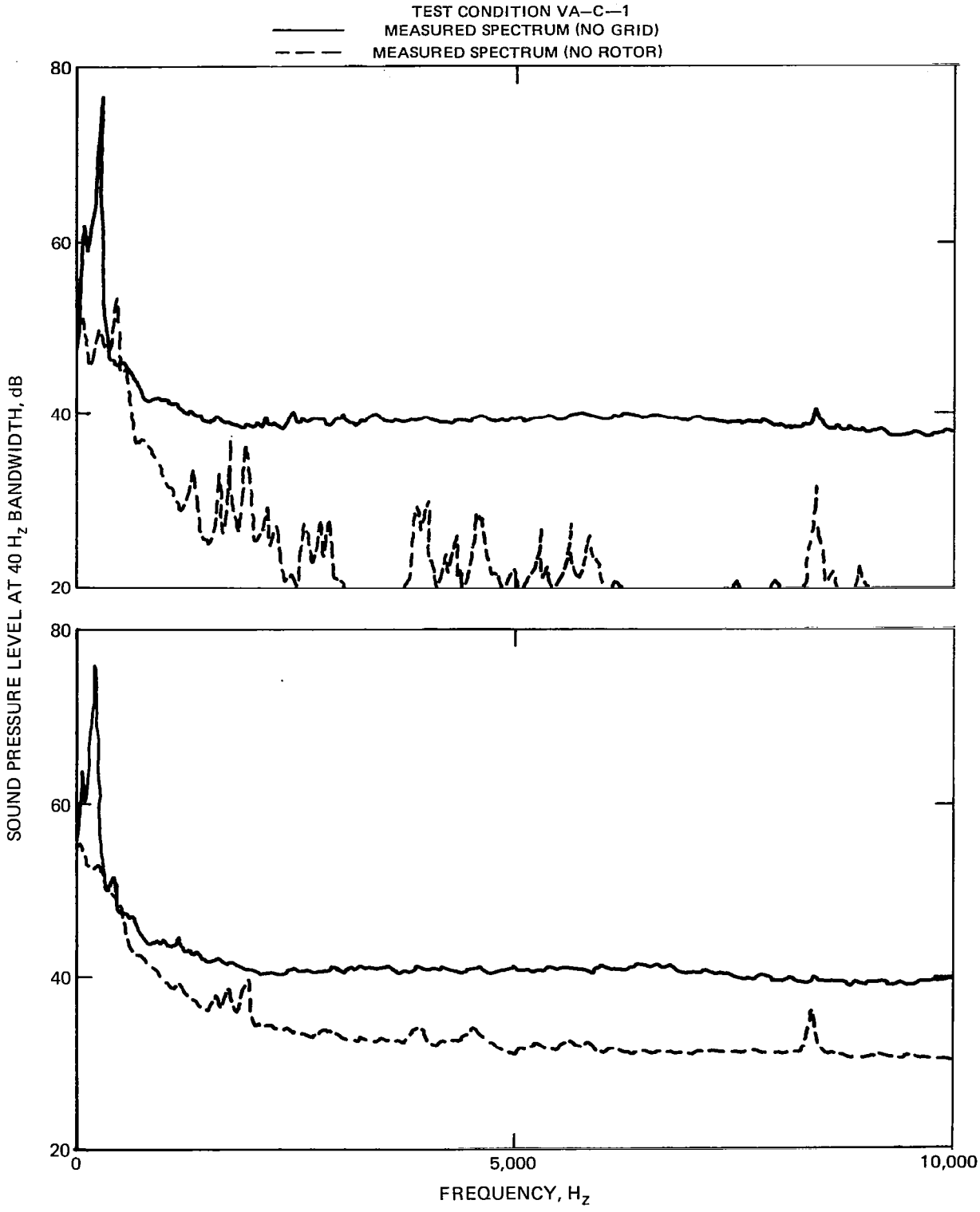

Figure 31 — Concluded

1. Report No.	2. Government Accession No.	3. Recipient's Catalog No.
NASA CR-3213		

4. Title and Subtitle	5. Report Date
Noise of a Model Helicopter Rotor Due to Ingestion of Turbulence	November 1979
	6. Performing Organization Code
7. Author(s)	8. Performing Organization Report No.
Robert W. Paterson and Roy K. Amiet	
9. Performing Organization Name and Address	10. Work Unit No.
United Technologies Research Center East Hartford, CT 06108	11. Contract or Grant No. NAS1-15094
12. Sponsoring Agency Name and Address	13. Type of Report and Period Covered Contractor Report
National Aeronautics and Space Administration Washington, DC 20546	14. Army Project No.

15. Supplementary Notes

Langley Technical Monitor: Robert J. Pegg
Final Report

16. Abstract

A theoretical and experimental investigation of the noise of a model helicopter rotor due to ingestion of turbulence was conducted. Experiments were performed with a 0.76 m dia, articulated model rotor at the United Technologies Research Center (UTRC) Acoustics Research Tunnel for a range of inflow turbulence and rotor operating conditions. Inflow turbulence levels varied from approximately 2 to 19 percent and tip Mach number was varied from 0.3 to 0.52. Test conditions included ingestion of atmospheric turbulence in outdoor hover as well as ingestion of grid generated isotropic turbulence in the wind tunnel airstream. In wind tunnel testing, both forward flight and vertical ascent (climb) were simulated. Far-field noise spectra and directivity were measured in addition to incident turbulence intensities, length scales and spectra.

17. Key Words (Suggested by Author(s))	18. Distribution Statement
Helicopter rotor Noise Turbulence	Unclassified - Unlimited Subject Category 05

19. Security Classif. (of this report)	20. Security Classif. (of this page)	21. No. of Pages	22. Price*
Unclassified	Unclassified	128	$7.25

*For sale by the National Technical Information Service, Springfield, Virginia 22161

NASA-Langley, 1979